Summer 2011

Nanofabrication of halloysite-PCL composite scaffolds and functionalization of titanium for tissue regeneration

Shraddha Parshottambhai Patel

NANOFABRICATION OF HALLOYSITE-PCL COMPOSITE

SCAFFOLDS AND FUNCTIONALIZATION OF TITANIUM

FOR TISSUE REGENERATION

by

Shraddha Parshottambhai Patel, B.Sc., M.Sc., M.S.

A Dissertation Presented in Partial Fulfillment
of the Requirements for the Degree
Doctor of Philosophy

COLLEGE OF ENGINEERING AND SCIENCE
LOUISIANA TECH UNIVERSITY

August 2011

UMI Number: 3480425

UMI®

Dissertation Publishing

ProQuest®

LOUISIANA TECH UNIVERSITY

THE GRADUATE SCHOOL

June 15, 2011
_____
Date

We hereby recommend that the dissertation prepared under our supervision

by Shraddha Parshottambhai Patel
_____

entitled_____

Nanofabrication of Halloysite-PCL Composite Scaffolds and
_____

Functionalization of Titanium for Tissue Regeneration
_____

_____

_____

be accepted in partial fulfillment of the requirements for the Degree of

Doctor of Philosophy in Biomedical Engineering
_____

_____
Supervisor of Dissertation Research

_____
Head of Department

Biomedical Engineering
_____
Department

Recommendation concurred in:

_____

_____   Advisory Committee

_____

Approved: **Approved:**

_____   _____
Director of Graduate Studies   Dean of the Graduate School

_____
Dean of the College

ABSTRACT

Major medical needs may be achieved through regenerative medicine. Nanotechnology has triggered a research revolution in many important areas such as the biomedical sciences and bioengineering at the molecular level which has grown significantly due to the availability of new analytical applications and tools based on nanotechnology. Clinical conditions and diseases being targeted by nanotechnology research include burns, Alzheimer's and Parkinson's disease, implant failure, improved wound healing, birth defects, osteoporosis and congestive heart defects. Therapeutic use of growth factors and drugs to stimulate the production and/or function of endogenous cells represents a key area of regenerative medicine. The development of methods to expand ex vivo and drug delivery through advances in cell culture and scaffold technology have led to successful new treatment modalities for bone and wound repair.

The studies in this dissertation focused on several regenerative medicine approaches, with a future goal of an implantable scaffold material that can efficiently act as a repair material for wound healing and repair or as a replacement material for bones, teeth and other tissues. In this study, two different materials were nanoengineered for regenerative medicine applications. Anodization was used to produce nanoporous titanium scaffolds. Electrospinning was used to form Poly (ε-caprolactone) (PCL) scaffolds, halloysite-PCL composite scaffolds and drug loaded halloysite-PCL scaffolds. Cellular response was assessed in each study through cell-based assays, including the

PicoGreen DNA assay, the Coomassie Plus total protein assay, and the Alizarin Red mineralization assay. Cell characterization methods were used to measure the potential of these nanoengineered materials to enhance cell proliferation, functionality, tissue formation and mineralization.

The results from the cell characterization assays suggest nanoporous titanium and the type I collagen coated halloysite-PCL scaffold both hold promise for bone tissue engineering and aiding in wound repair. Nanoporous titanium surfaces supported cell growth, cell differentiation and mineralization and are more biologically supportive compared to smooth titanium. The incorporation of HNTs up to 7wt%, within the PCL-scaffold did not extensively change the morphology of the PCL scaffold. Scanning electron microscopy and fluorescein isothiocyanate (FITC) labeling of halloysites indicated the nanotubes were not incorporated into PCL fibers but clustered together to form a ball-like structure that also linked adjacent fibers producing a complex, mesh-like (and extracellular matrix-like) composite scaffold. Type I collagen coated halloysite-PCL scaffold produced higher cell proliferation rates, increased protein synthesis and enhanced mineralization in comparison with halloysite-PCL and PCL only scaffolds.

In a companion study, hallyosite-loaded scaffolds containing more than one drug were created. Sustained release of Brilliant Green was achieved from both drug loaded PCL scaffolds and the drug loaded halloysite-PCL scaffold. This data supports the conclusion that drug loaded halloysite-PCL scaffolds may be a novel, biodegradable material for wound healing, producing anti-bacterial materials, or enhanced tissue bandages.

APPROVAL FOR SCHOLARLY DISSEMINATION

The author grants to the Prescott Memorial Library of Louisiana Tech University the right to reproduce, by appropriate methods, upon request, any or all portions of this Dissertation. It is understood that "proper request" consists of the agreement, on the part of the requesting party, that said reproduction is for his personal use and that subsequent reproduction will not occur without written approval of the author of this Dissertation. Further, any portions of the Dissertation used in books, papers, and other works must be appropriately referenced to this Dissertation.

Finally, the author of this Dissertation reserves the right to publish freely, in the literature, at any time, any or all portions of this Dissertation.

Author _S· P· Patel_

Date _8/4/2011_

DEDICATION

This dissertation is dedicated to my family.

TABLE OF CONTENTS

LIST OF FIGURES

LIST OF TABLES

ACKNOWLEDGMENTS

CHAPTER 1

INTRODUCTION AND BACKGROUND

1.1 Nanotechnology for Regenerative Medicine

Nanotechnology is a fast developing field with a wide range of potential applications. Nanotechnology involves understanding and controlling material at the nanometer scale [1]. Improving lifestyles, an aging population, and ever-increasing expectations for a better quality of life demand better, more proficient and cost effective health care [2, 3]. Regenerative medicine is a multidisciplinary field with contributions from biology, chemistry, engineering, material science and medicine [4]. The use of nanotechnology in regenerative medicine holds much promise for the development of new treatment modalities when applied to major medical challenges [4, 5]. The application of nanotechnology in regenerative medicine may drastically change the treatment of diseases in the future [1]. Nanotechnology has a broad area of application in regenerative medicine, for example, in improving contrast imaging for bioimaging, in biosensors and chemical sensors, tissue scaffolds, and in drug-delivery [6, 7]. The use of polymers for controlled drug-delivery helps in sustained drug release and also increases the effectiveness of the drug [1]. Nanoparticles and nanotubes are seeing increased use for drug-delivery. Nanoparticles can circulate in the body and can be taken up by the cell through endocytosis. Nanoparticles can also be used for diagnostic purposes. There are, however, some obstacles in transforming current drug-delivery methods to nano-based

therapies, for example, targeting nanoparticles at a specific site without being captured by organs such as the liver and spleen [1].

In the last few decades, nanomedicines have started coming onto the market; for example, superparamagnetic nanoparticles are used in MRIs for increasing contrast during imaging [8, 9, 10]. Shortage of organs for organ transplantation may be overcome by regenerative medicine [11, 12]. Regenerative medicine can be used to repair, retain, or improve tissue and organ functions [1]. With the help of regenerative medicine, tissues can be regenerated to replace or restore defective tissue or organs [4, 14]. Regenerative medicine may be able to rejuvenate damaged tissues and organs by provoking previously irrevocable organs to repair themselves [14].

At the present time, regenerative medicine has seen the development of tissue and organs which can be grown in the lab and implanted when the body cannot repair itself [14]. With the help of material science, engineering, and biology, tissue engineering can be done using biomaterial and nanotechnology scaffolds created for tissue engineering designs [1]. Using cells and scaffolds, regeneration of tissues can be achieved. Here, the scaffold acts as a surface for cell proliferation [8, 4, 15]. Cell-surface interactions are very important as it determines the success or failure of the implant; so it is essential that the scaffold used produces the right signal to guide cell growth and tissue formation in a suitable manner [4, 16].

In this dissertation, we have focused on three different applications of regenerative medicine. Our first objective was to investigate an anodization technique to produce surface modified nanoporous titanium that can be used as a potential system for engineering a distinctive biomaterial. Our second objective was to fabricate a halloysite-PCL (polycaprolactone) scaffold and assess the cell supportive ability. The final objective

was to examine drug release from drug-loaded halloysite nanotubes, drug-loaded PCL scaffolds, and drug-loaded halloysite-PCL scaffolds.

1.2 Nanoparticles and Nanotubes for Regenerative Medicine

Nanotechnology is undergoing fast development, and new research is continuously published [1, 10]. Nano means "one billionth" (10^{-9}) and examples of nanoparticles include buckyballs, liquid crystals, liposomes, nanoshells, quantum dots and supramagnetic nanoparticles [17]. Carbon nanotubes and halloysite nanotubes are other examples of nanotubes [18]. A couple of examples of potential application of nanomaterials are biosensor and drug carriers [19]. Nanomaterials can be used as intracellular drug carriers and as biosensors to monitor the real time level of biomolecules, enzymes, and cell differentiation [20]. Present methods of judging cell treatment include invasive and/or destructive methods, for example, tissue biopsies. Thus, non-invasive methods are very advantageous. Examples of non-destructive nanoimaging probes include nanoshells and quantum dots (QD) [18, 21].

1.2.1 Nanoparticles

1.2.1.1 Quantum Dots

Quantum dots are colloidal nanocrystalline semiconductors [22, 23]. Properties of quantum dots depend on their size. Quantum dots can be used as fluorescent probes for labeling [23]. To examine the cell and the cellular process, fluorescence labeling is used. Conventional fluorescence labeling has some limitations for example including sensitivity to thermal changes in local environment, blinking, photobleaching and lower contrast. However, by using quantum dots that are colloidal metal particles, we can overcome these limitations [23, 24]. The fluorescence wavelength of quantum dots depends on the size of

quantum dots [24]. The quantum dot can be observed with high resolution compared to fluorophores by electron microscopy [23].

1.2.1.2 Nanoshells

Nanoshells are nanoparticles which consist of a dielectric core coated with a metallic layer [25]. Nanoshells are produced by layer-by-layer self-assembling and can be used in drug-delivery [25]. Nanoshells can be manufactured by a one-step or two-step approach [26]. This shell can be made up of oxides or metals, depending on intended use [27]. As nanoshells are porous, drug-loaded nanoshells can be used for the delivery of a specific drug at a targeted site. Targeted drug-delivery can be achieved by attaching antibodies to the outer surface so that the nanoshell-antibody complex can bind to the specific antigen in the body [26]. Nanoshells can be used for cancer therapy [26].

1.2.1.3 Liquid Crystals

Liquid crystal (LCs) is a photoswitch material. They have the ability to flow while displaying anisotropic properties. They have solid-like and liquid-like properties [28]. Liquid crystals are sensitive to temperature, magnetic and electric fields [29]. They can be used in targeted drug-delivery and topical applications [30]. In topical application, drug diffusion depends on the amount of free water, length of diffusion pathway and arrangement of structural elements [28].

1.2.1.4 Liposomes

Liposomal drug-delivery is a lipid-based drug-delivery for the treatment of cancer, inflammation and pain relief [31]. It helps in reducing the dose dependent toxicity [32]. With the help of liposomes, drugs can be released all over the body. There are some limitations with liposomes; one of them is that since lipids are natural products, the immune system targets them, releasing the drugs too early [31].

1.2.1.5 Superparamagnetic Nanoparticles

Superparamagnetic nanoparticles are commonly used in the MRI for increasing contrast for imaging inflammation, tumors and degenerative diseases [33]. They can also be used for targeted drug-delivery and gene transfection. Iron oxides are most frequently used as core particles of superparamagnetic nanoparticles [33]. Endorem is an example of a superparamagnetic nanoparticle available in the market as a contrast agent for spleen and liver disease detection. Lumirem is an example of a superparamagnetic nanoparticle available in the market for detection of gastro-intestinal tract imagining [34].

1.2.2   Nanotubes

1.2.2.1 Carbon Nanotubes

Carbon nanotubes are made from a graphite sheet. There are two types of carbon nanotubes, single wall nanotubes (SWNTs) and multiwall nanotubes (MWNTs) [35]. Carbon nanotubes are made by chemical vapor deposition, laser ablation of carbon, and carbon-arc discharge [35]. There are many applications of carbon nanotubes, for example, cells tracking, bio-sensing, drug-delivery, chemical sensing, and many more [35, 36, 37]. The price of carbon nanotubes depends on the quality and method of production. The price of single wall carbon nanotubes is 50 to 100 times more than gold [38].

1.2.2.2 Halloysites

Halloysite nanotubes (HNTs) are natural nanotubes, very inexpensive and available in large quantities. Carbon nanotubes cost approximately \$500 per gram while halloysite nanotubes cost approximately \$500 per ton [39]. As halloysites have larger surface areas, they can be used for drug-loading. Drugs of a smaller molecular size will be trapped within the inner lumen of the halloysites, and drugs of a larger molecular size attach to the outer surface of halloysites [40]. Other potential applications of halloysites

include antifouling paint, fragrance, slow-release perfume, anti-scalants, pesticides, pest repellents, slow release of cosmetics, in electronic industry and radiofrequency shielding [39]. Thus, large surface area and low cost make halloysites superior compared to all other nanoparticles and nanotubes.

1.2.3 Nanomodified Surfaces

Surface properties of the scaffolds are very important as cell-surface interactions are dependent on the surface property of the scaffold. Cell-surface interactions impel protein adsorption and, finally, lead to cellular interaction [41, 42]. Protein adsorption relies upon the structure of the protein and the surface property [41]. Scaffolds used in tissue engineering should resemble natural, extra-cellular matrices (ECM) to increase implant biocompatibility [43]. Important surface properties of scaffolds to consider include surface roughness, chemistry, hydrophilicity, and hydrophobicity. Natural bone consists of organic compounds strengthened with inorganic compounds [44]. Collagen fibers are the major structure seen at nano-scale in the bone. Ninety percent of organic compound is collagen and the rest is noncollageneous protein and ground substances [44]. Thus if the scaffold has nanopores or nanofibers at the surface, it will resemble natural extra cellular matrix. According to some studies, adsorption of particular proteins increases subsequent cell adhesion to the material surface, for example, fibronectin. Calcium phosphate crystals (CaP) are the key feature determining Osseo-integration to surrounding bone tissue [45]. Growth factors mediate the differentiation of osteoblasts from immature, non-calcium depositing cells to mature calcium depositing cells [46].

They are many types of scaffolds. They can be mainly subdivided in two types: bio-resorbable and non-bio-resorbable. Scaffolds such as Poly(ε-caprolactone)(PCL), poly(d,l-lactide) PLA, Poly(lactide-co-glycolide) PLGA are all examples of FDA

approved bio-resorbable polymers, and titanium is an example of a non bio-resorbable scaffold [43].

The electrospinning technique is used for fabrication of the polymeric electrospun scaffold. This technique also allows the incorporation of nanoparticles, enzymes, proteins and chromophores directly during the preparation process. The application of these biohybrid nanosystems is extremely wide and includes drug-delivery, catalysis, and biosensors [47]. Titanium has good elastic modulus and mechanical properties similar to that of natural bone under a load bearing condition [44, 48]. Smooth titanium is a not sufficient bioactive to form a direct bonding with bone, which leads to implant failure. Therefore surface modification should be done to create porous material by sand blasting or plasma spraying techniques [49]. With the help of plasma spraying, hydroxypatite (HA) or other calcium phosphates can be used for coating titanium. These coatings have long term failures due to weak adhesion to the metal substrate and dissolution once implanted [44, 49]. These problems can be overcome by the anodization process by which we can produce micro and/or nanopores on the surface of the titanium implant which helps in biological fixation to the surrounding tissue through bone tissue.

1.3 Tissue Engineering in Dentistry and Orthopedics

Tissue engineering is based on materials science and biocompatibility. It incorporates cells, natural or synthetic scaffolds to create new tissues [50]. This field is increasingly being viewed as having enormous clinical potential. At present, the treatment of lost or deficient tissues includes prosthetic materials, drug therapies, and tissue and organ transplantation [51]. Nevertheless, all of these treatments have some type of limitations, for example, the failure of synthetic prostheses to replace any of the

simplest structural functions of a tissue. Each year, many patients are registered on transplantation waiting lists [52]. These problems have motivated the development of tissue engineering. Tissue engineering will have a significant effect on dental and orthopedic practice in the future, in the repair and replacement of mineralized tissues, support of oral wound healing and the use of gene transfer [51].

In the United States each year, over half a million people undergo total joint replacement [53]. The average lifespan of a reconstructive joint implant is approximately 15 years [54]. In all likelihood, this limitation means that each patient will have to undergo a second surgery to maintain functionality [54]. There are many drawbacks with replacement surgeries such as inferior recovery compared to the initial surgery, postsurgical complications and pain. The most common explanation for the implant failure is improper growth on the implant surface [44]. Currently, vanadium, cobalt, chromium and smooth titanium are used in dental and orthopedic implants [44]. Out of all these metals, titanium is most frequently used due to its tensile strength and corrosion resistance [55, 56, 57]. However, the problem with titanium implants is that they does not mimic the natural bone structure, so there is a higher chance of implant failure [58]. Natural bone is nanoporous at the surface [44]. Therefore, if we modify the surface of titanium such that it becomes nanoporous, these changes may help in increasing the life span of the implant. One of the objectives is to produce nanoporous titanium by the process of anodization.

1.4 Nanotechnology in Drug Release

Controlled drug-delivery is one of the most promising biomedical applications of nanotechnology. The use of nanomaterials as nanocarriers for improving delivery

methods has shown to be advantageous technically and viable economically [59]. The present generation of drugs is given systemically. Some of the harmful effects and problems of systemic drug-delivery include drug solubility, metabolism and excretion of drugs, trouble in maintaining drug concentrations and toxicity to non-target tissues [60]. Use of nanotechnology in drug-delivery methods may diminish current problems in drug-delivery [60]. Carbon nanotubes, halloysite nanotubes, superparamagnetic nanoparticles, liposomes and nanoshells can be used for targeted drug-delivery [61]. Drugs can be encapsulated in any of these nanoparticles and nanotubes, and used for drug-delivery [62]. This encapsulation protects drugs from metabolism or excretion [63]. This system can also be used in an internal and external signal triggered release. Examples of external signals include magnetic field, ultrasound, infrared light and radiofrequency; pH is an example of an internal signal [64].

Controlled release of antibiotics and antiseptic drugs from halloysite PCL scaffolds can be used for wound healing. The basic concept of healing in any tissue type (for example bone or skin) is the same. The second objective of this project is to electrospin a halloysite-PCL scaffold, to find the best concentration and the exact location of the halloysite in the halloysite-PCL scaffold by Fluorescein isothiocyanate (FITC) labeling of the halloysite and to check its biocompatibility. The third objective of this project is to check the drug released from drug-loaded halloysites, PCL scaffolds and halloysite-PCL scaffolds.

1.5   Project Objectives

1. To find out the best parameter of anodization to produce nanoporous titanium. Compare osteoblast cell proliferation and differentiation on smooth versus nanoporous

titanium surfaces. Nanoporous surfaces should lead to better cell proliferation and differentiation leading to enhanced implant durability and osteointegration for patients with degenerative joint problems, as the surfaces are similar to natural bone surface.

2. To electro-spin the halloysite-PCL scaffold and find the best concentration and the exact location of the halloysite in the halloysite-PCL scaffold by Fluorescein isothiocyanate (FITC) labeling of the halloysite, compare osteoblast cell proliferation and differentiation on PCL and halloysite-PCL scaffolds.

3. To load halloysite nanotubes with drugs, for example antibiotics and antiseptic, measure the drug released from the halloysites, PCL scaffolds and halloysite-PCL scaffolds.

CHAPTER 2

NANOFABRICATION FOR TISSUE ENGINEERING AND REGENERATIVE MEDICINE

This chapter describes the major topics of this dissertation. Nanofabrication of scaffolds can be done using many varied techniques [65]. These techniques can create unordered or ordered surfaces. Colloidal lithography, chemical etching, anodization, polymer demixing and electrospinning are example of nanofabrication technique that create unordered features [65, 66]. Photolithography and electron beam lithography are examples of nanofabrication techniques that create ordered features [65, 66]. Nanomodified surfaces resemble the nanoscale features presented to cells by extracellular matrix proteins. Collagen is major extracellular matrix proteins; it has a specific nanotopography that supports cell attachment, differentiation and functionality [66].

Tissue engineering has emerged as potentially superior therapeutic option in the field of regenerative medicine. Tissue engineering includes the use of cells and biomolecules in artificial or natural materials which can replace body functions that have been lost or damaged due to disease or accidents [12, 8]. Tissue engineering uses scaffold-guided tissue regeneration [67]. This process includes the seeding of scaffolds with cells which then differentiate and produce tissue mimicking natural tissues [68]. Once tissue engineered constructs are ready, they are implanted into the patient to replace unhealthy or injured tissues [68]. As time passes, host tissues invade the scaffold with blood vessels

11

and nerves, and with the scaffold degraded over time. Examples of successfully tissue engineered tissues include cartilage, bone and skin for autologous implantation [4, 69]. There are some implants which are not biodegradable, for example, titanium. Successful clinical use of resorbable, non-resorbable, bioinert and bioactive implants will significantly advance medical needs [70, 71, 72].

In this study, we used two different types of scaffolds: anodized titanium and halloysite-PCL scaffolds. Anodized titanium can be used in orthopaedic and dental implants. Halloysite-PCL scaffold may have use in drug-delivery, wound healing and tissue engineering applications.

2.1 Titanium Implants

Titanium implants are used in dental and orthopedic application [73]. It is difficult to produce properties of bone in synthetic implants [74]. These synthetic implants do not give satisfactory results. The average life of a knee, hip or ankle implant is 10 to 15 years [75]. Accordingly, patients need to undergo repeated implant surgery. The reason for implant failure is, that implants are unable to produce a sufficiently strong cellular response and so integrate the implant into surrounding tissue [76]. In this study, we examined if nanoporous titanium, manufactured by anodization, can be used to support cell attachment and functionality. Nanoporous titanium has a unique property due to nanopores that cover its surface; these nanopores provide improved magnetic, electrical properties and better structural integrity, leading to a better cellular response [76, 77, 78].

2.1.1 Anodization of Titanium

Titanium has corrosion resistant properties due to its titanium oxide layer [79]. This layer is formed automatically when titanium is exposed to the air [80]. Still, this

layer is not reactive enough, so it is unable to form a direct bond with the bone [81]. Due to this insufficient osseointegration, implant life is very short. Anodization should to improve surface properties creating a nanoporous surface similar to natural bone [82]. An oxide layer forms on the anode surface, when a constant voltage is applied between the anode and cathode [83]. The chemical reactions for anodizing titanium are described below. Figure 2.1 shows anodization set-up. Figure 2.2 shows smooth titanium used in the anodization.

Chemical reaction at Ti and Ti oxide interface:

$$Ti \leftrightarrow Ti^{2+} + 2e^-$$
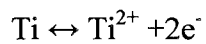
Chemical reaction at Ti oxide and electrolyte interface:

$$2H_2O \leftrightarrow 2O^{2-} + 4H^+$$
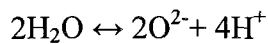
Chemical reaction at both interfaces:

$$Ti^{2+} + 2O^{2-} \leftrightarrow TiO_2 + 2e^-$$
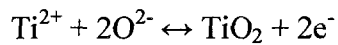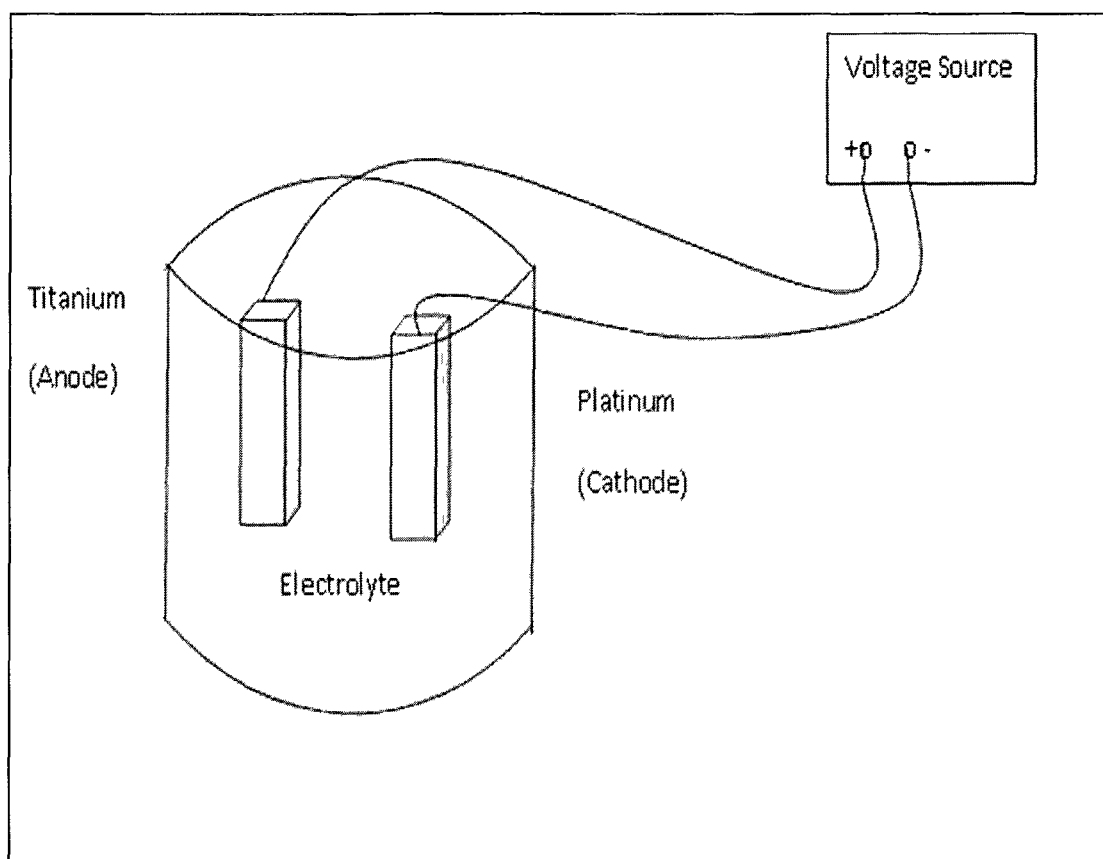
Figure 2.1 Anodization Set-Up [84].
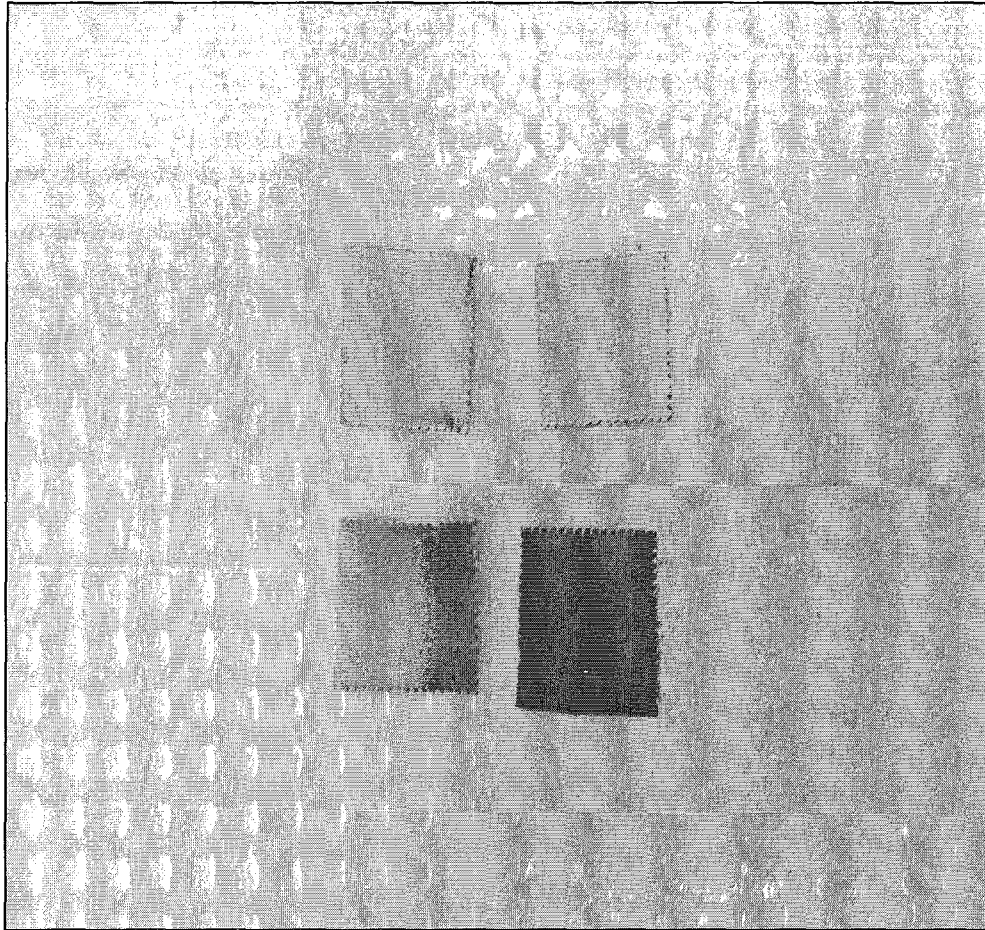
Figure 2.2 Smooth Titanium (0.5in × 0.5in).

As titanium oxide has more resistance compared to the electrolyte and the metallic substrate, the voltage will drop over the titanium oxide film on the anode [83]. Provided the voltage applied is sufficiently strong to drive the ion conduction through the oxide layer, the oxide film will keep on growing. Thus, the final oxide film thickness is almost linearly dependent on the applied voltage [83]. Anodization of titanium can be done with different chemicals, for example, in H_2SO_4/HF solutions, phosphate electrolytes, chloride-ion-containing media, acid/ethanol mixture [85, 86, 87, 88].

2.1.1.1 Effects of Processing Parameters

After the anodization process, morphology, chemistry and roughness of oxide film formed differ depending on the processing parameter used. These processing parameters are current density, voltage, pH, electrolyte composition, time and temperature [44]. Different types of acids, alkaline solutions and neutral salts are used as electrolytes for the anodization process. Commonly, it was observed that compared to all the electrolytes the titanium oxide layer thickness in H_2SO_4 was the highest [44]. In this study, therefore we have used H_2SO_4 and HF as electrolytes.

2.1.1.2 Anodized Oxide Film

Properties of anodic oxide films include surface roughness and porous texture. After anodization, the thickness of the protective oxide layer increases and it could lead to less ion release in the human body. The oxide barrier layer is considered to contribute to the improvement of corrosion resistance [89]. Structure and properties of anodic oxide films depends on the processing parameters [90].

2.1.2 Chemical Properties

Currently, many different implant materials are under investigation including titanium, ceramics, polymers, and biologically synthesized substances. Compared to all material, titanium is the best material because it is more biocompatible, durable and corrosion resistante [79]. Still, according to previous studies, metal such as smooth titanium, failed to produce proper osseointegration [78]. Accordingly, in this study we modified the surface of smooth titanium to obtain a surface that would promote osseointegration.

2.1.3 Need for Long Lasting and Better Quality Implants

Current implants do not help in changing bone mass that occurred due to osteoporosis and fractures. The average life of these implants is 10 to 15 years [75]. The lifetime of the implant is very short for infants and young people. Bone implants replace missing bone and provide surface where bone and a vascular network can be regenerated and better osseointegration can occur [91]. Once the implant is implanted at the injured site, protein from blood, bone marrow and other tissues, for example, fibronectin and vitronectin, starts adhering to the implant surface [92]. These proteins then control subsequent cell adhering. Protein bound to the implant surface osteoblast cells then binds to the implants. Thus, it is very important to have a proper surface where initial protein adsorption occurs [93]. Here, chemical and physical properties of the implant's surface determine the initial adsorption of the protein. So the goal is to produce implants with such chemical and topographic properties that may have the potential to solve current problems in orthopedic and dental implants [76, 77, 78].

2.1.4 Osteoporosis and Implants

Osteoporosis is a bone disorder resulting in reduced bone density and bone strength [94]. Osteoporosis can be asymptomatic. Symptoms and problems of osteoporosis include fractures, pain, and deformity [94]. Osteoporosis is usually found in the aged population, especially women, who are very prone to this disorder. Implants that provide better structural integrity by providing quicker and better cellular response are very useful for repairing a fracture in osteoporosis patients [76, 78]. Anodized titanium may prove useful in generating faster and better cellular response in osteoporosis and aged people.

2.2 Electrospinning Halloysite-PCL Scaffolds

Scaffolds of microscale and nanoscale polymer fibers can be fabricated by placing a polymer solution to an electric field [96]. This technique is known as "electrospinning." The electrospinning set-up is shown in Figure 2.3. The electrospining set-up consists of a syringe pump, a high voltage source and a collector [97]. Surface tension holds a polymer solution at the tip of the needle. Higher voltage in the needle causes induction of charges in the polymer solution. The polymer jet is formed when the charge repulsion within the solution overcomes the surface tension [98, 99, 100]. Fluid jet experience instability when jet leaves the tip of the needle. This results in the bending of the fluid jet due to applied electric field [101]. During the polymer jet travel path, the evaporation of the solvent occurs, and the fibers are collected on a collector plate. Solutions with higher conductivity have more tendencies for jet formation [102, 103, 104]. In this study, we are trying to electrospin halloysite-PCL composite scaffolds and drug-loaded halloysite-PCL scaffolds.
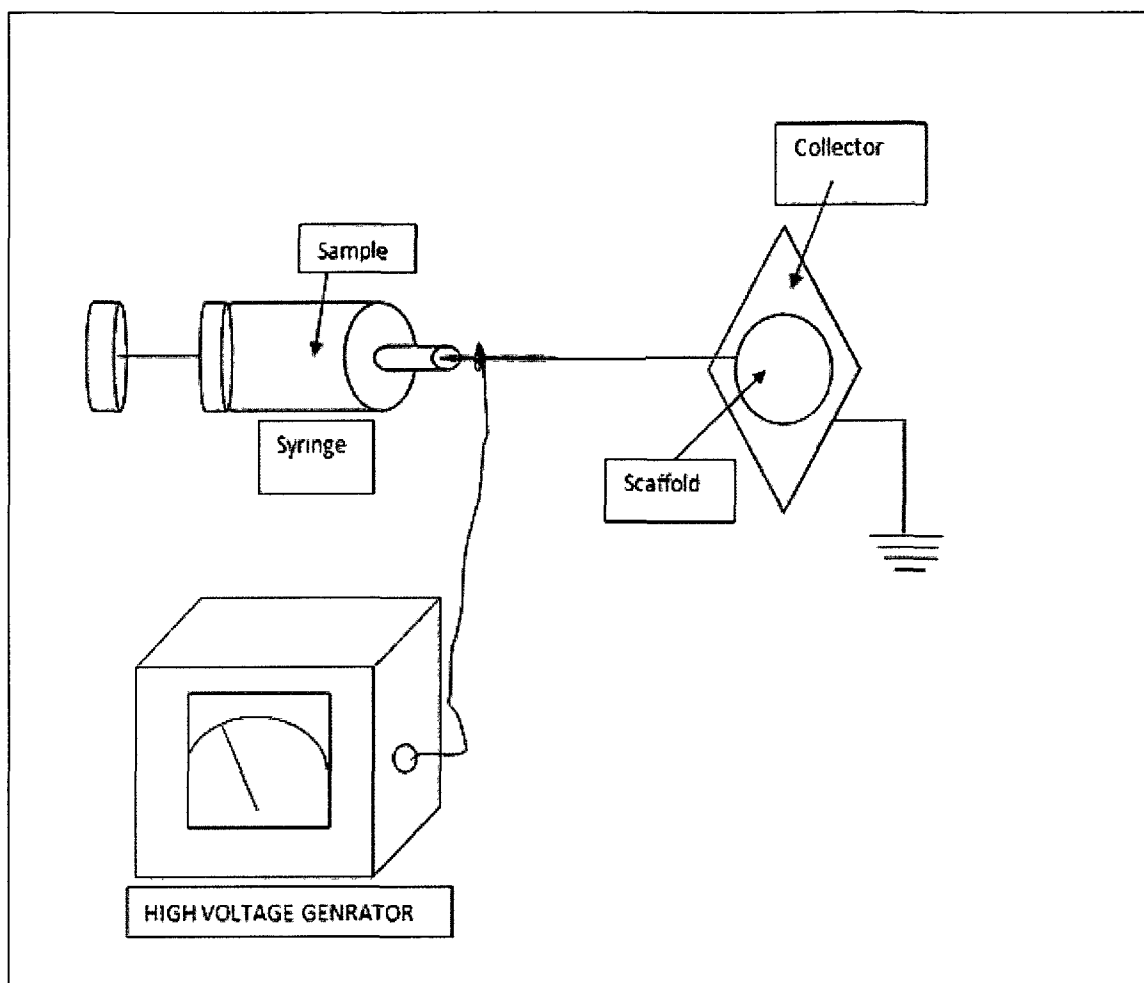
Figure 2.3 Electrospinning Set-Up [95].

There are different parameters which can affect the diameter of the electrospun fiber including distance between needle tip and the collection screen, the rate of the syring pump, voltage applied and solution parameters [105]. Solution parameters include weight percent of polymer, weight percent of solvent, molecular weight of polymer, viscosity and surface tension [105]. There are some other parameters which have some effect on fiber morphology; these parameters includes includes air-flow, humidity and temperature [105].

2.3   Drug-Delivery

Drug-delivery, is one of the promises of nanotechnology. The use of nanomaterials as nanocarriers for improving the delivery methods has been advantageous technically and viable economically. These nanocarriers, formed by the process of nanoencapsulation, are of two types: nanospheres and nanocapsules [106]. Halloysite is an example of nanocapsules.

2.3.1 Halloysite

Halloysite is a naturally occurring nanotubular clay particle [107]. It is mined from natural deposits in different countries. Utah has the biggest halloysites deposit in the USA [108]. Halloysite is a two-layered aluminosilicate [109]. It has an empty tubular structure. Halloysite is chemically analogous to kaolinite [110, 111, 112, 113, 114]. Hydrothermal processe convert kaolinite to halloysites [115]. This process takes more than millions of years. The strain caused due to lattice mismatch between adjacent silicone dioxide and aluminum oxide layers cause them to become are rolled into nanotubes [110, 111, 112, 114]. Figures 2.4 and 2.5 show SEM images of halloysite. Figure 2.6 shows TEM image of halloysites.
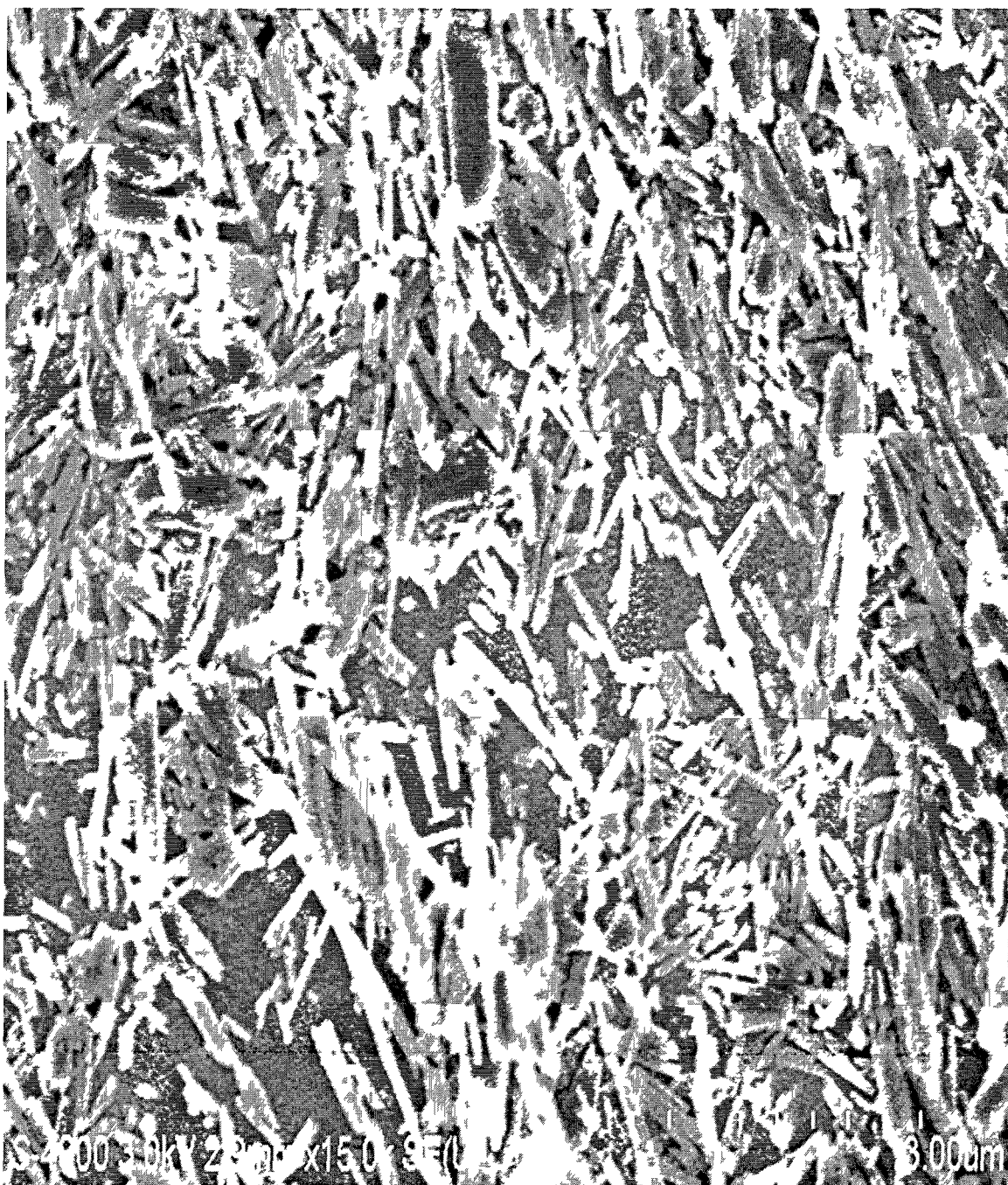
Figure 2.4 SEM Image of Halloysites.
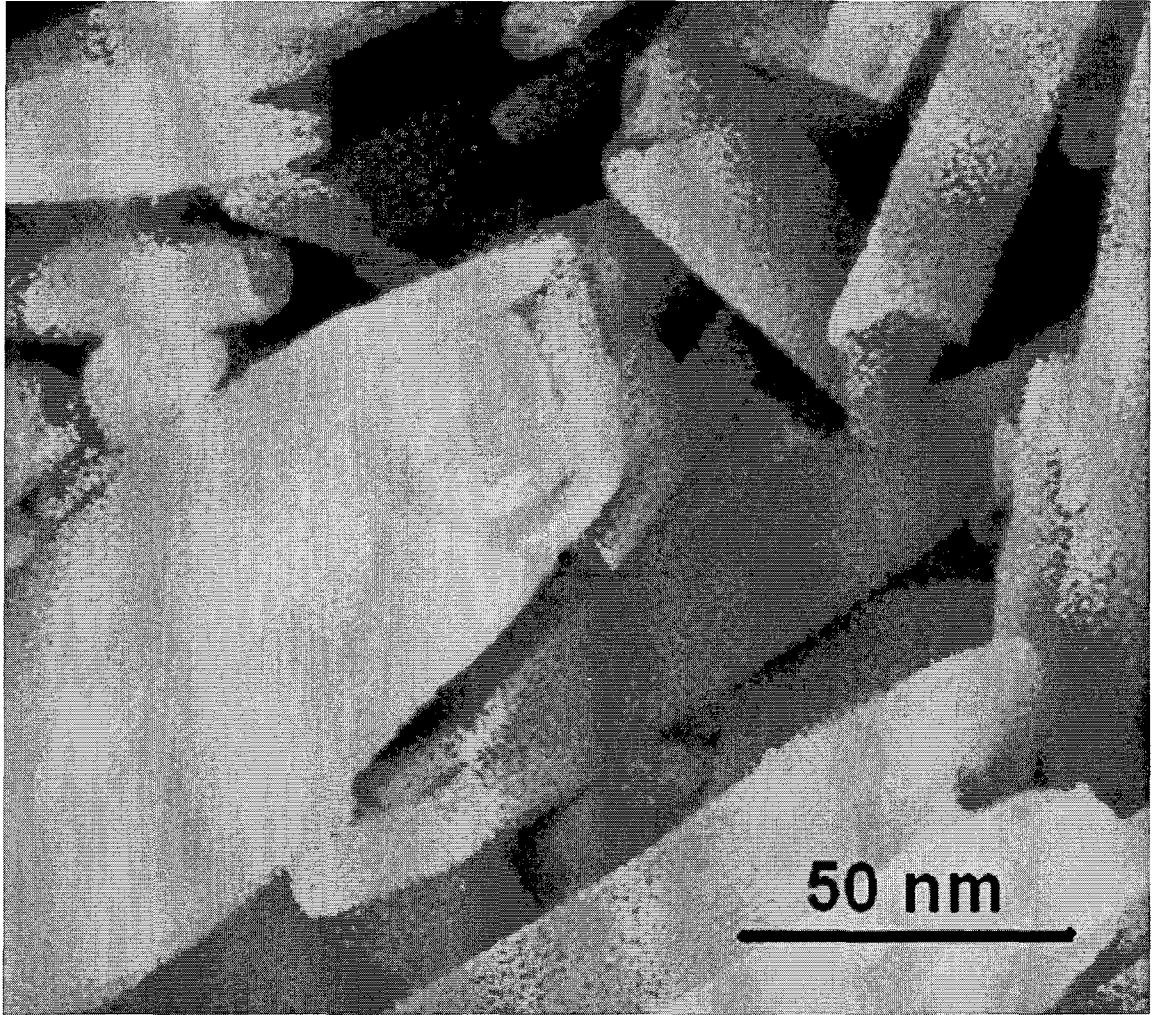
Figure 2.5 SEM Image of Halloysites.
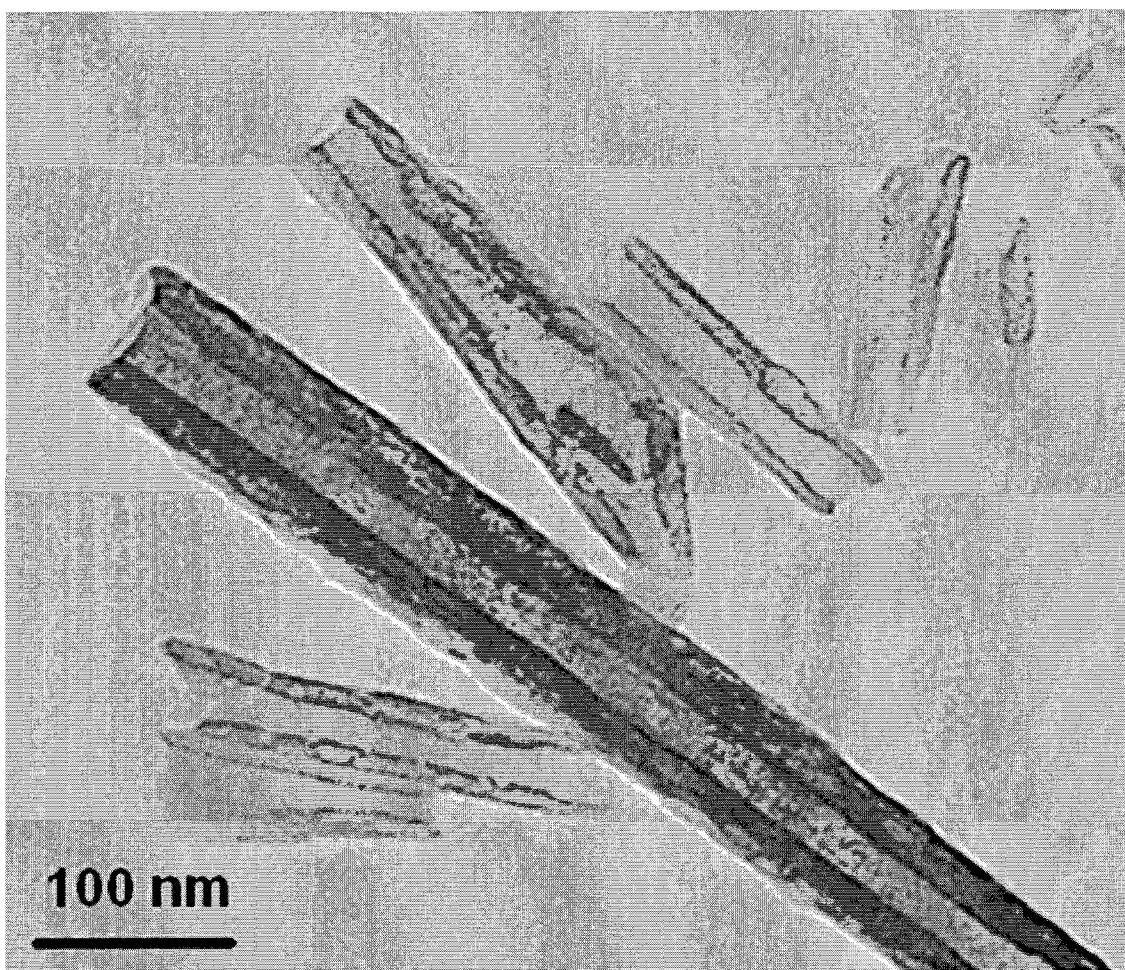
Figure 2.6 TEM Image of Halloysites.

2.3.2 Structure and Chemical Constitution of Halloysite

Halloysite occurs as a hydrated mineral; it contains H_2O in the interlayer.

Hydrated halloysites are represented as halloysite (10 Å). Heating hydrated halloysite (10

Å) converts it to dehydrated halloysite (7 Å) [116]. The chemical formula of halloysite

is $Al_2Si_2O_5(OH)_4.2H_2O$. The chemical formula is alike to kaolinite, except the

existence of an extra water monolayer between the adjacent layers [117]. Figures 2.4 -

2.6 show the halloysite nanotubes. The outside diameters of the halloysite vary from 50 to

70 nm [118]. The average inner diameter is 15 nm [118]. The lengths of halloysite vary

from 1 to 1.5 μm [118]. The morphology of halloysite nanotubes vary depending on chemical composition, crystal structure and effect of dehydration [119].

2.3.3 Physical and Chemical Properties of Halloysite

Halloysites have large specific surface areas [120]. According to a study done by Churchman et al., small halloysite particles (in terms of width) were plentiful with fine cylindrical pores, whereas larger halloysites (in terms of width) had very few pores [121]. Due to this reason, the halloysites are able to absorb a fairly large class of compounds. This absorption includes drugs, biologically active agents and anticorrosion agents [108]. If suitable pre-treatment of halloysite is done, then both hydrophilic and hydrophobic compounds can be entrapped in halloysites [112]. The loading of small molecules occur by intercalation of small molecules into their interlayer space [122, 123, 124] whereas, larger molecules (proteins) binds to outer face. Intercalation does not take place with bigger molecules because of their large molecular size [111, 125]. Halloysites can be used as a enzymatic nano-reactor [108]. Different metals (iron, copper etc.) can be used to form conductive and paramagnetic coating on halloysites [108]. The inner surface of halloysite is similar to alumina and the outer surface of the halloysite is similar to silica. When pH is below 8.5, halloysites have inner surface positively charged and outer surface negatively charged. This helps in loading negatively charge molecules in inner lumen of halloysites. Surface charges are pH-dependent [110, 40]. The capillary force facilitates adsorption of several materials. The capillary force is calculated by, $h = (2\gamma \cos\theta) / (\rho g r)$ [126]. Here ρ is density of liquid, r is radius of halloysite and g is acceleration due to gravity. For a water-filled tube in air at sea level, $h = (1.4 \times 10^{-5})/r$. Halloysite has average inner radius of 7nm, so the capillary force this halloysite in terms of the height of the water column is $h - 2000^{in}$. Thus, halloysites have higher

capillary forces so they can quickly adsorb numerous materials [126]. These drug-loaded

halloysites can be added to PCL-chloroform mixture and drug-loaded halloysite-PCL

scaffold can be prepared and may potentially be used as drug-loaded bandage.

CHAPTER 3

METHODS AND INSTRUMENTATION FOR EXPERIMENTATION AND ANALYSIS

This chapter describes the instruments and methods used in these projects.

3.1   Instruments

Current research involves many different instruments; different instruments were used in this project according to need. The anodization set-up was used for anodizing titanium at room temperature. The electrospinning set-up was used for spinning PCL scaffolds, Halloysite-PCL scaffolds, drug-loaded PCL scaffolds, drug-loaded halloysite-PCL scaffolds and FITC labeled halloysite-PCL scaffolds. The scanning electron microscope (SEM) was used for observing surface modification on titanium after the anodization process and fiber organization in PCL scaffolds and halloysite-PCL scaffolds after electrospinning. An epifluorescence microscope was used to observe the location of FITC labeled halloysites in a halloysite-PCL scaffold. A benchtop vacuum station was used for loading drugs into the halloysites. Ultraviolet visible (UV-Vis) spectroscopy was used to measure the different drugs released from the halloysites, drug-loaded PCL scaffold and drug-loaded halloysite PCL scaffolds. A visible spectrophotometer was used for Coomassie plus protein assay and alizarin red staining.

3.1.1 Anodization Set-Up

Figure 3.1 shows the anodization set-up used in this project. The anodization technique has been used widely for different metals, for example, aluminum, titanium, zinc and magnesium [127]. Anodization is an electrochemical conversion process and increases the oxide layer on the metal surface [128]. As the part to be treated is kept at anode, this process is known as "anodization". This process increases the wear resistance and the corrosion resistance [129]. Anodization changes the surface texture of the metal This process can be performed in a variety of chemical solutions; chromic acid, oxalic acid, phosphoric acid, sulfuric acid, boric acid and organic acids [129, 130, 131]. In this study, sulfuric acid and hydrofluoric acid were used for the anodization of titanium.
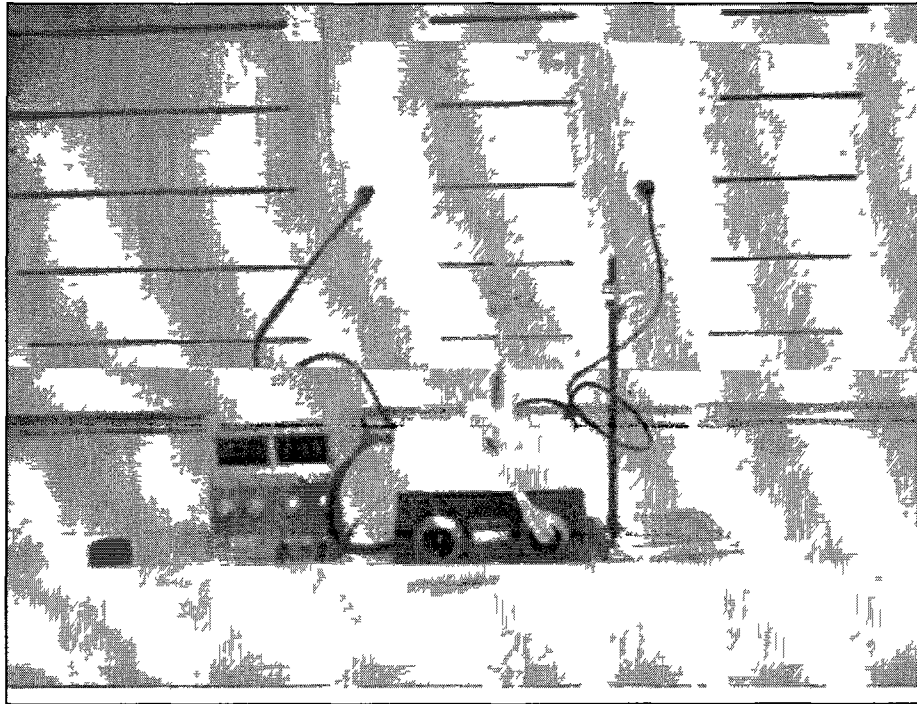
Figure 3.1 Anodization Set-Up (Located at IFM).

3.1.2   Scanning Electron Microscope

Figure 3.2 shows the scanning electron microscope (SEM) used in this project. The scanning electron microscope is a type of electron microscope which uses an electron beam as an alternative of light to form an image [132, 133]. An electron gun produces a beam of electrons at the top of the microscope. The electron beam passes through electromagnetic fields and lenses. These electromagnetic fields and lenses focus the electron beam on the sample. As soon as the electron beam strikes the sample, X-rays and electrons are expelled from the sample. A detector collects and converts all secondary electrons, backscattered electrons, and X-rays into a signal. These signals are then sent to a screen to produces the image [134, 135, 132]. The signals that are received from the electron-sample interactions disclose information about the sample including structure, composition, morphology and arrangement of materials making up the sample [132, 133]. SEM has developed new areas of study in the science communities. As the SEM uses electromagnets instead of lenses, the researcher has more control over the level of magnification. Besides these benefits, the outstandingly clear images make the SEM one of the most helpful instruments for research [136, 132]. In this study, SEM was used for observing surface modification on the titanium after the anodization process. It was also used for observing fiber and halloysite organization in PCL and halloysite-PCL scaffolds.
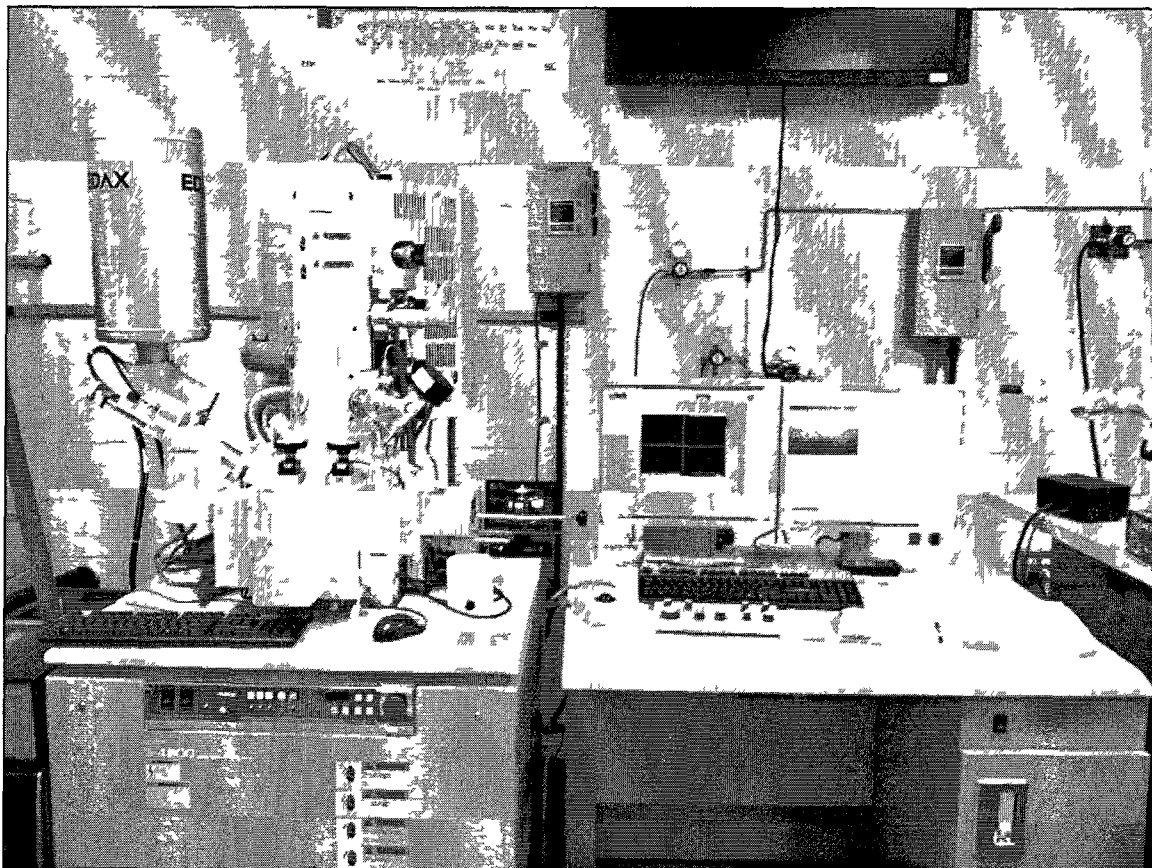
Figure 3.2 Scanning Electron Microscope (Located at IFM).

3.1.3 Electrospinning Set-Up

Figure 3.3 shows the complete electrospinning set-up. Electrostatic forces are used in the electrospinning set-up for the production of polymer fibers [137]. Process of spinning fibers using electrospinning set-up is known as "electrospinning process". In this process, a jet of polymer solution is created by applying voltage. In electrospinning set-up, one electrode is attached to syringe containing spinning solution, and the other electrode is attached to a collector. When the strength of the applied electric field is increased, the solution at the tip of needle elongates to form a Taylor cone (conical shape) [137]. When a significant electric field is achieved, the repulsive force overcomes the surface tension and the jet of solution formed from the Taylor cone. During travel,

solvent evaporates from the polymer jet and polymer fiber is formed; these fibers are arranged randomly on collector plate (metal screen) [138, 139, 140]. In the current research, an aluminum screen is used as a collector plate Figure 3.4 shows a syringe pump and syringe. Figure 3.5 shows a collector plate, and Figure 3.6 shows a high voltage electricity source.
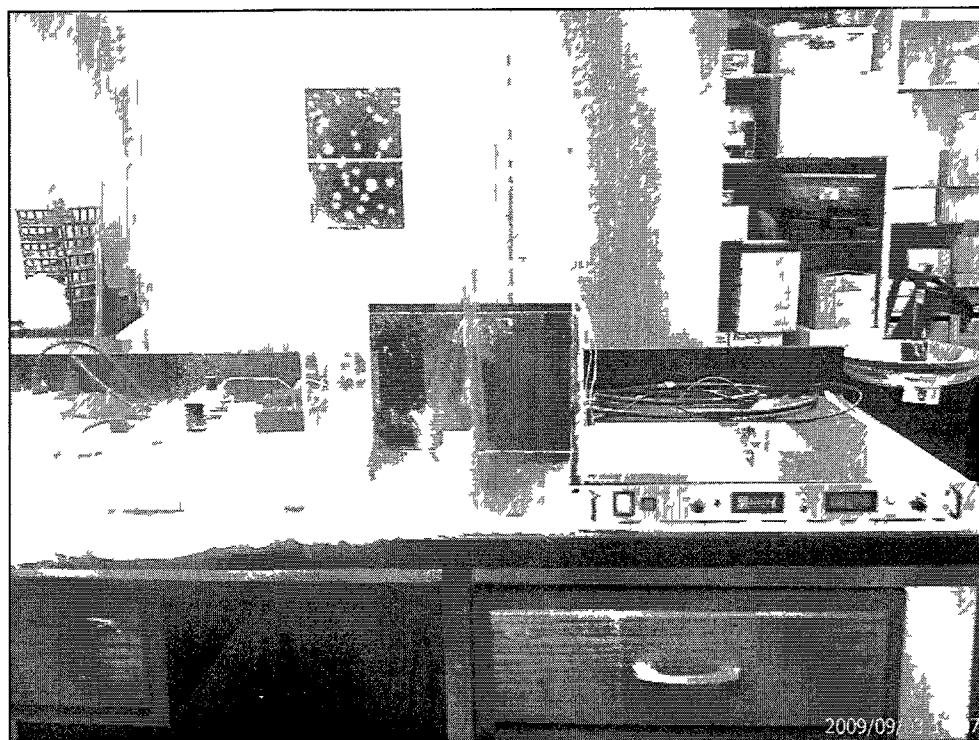
Figure 3.3 Electrospinning Set-Up (Located at CTH).
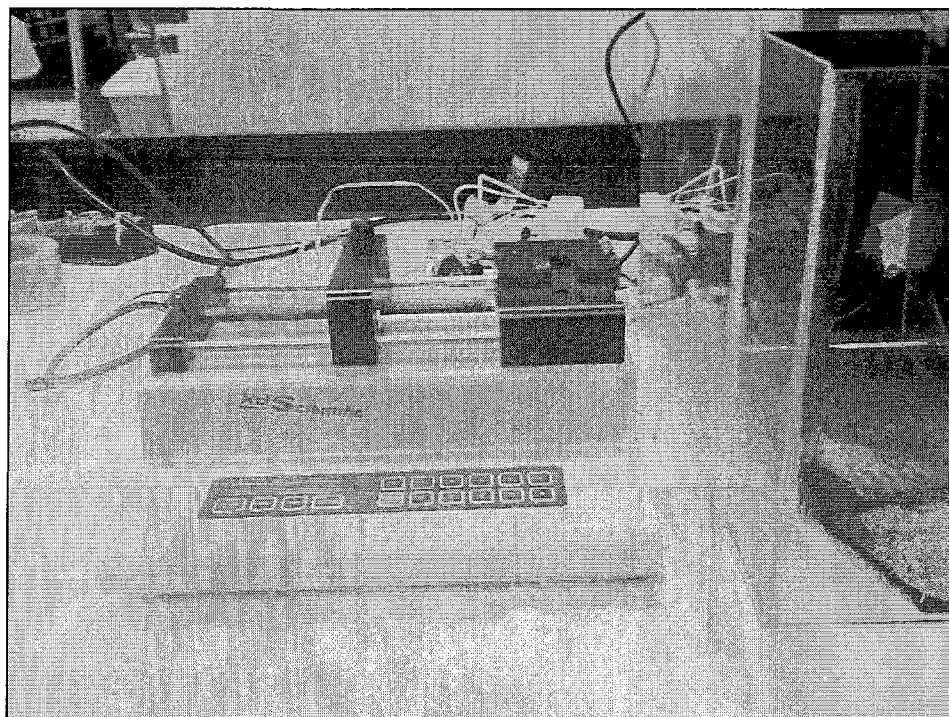
Figure 3.4 Syringe Pump and Syringe (Located at CTH).
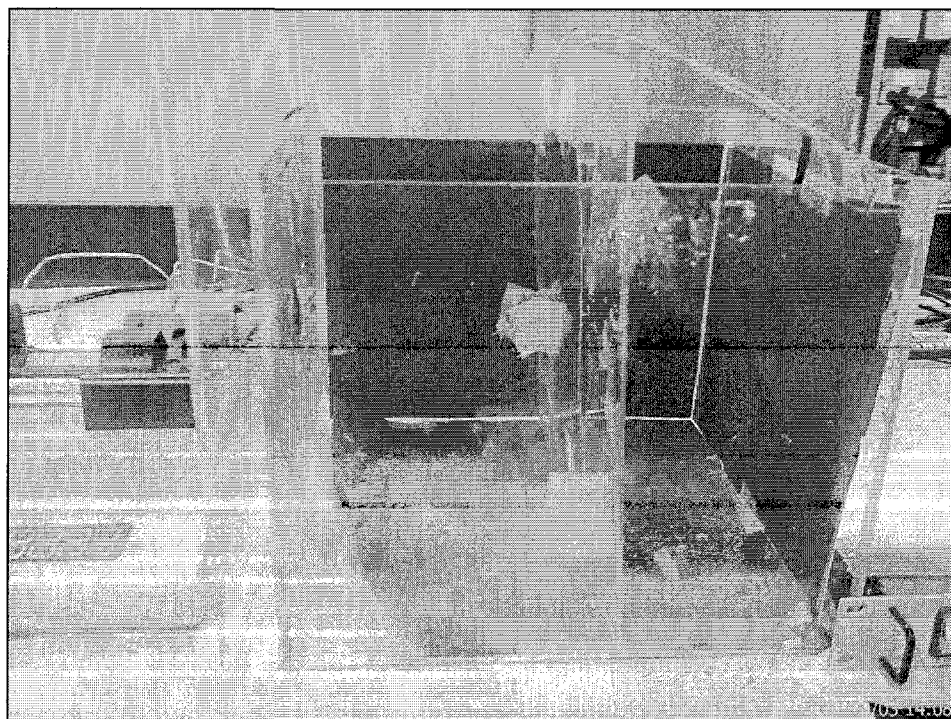
Figure 3.5 Collector Plate (Located at CTH).

Figure 3.6 High Voltage Electricity Source (Located at CTH).

With the help of the electrospinning process, we can make fibers with diameters ranging from a few micrometers to a nanometer [141, 142, 143]. Fibers produced by this process have a larger surface area per unit mass. Thus, a scaffold collected on a collector plate can be used for many different applications: tissue engineering scaffolds, filtration of submicron particles and wound dressing band aid [140]. In this study, electrospinning was used to spin PCL scaffolds, halloysite-PCL scaffolds, drug-loaded halloysite-PCL scaffolds and FITC labeled halloysite-PCL scaffolds.

3.1.4 Epifluorescence Microscope

Figure 3.7 shows the epifluorescence microscope used in this project. Epifluorescence is an optical arrangement used in a fluorescence microscope. In this set-up, light is focused on the sample and collected from the sample by objective lens [144, 145]. As separate lens are used in transmitted fluorescence microscope to focus UV light on the sample, the epifluorescence microscope is more efficient compared to transmitted fluorescence [146]. In the epifluorescence microscope, both the excitation and emission light pass through the objective lens. Thus, in epifluorescence, an important aspect is separation of the excitation light from the emission light coming from the sample [145]. In this type of microscope, the UV light strikes on a dichroic mirror. This mirror returns one range of wavelengths and lets another range of wavelength to pass through. Here, the mirror returns the UV light to the specimen, which excites fluorescence within the sample. The objective lens collects the fluorescent light produced by the sample, and this light then goes to the dichroic mirror and a filter. Here, wavelengths other than fluorescent are eliminated, so only fluorescent light travels to the eyepiece [147, 145]. In this project, an epiflurescence microscope was used for finding the location of FITC labeled halloysites in halloysite-PCL scaffolds.
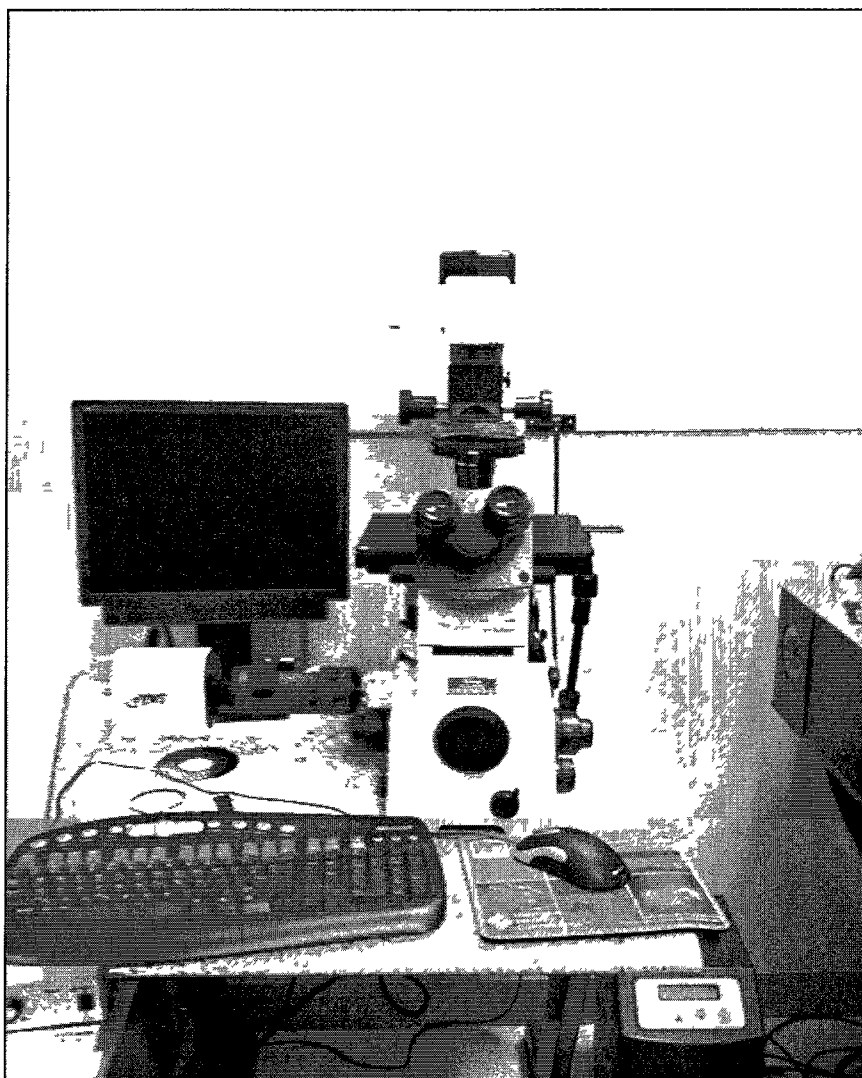
Figure 3.7 Epifluorescence Microscope (Located at IFM).

3.1.5 Benchtop Vacuum Station

Figure 3.8 shows the benchtop vacuum pump used in the current study. It creates a vacuum in the chamber by removing air from the chamber. It is used for drug-loading in the halloysites. Halloysites are mixed with a drug solution and kept in the chamber; when the vacuum pump starts, it removes the air from the halloysites and loads the drug into the halloysites.
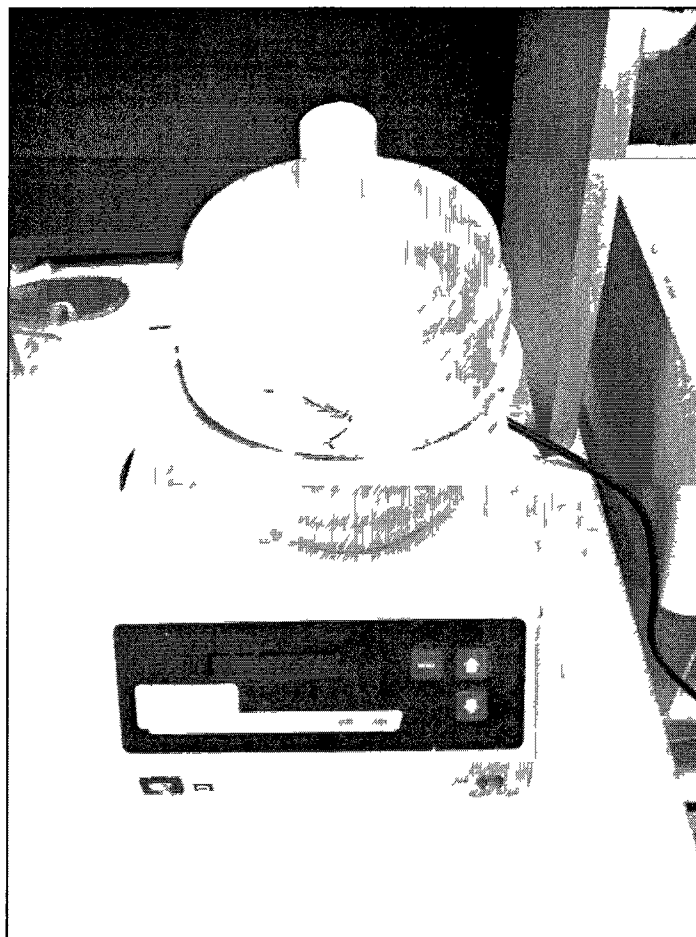
Figure 3.8 Vacuum Pump (Located at IFM).

3.1.6 Ultraviolet Visible Spectroscopy

Figure 3.9 shows the ultraviolet-visible (UV-Vis) spectrophotometer used in this project. The ultraviolet-visible spectrophotometer is used for examine samples in the visible and ultraviolet regions of the electromagnetic spectrum [148]. In UV-Vis spectroscopy, the wavelength and maximum absorbance of compounds are determined by examining electronic transitions. Concentration or molar absorbance of a sample can be determined by beer's law if the molar extinction coefficient is known or the molar absorptivity of sample is known [149, 150, 151]. As molar extinction coefficients are precise for specific compound, UV-Vis spectroscopy can be used for   finding an

unknown compound's identity [151]. In this study, UV-Vis spectroscopy was used to determine the amount of drug released from the halloysites, PCL scaffolds, halloysite-PCL scaffolds.

Figure 3.9 Ultraviolet-Visible Spectrophotometer (Located at IFM).

3.1.7 Visible Spectrophotometer

Figure 3.10 shows the visible spectrophotometer used in this study. It is also known as a colorimeter, as it determines absorbance of light in the visible region [152]. In the visible spectrophotometer, light coming from the tungsten filament lamp is focused onto the entrance slit using condensing lens. The light from the slit is focused on the cuvet containing the sample. When light hit the curvet containing sample, the beam of light is dispersed and the spectrum is obtained. This spectrum, then, is focused on the

exit slit. The visible Spectrophotometer is used for qualitative and quantitative analysis [152, 153, 154]. In the current project, a visible spectrophotometer was used for Coomassie plus protein assay and alizarin red staining.
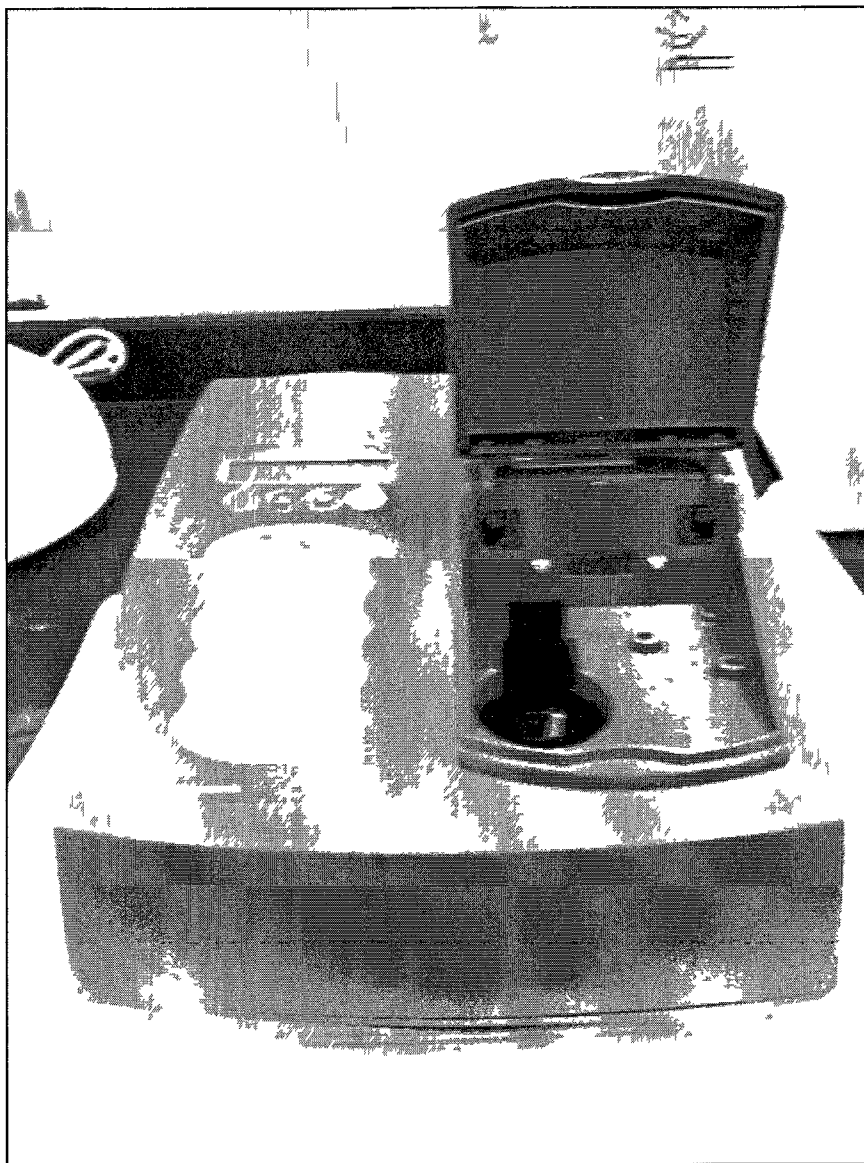
Figure 3.10 Visible Spectrophotometer (Located at BEC).

3.1.8 Fluorescence Plate Reader

Figure 3.11 shows the fluorescence plate reader used in this project for PicoGreen Assay. In this instrument, top and bottom readings are available to read anything from 6 wells to 384 wells at a same time. The FLx800™ is a multi-Detection microplate reader. It has excellent specifications and the design incorporates powerful performance at much lower price [155].

Figure 3.11 Fluorescence Plate Reader (Located at IFM).

3.1.9 Inverted Microscope

Nikon TS100 is an inverted microscope (Figure 3.12). It produces intensely clear and sharp images. Applications of an Inverted microscope include blood typing, genetic engineering, developmental genetics, electrophysiology, pharmacology, tissue culture and neurochemistry [156, 157].
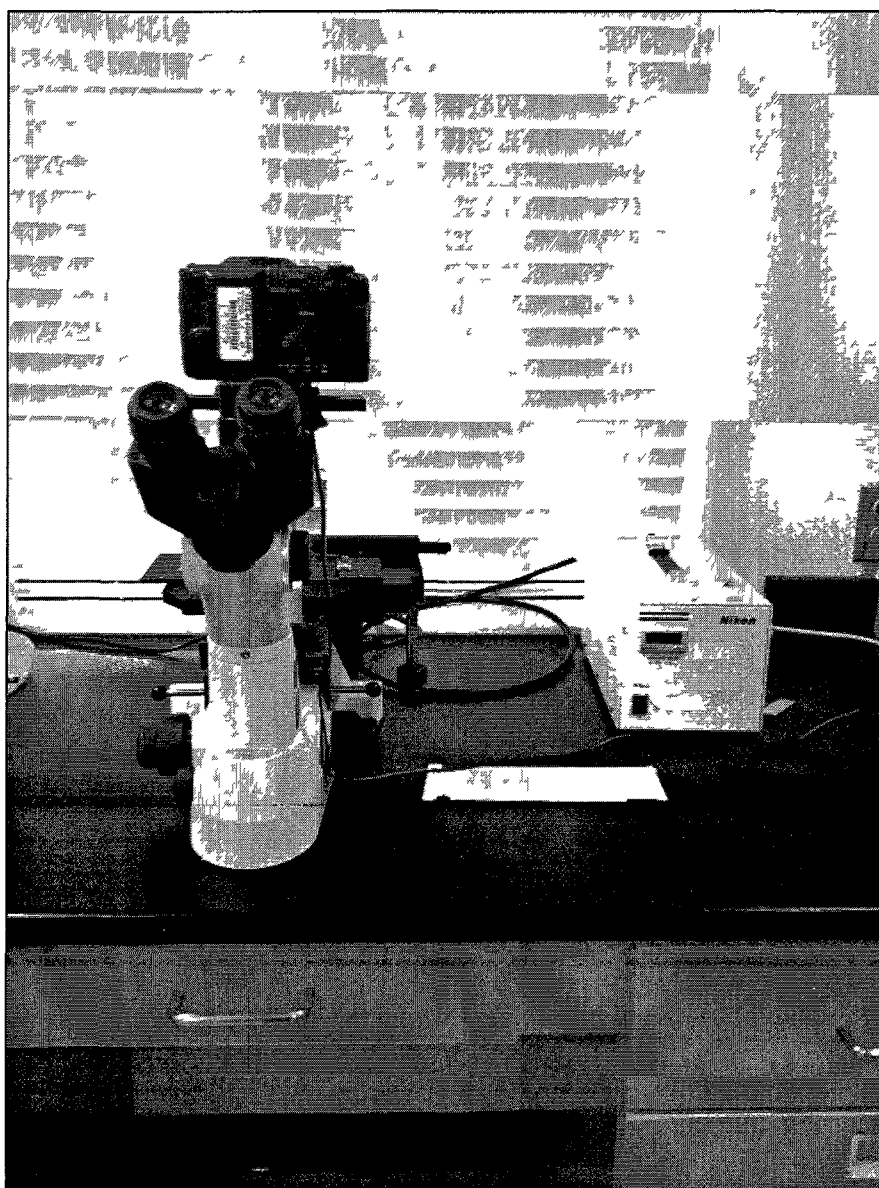
Figure 3.12 Inverted Microscope (Located at BEC).

3.2   Cell Assays

There are many different techniques to determine cellular response. We have used three of them to determine cellular response including PicoGreen assay, Coomassie plus protein assay and alizarin red staining.

3.2.1   PicoGreen Assay

PicoGreen assay is used to quantify double-stranded (ds) DNA within a sample. PicoGreen is a fluorescent nucleic acid stain, which is very sensitive and specific for double stranded DNA, enabling researchers to quantitate as little as 250pg/ml ds DNA in a 200µl assay volume. Results of PicoGreen assay are not affected even in the presence of salt, urea, ethanol, chloroform, detergents, protein and agarose compared with traditional Hoechst or UV absorbance-based ds DNA quantification methods [158]. Thus in this study, the PicoGreen assay was used to obtain measurement on the rate of cell proliferation determined by quantifying ds DNA content produced by dividing cells.

3.2.2   Coomassie Plus Protein Assay

Coomassie plus protein assay is a colorimetric method for total protein quantitation. In an acidic medium, when Coomassie dye attach to protein, the color changes from brown to blue. Here change in absorption maximum also takes place from 465nm to 595nm [159]. In the current study, we examined how the surface modification of titanium can increase the rate of protein synthesis. We also tried discovering the effect of the addition of halloysites in PCL scaffold.

3.2.3   Calcium (Alizarin Red) Assay

Calcium deposition by cells in culture can be estimated with help of alizarin red staining. To determine amount of calcium deposition, distaining of stained monolayer should be done and assayed. Alizarin red assay is more sensitive compared to

cetylpyridinium chloride extraction method [160]. Using alizarin red staining method, a detailed analysis of mineralization can be done by microscopy, and quantification can be done by visible spectroscopy. Alizarin red staining can be used for osteogenic compound screening, stem cell evaluations, tumor characterization and many more [160]. This assay gives more reliable results for weakly mineralizing samples. Alizarin red stain forms alizarin red S- calcium complex in the presence of calcium [161]. The reaction complex formed can be recovered and measured at 410nm.

CHAPTER 4

OSTEOBLAST CELLULAR RESPONSE ON NANOPOROUS TITANIUM

4.1   Introduction

As titanium has outstanding mechanical and corrosion resistance properties, it is extensively used in dental and orthopedic applications [162, 163]. The corrosion resistance property of titanium is due to titanium oxide (TiO_2) layer [164, 165]. This layer is formed automatically when titanium comes in contact with an oxygen containing environment. The titanium oxide layer is not bioactive, due to this it is unable to form a proper bonding with bone; this leads to a lack of osseointegration. This may cause implant failure [44, 93]. Thus, improving surface properties of titanium implants, which determine cell-surface interactions after implantation, will help extend the life of titanium implants. There are different surface modification techniques available, for example plasma spraying, acid etching and sand-blasting [166]. The organic matrix of bone contains type I collagen. It has specific nano-topography [44]. These indicate that bone cells may be more used to an environment in nano-scale rather than micro-scale [93] so, in this chapter; we are discussing the anodic oxidation (anodization) technique for surface modification. In this project, the strategy is to modify titanium to possess nanoporous and/or microporous surface features as natural bone is nanoporous. This chapter will

describe the anodization and different processing parameters and biological responses of anodized nanoporous titanium.

Human bone is composed of collagen, proteoglycan and calcium phosphate crystals [167]. It is a rigid structure. Bone is considered to be nanophase material; it has nanometric surface roughness [93]. Bones are made up of intercellular calcified material, known as the bone matrix and three cell types: osteocytes, osteoblasts and osteoclasts [168; 169; 170]. Bone is composed of 30% of bone matrix and 70% of bone salts [171]

4.1.1 Bone Fracture Repair

Hematoma formation occurs as an initial leading process in bone repair. Subsequently, infiltration of monocyte, macrophage, lymphocytes and polymorphnuclear cells occur, helping in removing the tissue debris [172]. After that, the fibroblast come into action and produces the granulation tissue and help in angiogenesis [173, 174]. During the repair process, the mesenchymal cell differentiates into osteoblast cells, which helps in laying down matrix [174], known as a callus. This callus is very weak and further strengthened by the osteoblast. Remodeling is the last process in bone repair. During remodeling, weak tissue is resorbed by the osteoclast and replaced by osteoblast, forming the new bone [172, 174].The steps of the bone repair process are shown in Figure 4.1.

| Inflammatory Phase |
| Reparative Phase (Callus Formation) |
| Remodeling Phase |
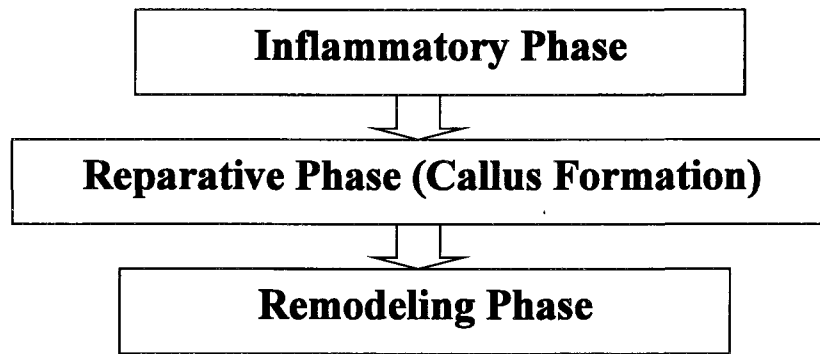
Figure 4.1 Bone Repair Process.

4.1.1.1 Current Strategies for Bone Repair

Usually, bone regenerates on its own but in certain pathological states like infection, excessive injury in accident or with immunocompromised, bone loses its potential to regenerate. In these scenarios, bone grafts are employed to replace damaged bones. There are several types of grafts like autografts, allografts, xenografts and alloplasts [175]. Due to issues of availability, immune rejection and transmission of potential infectious diseases, alloplasts are nowadays the preferred modality [176].

4.1.1.2 Limitations of Current Implants

Usually, implants are made up of different metals like vanadium, titanium and cobalt-chromium. Out of these metals, titanium is used very commonly in dental and orthopedic implants as it is more biocompatible and provides more mechanical support. It has also shown a lower propensity for corrosion [79]. Despite all of these advantages, the current clinical issue is about longevity of titanium implants [44]. This study attempts to understand osteoblast cell adhesion, growth and functionality on smooth and nanoporous titanium, and tries to find out what modifications can be done on titanium so that the life of implants can be increased.

4.1.2 Dental Structure

The core of the human tooth is made up of dentin. Dentin is calcified connective tissue. Dentin is covered by enamel which is an extremely hard and brittle material. Compared to all other skeletal elements, teeth are more resistant to all kinds of physical and chemical destruction [177]. The cervical level of the tooth is surrounded by the gingiva and the alveolar bone [178]. Three cell types are responsible for alveolar bone formation: osteoblasts, osteocytes and osteoclasts [179].

Replacement of the missing teeth is very important; for this purpose, titanium implants are used. In the current study, we used osteoblast to grow on smooth and anodized titanium to see which one will help in increasing alveolar bone volume faster and better as dental implant technology is dependent on bone volume.

4.1.3 Missing Teeth

People sometimes have a missing tooth or teeth since birth, and many lose a tooth or teeth due to disease, age, or accident. This problem of missing or broken teeth can be treated. On the other hand, ignoring these problems may lead to extra tooth and bone loss. Thus, it is important to take care of missing teeth as soon as possible. If missing teeth are left untreated, then other teeth start moving into the space. Opposing teeth also start moving when opposing teeth are missing. Thus, to keep all other teeth in the right position, it is important to treat missing teeth.

4.1.4 Implant Bone Volume

Bone volume is one of the important factors for implant success. It is essential to assess this parameter prior to implant placement. An adequate amount of bone available for implant placement is one of the requirements for implant success [180]. Long-term

tooth loss can decrease bone volume in patients [181]. With proper treatment planning, the bone and peri-implant soft tissue can be reestablished. Providing the support required for long-term function of implant. Implants are more likely successful when placed into better quality bone in term of both quantity and density [180]. It is, therefore required to have appropriate bone volume. In this study we are trying to find out whether anodization of titanium helps in improving bone volume.

4.2 Materials and Methods

Titanium was first anodized by the anodic oxidation method, followed by the surface characterization by the scanning electron microscope (SEM). Then the selected titanium samples were used for cell culture work.

4.2.1 Anodization of Titanium

For Anodization of titanium, titanium was purchased from Goodfellow Cambridge Ltd, UK. Titanium specimens of 0.5in × 0.5in (thickness 0.25mm) were cut from the commercially 99.6+% pure titanium foils. Prior to further use, the specimens were mechanically polished to a 0.05μm diamond past finish, degreased by ultrasonic cleaning in acetone, and air dried. During anodization, a circular area of 0.25^2 in was exposed to the electrolytes. The counter-electrode was a platinum slate placed at a distance of 2cm from the anode. All experiments were carried out at a constant cell voltage (range 10-40V). The electrolyte was unstirred during anodization. The electrolyte was composed of 0.1 to 1M H_2SO_4 and 0.05 to 0.9wt% HF, prepared from reagent grade chemicals and deionized water. After the anodization, samples were thoroughly rinsed in DI water and finely air dried.

4.2.2 Surface Characterization of Titanium

The scanning electron microscope (SEM) was used to observe the surface topography of the anodized titanium; electrically conductive carbon tapes were used for mounting a titanium sample on SEM pin mount specimen holder. The double sided adhesive tape allows faster sample mounting with no liquid or colloidal adhesives. It is helpful for investigative samples in an uncoated state.

4.2.3 Osteoblast Cell Culture

After anodization and surface characterization, selected anodized titanium samples were used for cell culture. Osteoblasts obtained from ATCC (7F2 CRL-12557) were cultured on titanium samples for 14 and 21 days. The culture was incubated at 37°C, 5% CO_2 and 95% humidified air.

4.2.4 Cellular Characterization Methods

4.2.4.1 Cell Lysis Protocol

Osteoblasts cells were cultured in 12 well plates with three wells as negative control, three wells as positive control, three wells as smooth titanium samples and three wells as anodized titanium samples. Cells were detached from the plate and titanium samples by trypsinization and transferred to 15ml tubes. They were centrifuged at 1200rpm for 5 minutes. The supernatant was discarded; and the pellet was resuspended in 300μl of the cell lysis solution. It was kept on ice for 15 minutes. It was then centrifuged at 3200rpm for 20 minutes at 4°C. The supernatant was collected and stored at -70°C until needed for further use.

4.2.4.2 DNA (PicoGreen) Assay

PicoGreen assay was used to measure the rate of cell proliferation. It was determined by quantifying ds DNA content produced by dividing cells. DNA standers

were prepared from DNA stock by diluting it in an appropriate amount of 1X TE buffer [158]. For standards, 100μl was mixed with 100μl of picogreen working reagent. For titanium samples, 100μl of cell lysate sample obtained from cell grown on titanium samples was mixed with 100μl of picogreen reagent. It was incubated in dark at room temperature for 2-5 minutes. Then from each tube 100μl was transferred in 96 black well plates to avoid photodegradation. A fluorescence plate reader was used to detect fluorescence emitted by the samples at an excitation wavelength of 485nm and emission wavelength of 528nm.

4.2.4.3 Coomassie Plus Protein Assay

Fifty microliters (0.05ml) of each sample (cell lysate) was pipetted into the appropriate test tube. Thousand five hundred microliters (1.5ml) of the Coomassie® Plus Reagent was added to each well and mixed. The test tubes were incubated for 10 minutes at room temperature. The absorbance was measured at 595nm with a spectrophotometer [159].

4.2.4.4 Calcium (Alizarin Red) Staining

Alizarin red stain forms alizarin red S- calcium complex in the presence of calcium. The reaction complex formed can be recovered and measured at 410nm. Alizarin Red solution (40mM) was prepared by adding 2g of Alizarin Red-S to 100ml of distilled water. 10mM Sodium Phosphate solution was prepared by adding two different solutions. solution A, consisting of 138g of Sodium Phosphate Dibasic in 100ml of distilled water, and solution B, consisting of 142g of Sodium Phosphate Monobasic in 100ml of distilled water. Solution A (42.3ml) and Solution B (47.7ml) altogether made 100ml of 10mM sodium phosphate solution. To this solution, 10% cetyl pyridinium chloride was added to prepare the destaining solution. The cells gown on titanium

samples were then stained with alizarin red for 10 minutes. All the excess stain was removed, and the scaffolds were destained with 10% cetyl pyridinium chloride in 10mM sodium phosphate solution. This was measured on a spectrophotometer at 410nm.

4.2.4.5 Statistical Analysis

Analysis of variance (ANOVA) was used for quantitative analysis of osteoblast cells proliferation, total protein synthesis and calcium deposition. In all these assays, each reading was the mean of three trials to eliminate experimental errors. In this study, ANOVA was used to assess the statistical difference between samples types (smooth titanium and anodized titanium) and culture time. Here α was taken as 0.05. The null hypothesis for this study stated that measured parameters such as osteoblast cells proliferation, total protein synthesis and calcium deposition would not be affected by factors such as surface roughness and different culture days. Additionally, an alternative hypothesis stated that osteoblast cells proliferation, total protein synthesis and mineralization would be affected by factor of surface roughness and different culture day. Results of different assays will be considered significant when $p<0.05$.

4.3   Results

Anodization is a widely used surface modification technique for many metals by varying voltage, molar concentration of sulfuric acid, and weight percent of hydrofluoric acid. In this project, the anodization technique was used to produce nanoporous titanium. Image Pro software was used to analyze the SEM images of anodized titanium samples to determine inner pore diameter. In this study, the surface modification process was performed using a hydrofluoric acid (HF) solution. Figure 4.2 shows titanium after the anodization.
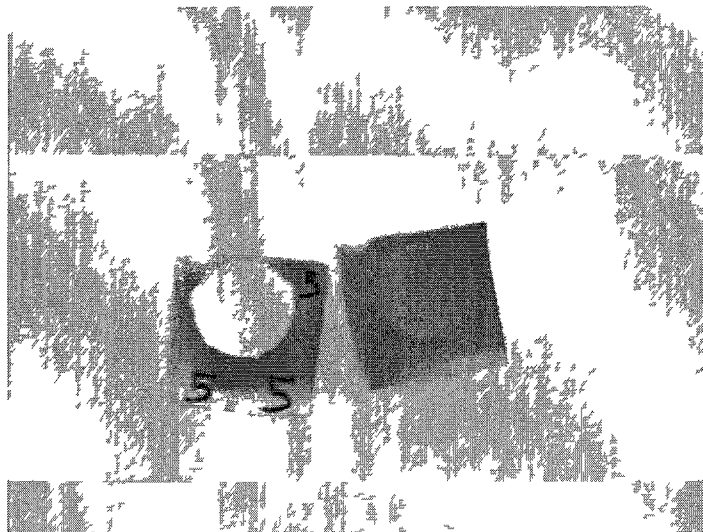
Figure 4.2 Titanium After Anodization (0.5in × 0.5in).

4.3.1 Surface Characterization

4.3.1.1 Effect of Voltage

Results of this study indicated that cell voltage affects the pore size. Figures 4.3-4.7 show the SEM images of titanium oxide films obtained by the anodization in 1M H_2SO_4 and 0.5wt% HF solution at room temperature at 15, 20, 25, 25 and 30V, respectively. When 15V were applied, the average pore diameter was 215nm. For voltage 20, the average pore diameter was 78nm. For voltage 25, the average pore diameter was 297nm and for voltage 30, the average pore diameter was 268nm.
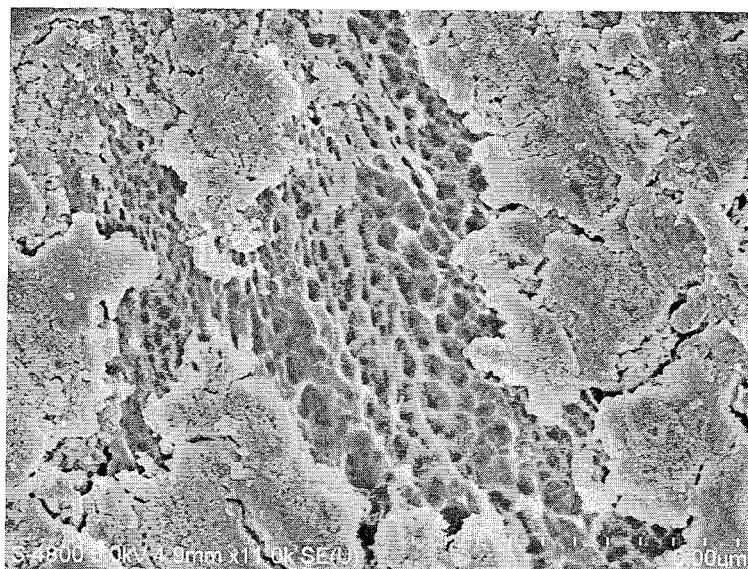
Figure 4.3 SEM Image of Titanium Oxide Films Obtained by Anodization in 1M H_2SO_4 and 0.5wt% HF at Room Temperature at 15V.
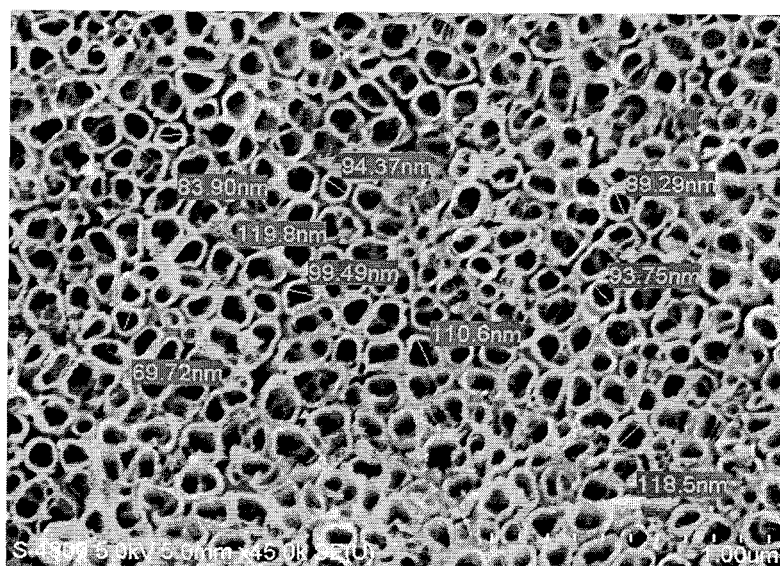
Figure 4.4 SEM Image of Titanium Oxide Films Obtained by Anodization in 1M H_2SO_4 and 0.5wt% HF at Room Temperature at 20V.
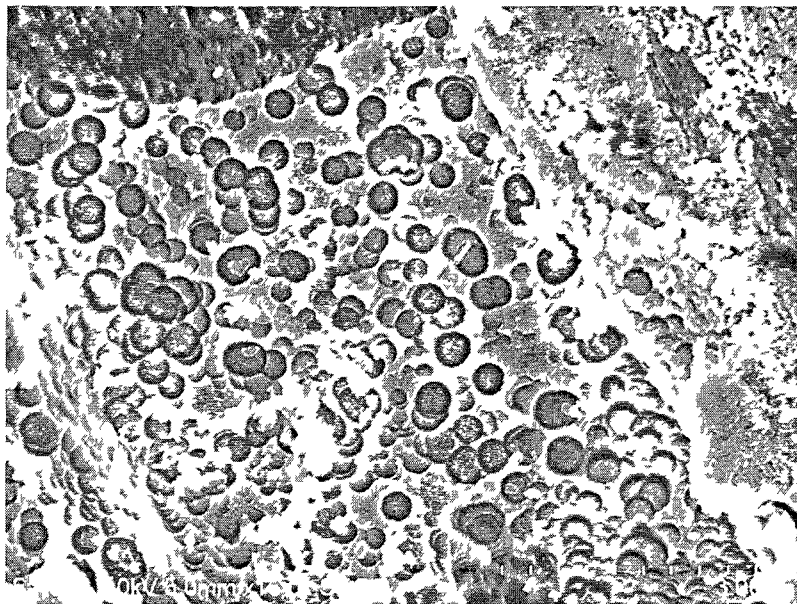
Figure 4.5 SEM image of Titanium Oxide Films Obtained by Anodization in 1M H_2SO_4 and 0.5wt% HF at Room Temperature at 25V.
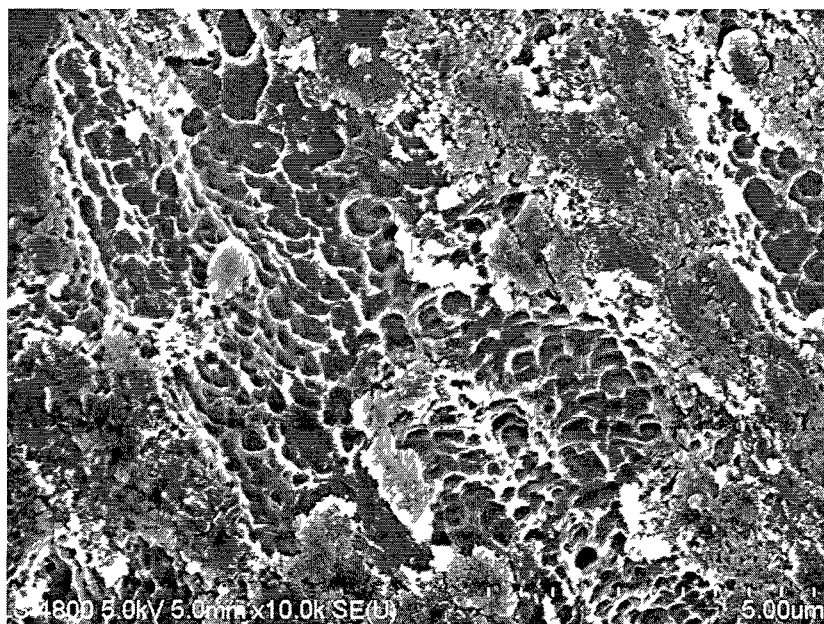
Figure 4.6 SEM Image of Titanium Oxide Films Obtained by Anodization in 1M H_2SO_4 and 0.5wt% HF at Room Temperature at 25V.
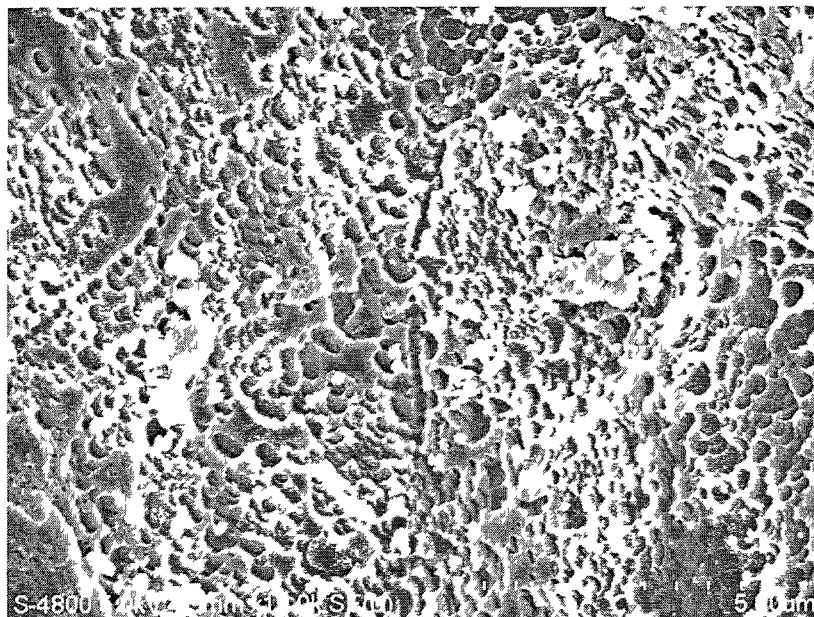
Figure 4.7 SEM Image of Titanium Oxide Films Obtained by Anodization in 1M H_2SO_4 and 0.5wt% HF at Room Temperature at 30V.

4.3.1.2 Effect of Hydrofluoric Acid Concentration

According to the results of the current study, 0.5wt% HF concentrations worked best for producing nanopores. As shown in Figure 4.9, titanium samples were anodized in 1M H_2SO_4 and 0.5wt% HF at 20V; the average pore diameter was about 78nm. As the HF concentration increased to 0.7wt% and 0.9wt% in 1M H_2SO_4, the increased wt% of HF yielded the almost completely etched titanium surface as shown in Figure 4.10. HF concentrations of less than 0.5wt% resulted in the disordered and spongy-like, porous titanium shown in Figure 4.8.
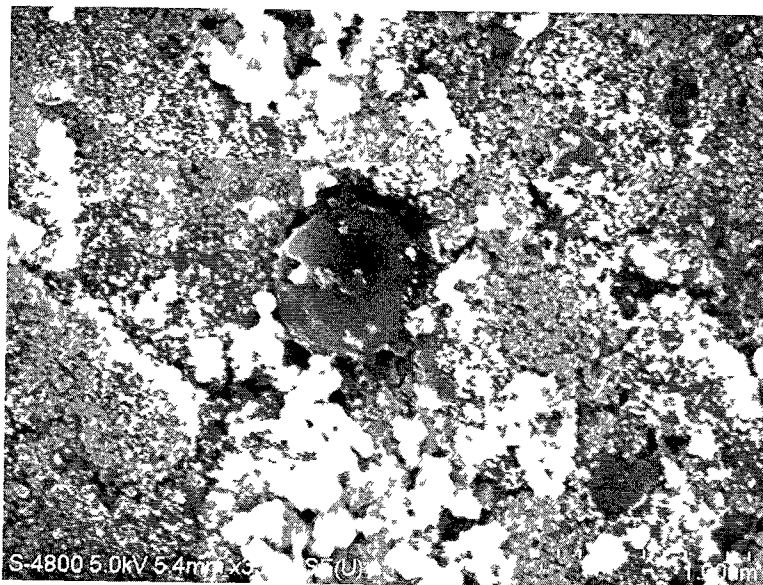
Figure 4.8 SEM Image of Titanium Oxide Films Obtained by Anodization in 1M H_2SO_4 and 0.15wt% HF at Room Temperature at 20V.
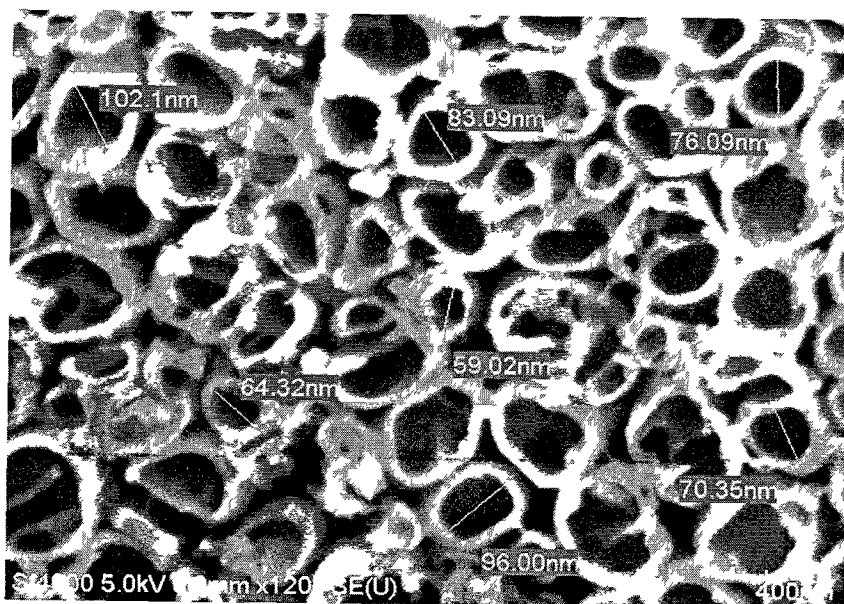
Figure 4.9 SEM Image of Titanium Oxide Films Obtained by Anodization in 1M H_2SO_4 and 0.5wt% HF at Room Temperature at 20V.
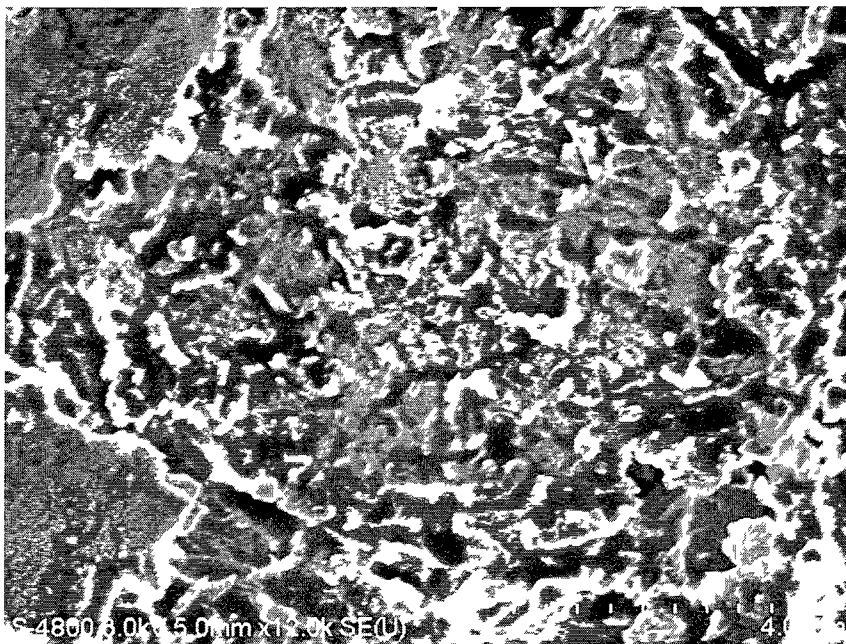
Figure 4.10 SEM Image of Titanium Oxide Films Obtained by Anodization in 1M H_2SO_4 and 0.9wt% HF at Room Temperature at 20V.

4.3.1.3 Effect of Molar Concentration of Sulfuric Acid

When Titanium was anodized in 0.1M H_2SO_4 and 0.5wt% HF at 20V, there was no pore formation. When the same molar concentration of H_2SO_4 and wt% of HF was used at 25V, still there was no pore formation. As shown in Figure 4.11, when molar concentration of sulfuric acid was increased to 1M with 0.5wt% HF at 20V, nanopores were present. Thus, these results indicate that 1M concentration of H_2SO_4 was responsible for the pore formation.
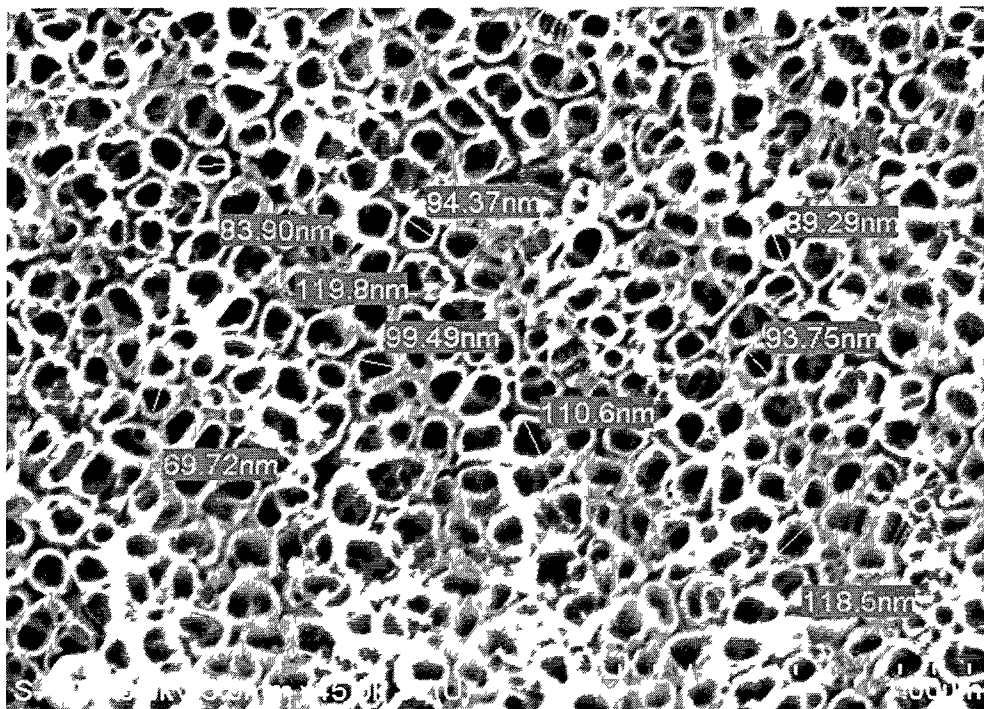
Figure 4.11 SEM image of Titanium Oxide Films Obtained by Anodization in
1MH$_2$SO$_4$ and 0.5wt% HF at Room Temperature at 20V.

Table 4.1 shows different parameters affecting pore size. Based on results of

different experiments preformed, we have found that anodization in 1M H$_2$SO$_4$ and

0.5wt% HF at room temperature at 20V is the excellent combination as it produced

uniform nanopores on the surface of titanium.

Table 4.1 Different Parameters Affecting Pore Size.

Wt% HF	0.15	0.5	0.7	0.9	wt% HF
M H_2SO_4					Voltage
1 M H_2SO_4	No pores	215nm	No Pores	No Pores	15
0.1 M H_2SO_4					15
1 M H_2SO_4		78nm			20
0.1 M H_2SO_4		No Pores			20
1 M H_2SO_4		297nm			25
0.1 M H_2SO_4		No Pores			25
1 M H_2SO_4		268nm			30
0.1 M H_2SO_4					30
	Average pore diameter	Average pore diameter	Average pore diameter	Average pore diameter	

4.3.2 Cellular Characterization Analysis

7F2 osteoblast cells were cultured in tissue culture plastic. Osteoblasts were obtained from ATCC (7F2 CRL-12557). Figure 4.12 shows the growth of 7F2 osteoblast cells on days 1, 2, 3 and 4. On day 4, cells reached almost 85-90% confluence. These cells were trypsinized and seeded on the PCL scaffolds, on the halloysite-PCL scaffolds, on the smooth titanium, and on the anodized titanium. The remaining cells were either plated again for culture or they were frozen.
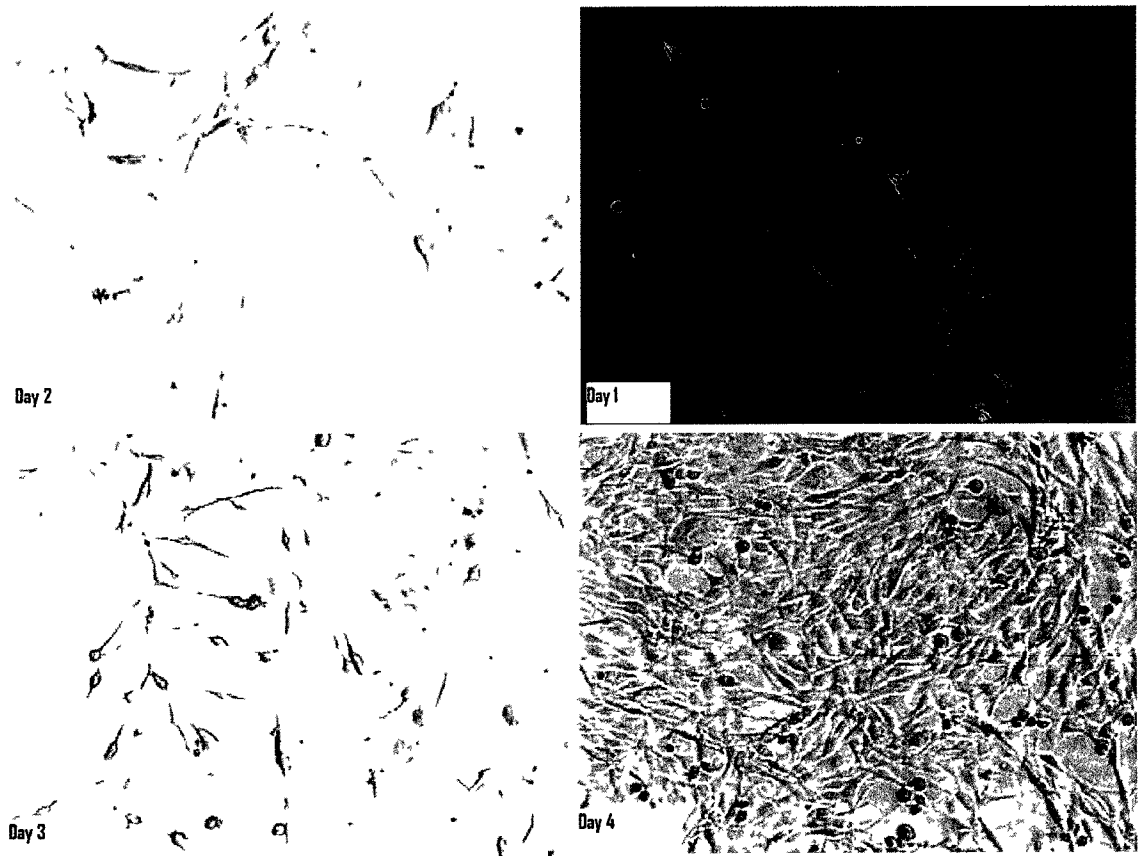
Figure 4.12 Monolayer of Osteoblast on Day 1, Day 2, Day 3 and Day 4.

4.3.2.1 DNA (PicoGreen) Assay

The PicoGreen assay was used as it provided accurate measurements on cellular proliferation. This assay measures the total amount of ds DNA produced. The assay was performed on 14 and 21 culture days to closely observe the cellular proliferation over 21 culture days. A high-range and low-range standard curve of fluorescence versus DNA concentrations was generated by the lambda DNA standard to determine the amount of ds DNA produced by the assay samples. DNA concentrations were prepared by diluting the lambda DNA stock solution (2μg/ml) with the appropriate amount of TE buffer and the PicoGreen working reagent as shown in Tables 4.2 and 4.3. A standard curve was generated by plotting the fluorescence obtained for different concentrations of the prepared DNA standards (ng/ml). The fluorescence value of the reagent blank was subtracted from the measured values. Triplicate samples were employed for each DNA concentration to ensure accuracy. Figure 4.13 shows a high-range standard curve, and Figure 4.14 shows a low-range standard curve.

Table 4.2 Standards for High Range DNA Calibration Curve [158].

Volume (μl) of TE	Volume (μl) of 2μg/ml DNA Stock	Volume(μl) of Diluted Quant-iT PicoGreen Reagent	Final DNA Concentration in Quant-iT PicoGreen Assay
0	1,000	1,000	1 μg/ml
900	100	1,000	100 ng/ml
990	10	1,000	10 ng/ml
999	1	1,000	1ng/ml
1,000	0	1,000	Blank

Table 4.3 Standards for Low Range DNA Calibration Curve [158].

Volume (μl) of TE	Volume (μl) of 50 ng/ml DNA Stock	Volume(μl) of Diluted Quant-iT PicoGreen Reagent	Final DNA Concentration in Quant-iT PicoGreen Assay
0	1,000	1,000	25 ng/ml
900	100	1,000	2.5 ng/ml
990	10	1,000	250 pg/ml
999	1	1,000	25 pg/ml
1,000	0	1,000	Blank
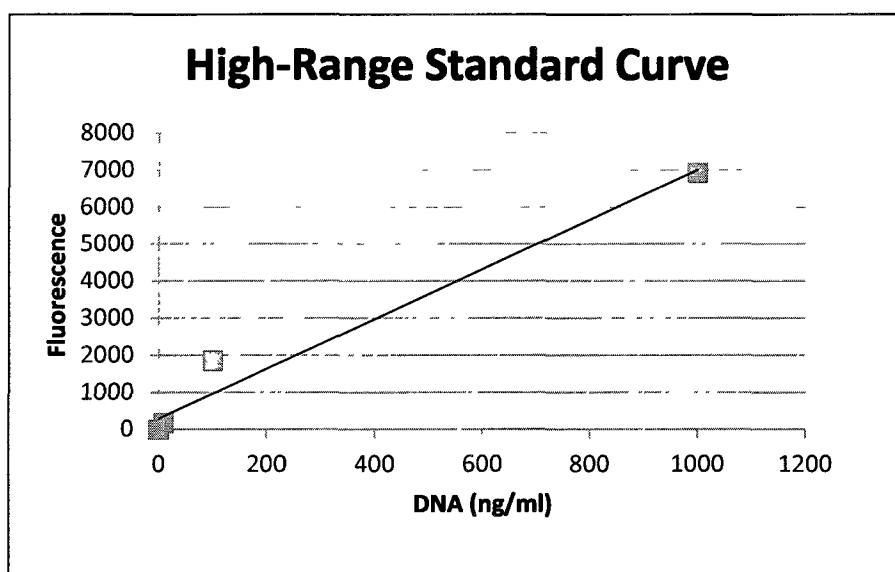
Figure 4.13 High-Range Standard Curve.
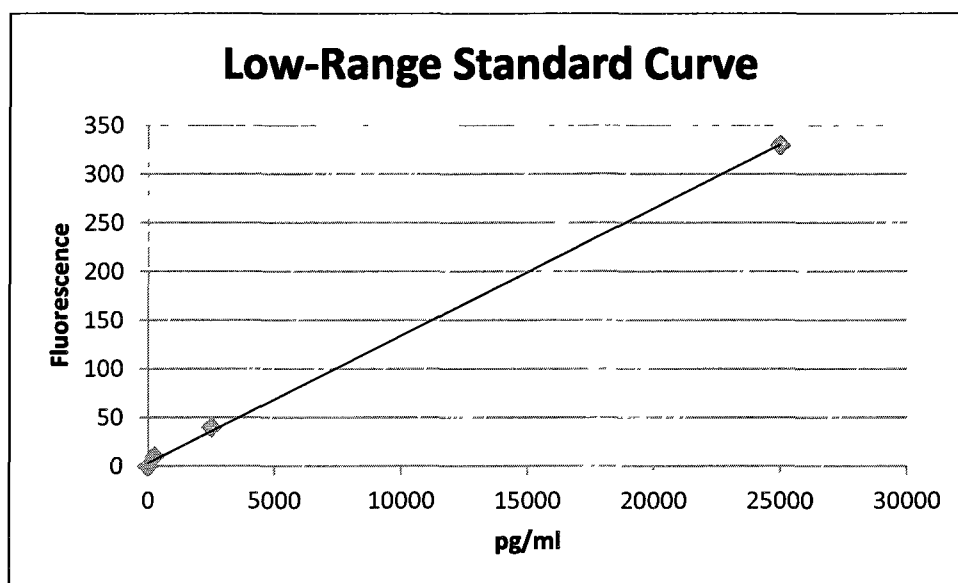
Figure 4.14 Low-Range Standard Curve.

Cell lysate samples obtained from the osteoblast cells cultured on the nanoporous titanium, on the smooth titanium, on the positive and on the negative control were used for the assay. The assay was performed over a culture period of 21 days, on 14 and 21 days. The lysate samples were placed in a 96 well plate, and the total DNA content was evaluated with the addition of PicoGreen. The quantity of ds DNA produced was measured from the fluorescing cell lysate samples at 528nm. The standard curve was used to evaluate the quantity of ds DNA produced from the fluorescence of the cell lysate samples. Each fluorescing value was a mean of the triplicate samples employed.

It was observed that nanoporous titanium showed an increased rate of osteoblast cell proliferation (Figures 4.15) on day 14, compared to the negative control, the positive control and the smooth titanium. An enhanced proliferation was seen on culture day 21 compared to day 14 for the negative control (media and no cells), positive control (media and cells) and smooth titanium (Figure 4.15 and Figure 4.16). On day 21, cell

proliferation was decreased compared to day 14 for anodized titanium, but it was still higher than the negative control, the positive control and the smooth titanium (Figure 4.15 and Figure 4.16). It was also observed that the cells' proliferative activity was dependent on the substrates' surface roughness; thus, nanoporous titanium had a higher rate of cell proliferation compared to the smooth titanium.
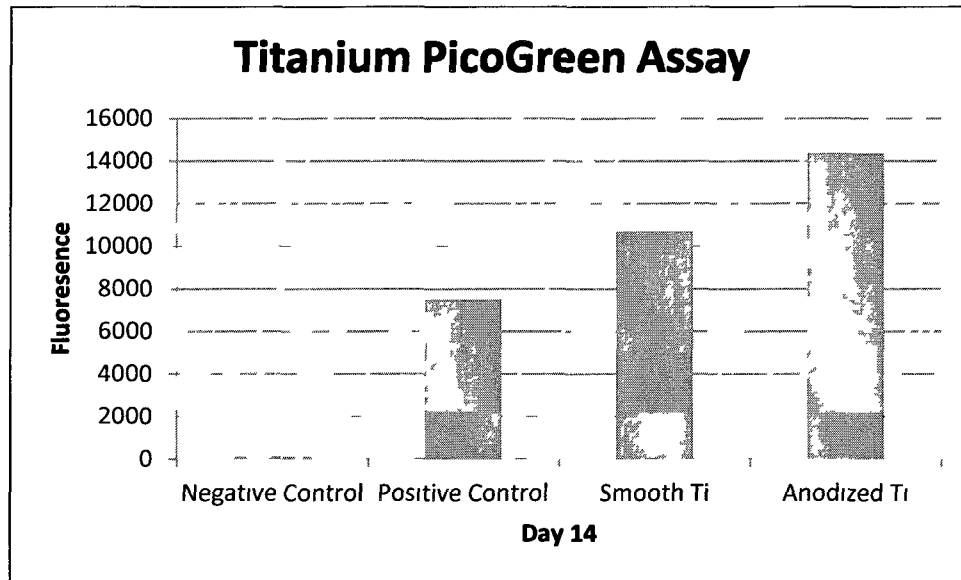
Figure 4.15 Ti PicoGreen Assay Day 14 ($p>0.05$ Not Statistically Significantly Different).
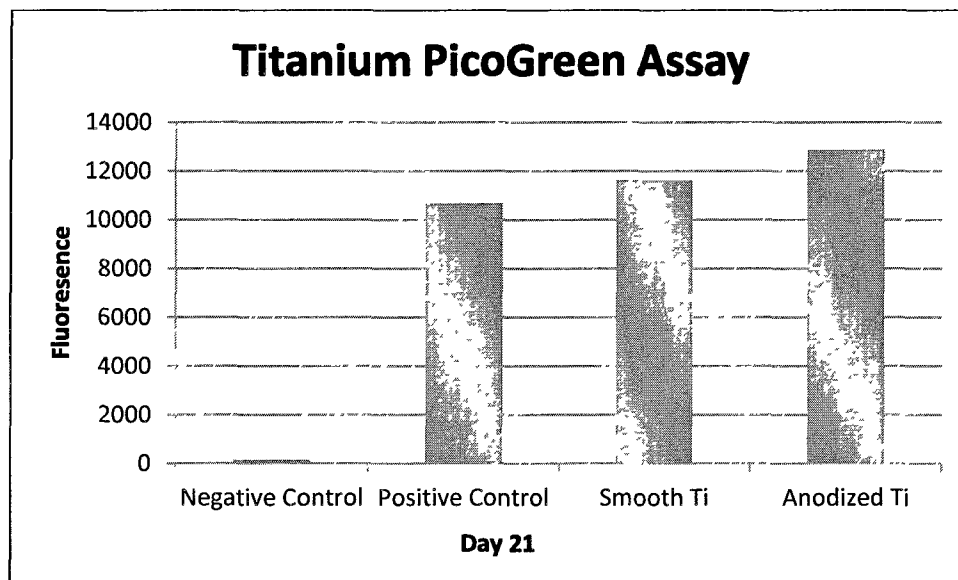
Figure 4.16 Ti PicoGreen Assay Day 21 (p>0.05 Not Statistically Significantly Different).

4.3.2.2 Coomassie Plus Protein Assay

Coomassie Plus protein assay was used to quantify the total protein production of the negative control, the positive control, the smooth titanium and the nanoporous titanium. The total protein content was assessed in cell lysate samples obtained from the cells cultured on the negative control, the positive control, the smooth titanium and the nanoporous titanium. Triplicates were used for each sample considered. The lysate of 0.05ml of each sample was mixed with 1.5ml of the Coomassie Plus reagent; the resulting colorimetric reaction was measured for absorbance (595nm) and the total amount of protein quantified.

Figures 4.17 and 4.18 depict the amount of total protein produced by osteoblasts cultured on the negative control, positive control, smooth titanium and nanoporous titanium at the culture period of 14 and 21 days respectively. Results indicated that the total amount of protein production on nanoporous titanium was more than the negative control, the positive control and the smooth titanium on day 14 and day 21. With time,

protein synthesis was increased for both smooth titanium and anodized titanium; whereas,

it reduced slightly for positive control and negative control (Figures 4.17 and 4.18).
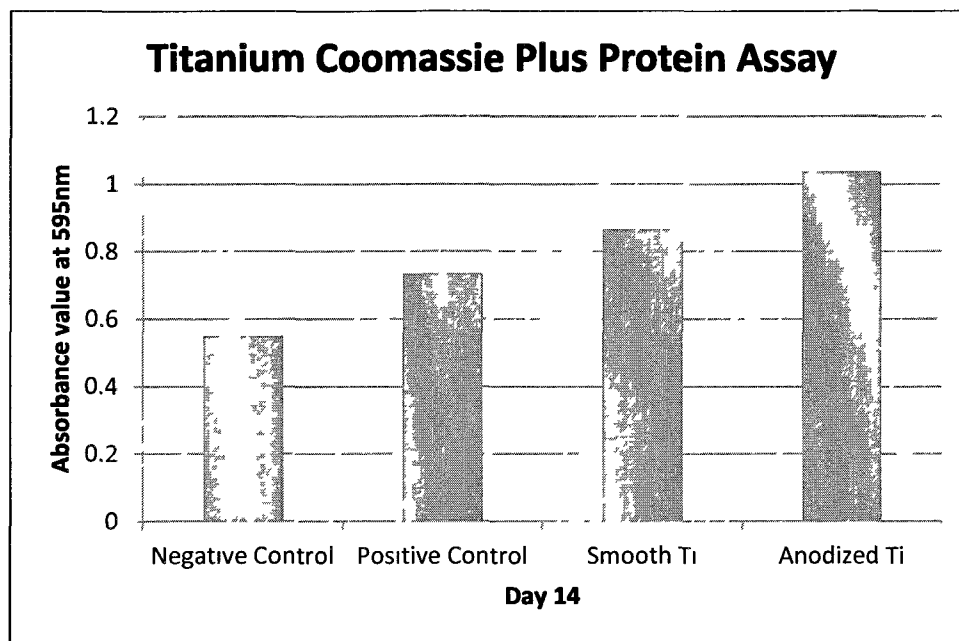
Figure 4.17 Ti Coomassie Plus Protein Assay Day 14 ($p>0.05$ Not Statistically Significantly Different).
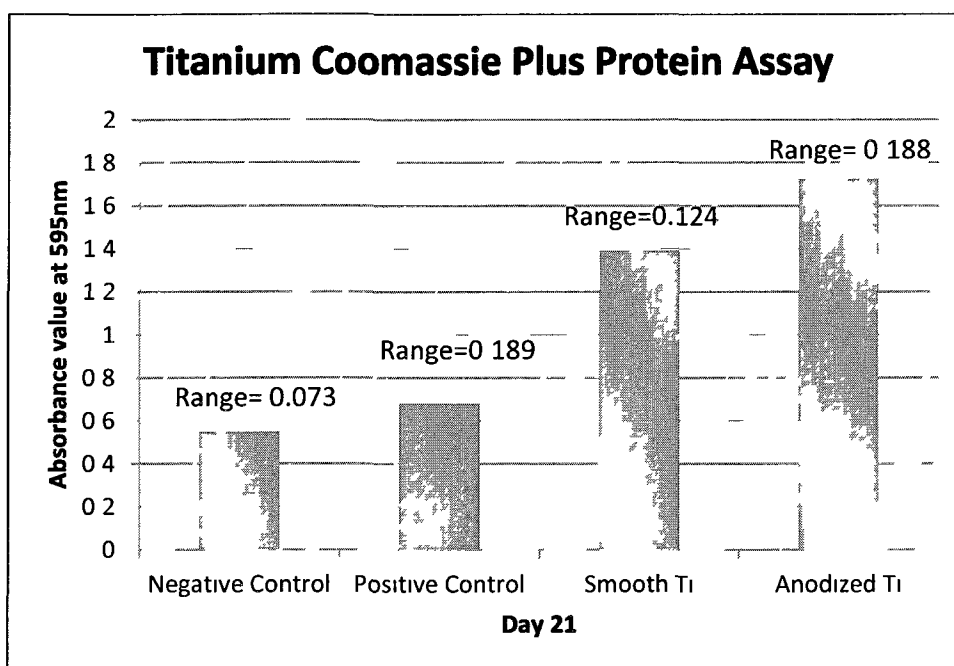
Titanium Coomassie Plus Protein Assay

Figure 4.18 Ti Coomassie Plus Protein Assay Day 21 ($p<0.05$ Statistically Significantly Different)

4.3.2.3 Calcium (Alizarin Red) Assay

To estimate calcium-rich deposition by cells in a culture, Alizarin red assay is used frequently. In this method dye from the stain cells can be extracted and evaluated. Here, distaining is performed with 10% Cetyl pyridinium chloride in 10mM Sodium Phosphate solution which can be measured by spectrophotometer at 410nm. Figures 4.19 and 4.20 shows the absorbance value of the alizarin red stain distained from the monolayer on days 14 and 21, respectively. It was observed that anodized titanium showed a higher absorbance value than the controls. The absorbance value increased constantly with time for all the substrates except the positive control and the negative control. Enhanced calcium deposition was seen on culture day 21 compared to 14 for the smooth titanium and the anodized titanium. It was also observed that the cells' calcium

deposition was dependent on the substrates' surface roughness; hence, more absorbance was observed on nanoporous titanium.
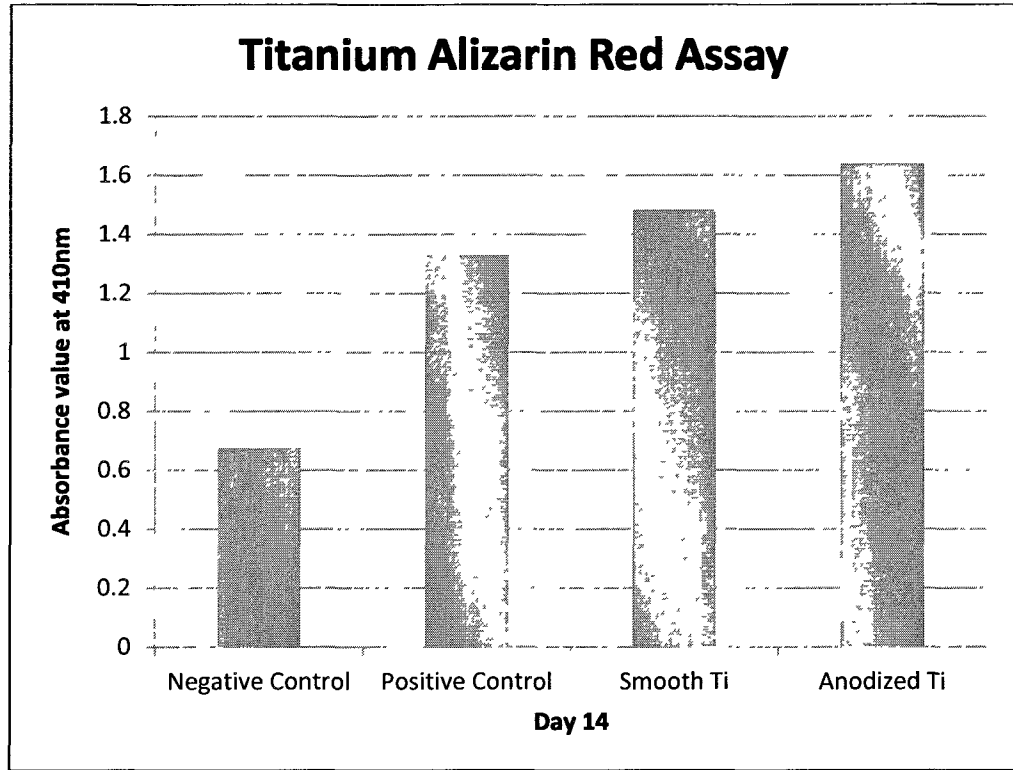
Figure 4.19 Ti Alizarin Red Staining Day 14 ($p>0.05$ Not Statistically Significantly Different).
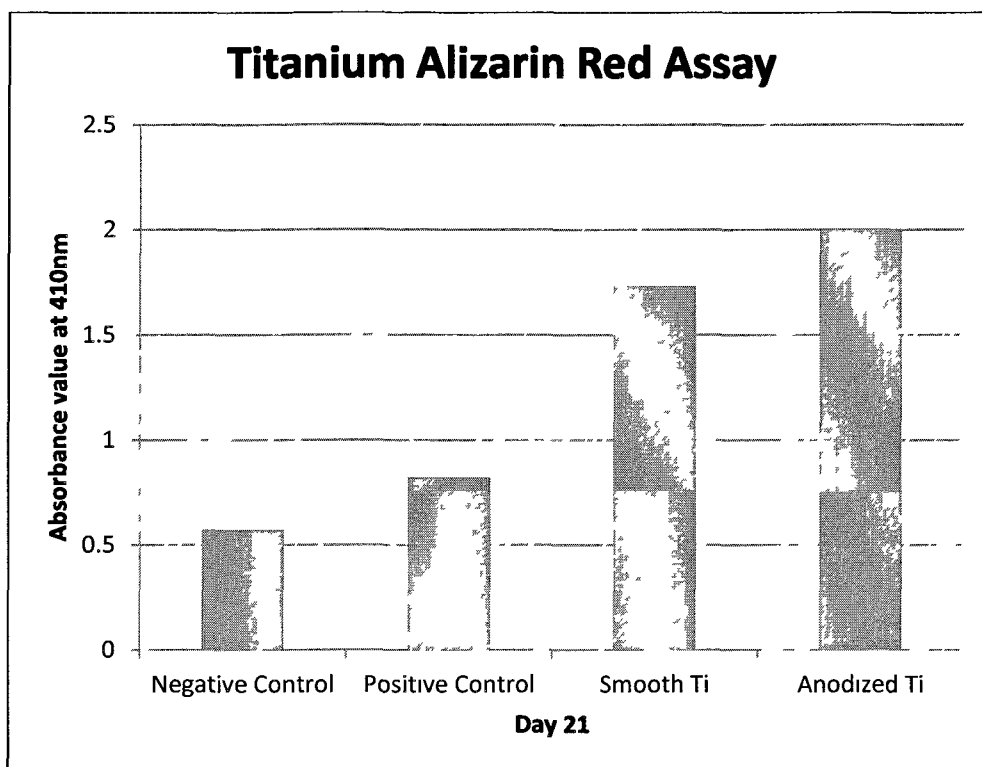
Figure 4.20 Ti Alizarin Red Staining Day 21($p>0.05$ Not Statistically Significantly Different).

4.3.2.4 Statistical Analysis of Results

Reading of cell proliferation, total protein synthesis and calcium deposition was mean of three trials to remove experimental errors. The statistical significance of results with respect to surface roughness and different culture period was analyzed using ANOVA. The calculated p value for total protein synthesis showed significant differences for the employed samples (smooth titanium and anodized titanium) at different culture period. Calculated p value of total protein synthesis for smooth titanium and anodized titanium on day 21 found to be statistically significantly different.

4.4   Discussion

Titanium is widely used in orthopedic and dental implants [162, 163]. However, smooth titanium is not bioactive enough to form bonds with the bone, and hence, there is a lack of osseointegration [93]. There are chances of implant failure or a shorter life of the implant; so many attempts have been made to improve the surface properties of titanium. Surface modification plays a very important role in the development of biocompatible scaffolds. Previous studies have shown the importance of surface topography in cell attachment and growth. Surface modification techniques (including self-assembled monolayer, plasma spraying, laser surface treatment and microcontact printing in conjunction with nanostructured materials such as protein, polymers and nanoparticles) have shown promising results in terms of cell attachment and growth [44, 93]. Among the several surface modification techniques available, anodization is a well-established surface modification method. Anodization is performed in an electrochemical cell which has a titanium anode and a platinum cathode. Constant voltage is applied between the anode and the cathode. The degree of nanometer roughness after anodization varies according to the process parameters such as voltage, electrolyte composition and different kinds of acids. Compared to all the electrolytes, H_2SO_4 has shown the highest oxide thickness. A fluoride solution was found to have the ability of producing a biologically-inspired nano-tubular structure [44].   In this study we have used a combination of H_2SO_4 and HF.

4.4.1   Effect of Hydrofluoric acid Concentration

Nanopores were produced when titanium samples were anodized in 1M H_2SO_4 and 0.5wt% HF at 20V for 30 minutes. A HF concentration of higher than 0.5wt% yielded completely etched titanium. These results disagree with a study done by Schmuki

et al., that in 1M H_2SO_4 containing HF concentration higher than 0.2wt% yielded a completely etched titanium surface [182]. Previous findings suggest that disordered and spongy, porous titanium oxide films were formed when anodization was performed in H_2SO_4 containing 0.05wt% HF or less, but in this study a spongy nanoporous titanium oxide file was produced below 0.5wt% HF [182]. According to Bestetti et al., by increasing the HF concentration (0.15, 0.2, 0.3, 0.4wt%) in 1M H_2SO_4 a more regular porous structure is observed. The current study also disagrees with the results of the study done by Bestetti et al [85].

4.4.2 Effect of Voltage

According to Bestetti et al., cell voltage significantly affects pore size [85]. When increasing anodization voltages from 10 to 25 in increments of 5V in 1M H_2SO_4 and 0.15wt% HF, an increase in pore diameter was observed while at a cell voltage higher than 30V, the nanopores disappeared [85]. In the current study, as nano pores were not formed at 0.15wt%, as discussed in the effect of hydrofluoric acid concentration. 1M H_2SO_4 and 0.5wt% HF were used for anodization of titanium at 15, 20, 25 and 30V. Results of this study do not agree with results of bestetti et al [85]. An increase in pore diameter was not observed with the increased in a cell voltage. Nanopores were formed at all voltages (15, 20, 25 and 30V), but the pores formed at 20V were more uniform than pores formed at other voltages.

4.4.3 Effect of Molar Concentration of Sulfuric acid

Titanium was anodized in 0.1M H_2SO_4 and 0.5wt% HF at 20V and 25V, but there was no pore formation. However, pore formation was observed in 1M H_2SO_4. Thus, in this study, the best condition when nanopores were formed was 1M H_2SO_4 and 0.5wt%

HF at 20V for 30 minutes. These results are consistent with the results obtained by Gong et.al [183].

4.4.4 Cellular Characterization Analysis

Nanoporous surface topography on titanium is produced using anodization. In the current study, nanoporous titanium showed higher cell proliferation, total protein synthesis and mineralization (calcium deposition) compared to smooth titanium. Higher cell proliferation results in more cell colonization on the implant surface, probably leading to a larger mass of bone tissue around the implant. Faster cell differentiation may result in faster maturation of bones around the implant and stronger bone-implant bonding. Our results suggest that nanoporous surfaces may be biologically friendlier and may promote multiple cell functions. The biological performance of the titanium nanotube is still not well understood, and conflicting results have been reported. Our study reveals the role played by nano-topographies on osteoblast function and provides insights into future implant surface design.

CHAPTER 5

HALLOYSITE-PCL COMPOSITES SCAFFOLD FOR OSTEOBLAST TISSUE ENGINEERING

5.1   Introduction

Tissue engineering is an emerging field. It has many promising applications for the development of novel artificial repair and replacement materials [184, 185]. This material can be used in the treatment of tissue and organ regeneration [186, 187]. Tissue engineering would be especially useful in developing bioengineered tissue for treatment of orthopedic implants, dental implants and wound healing where current treatment methods have proven refractory for many patients [188, 51]. The major component of any tissue engineering approach includes cells and scaffolds [189, 190]. The current study used PCL scaffolds, halloysite-PCL scaffolds and type I collagen coated halloysite-PCL scaffolds.

Halloysite nanotubes can be loaded with different drugs, followed by their slow release. The halloysite is an environmentally friendly object available in nature, which can be used commercially. Halloysites are added to the PCL to make the halloysite-PCL scaffold. PCL-scaffolds have been extensively studied and used in bone tissue engineering applications. These PCL scaffolds possess preferred characteristics to be used as a biodegradable scaffold. Polycaprolactone-based scaffolds generally tend to degrade at a slow rate due to the high molecular weight and hydrophobic nature

[191]. When these scaffolds are used for dentoalveolar reconstruction, they should be degraded over a long period of time. Now, researchers are trying to modify the architecture and surface characteristics of scaffolds used for tissue engineering. A recent study investigated whether the adding of halloysite in PCL scaffolds would modify the surface characteristics and osteoblast growth on the scaffolds. If halloysite-PCL scaffolds are proved to be biocompatible, then they can be used for drug-delivery in orthopedic implants, dental implants and wound healing.

5.2 Materials and Methods

Electrospinning was used to make halloysite-PCL scaffolds. The arrangement of halloysites and PCL fibers was characterized by the scanning electron microscope. To further confirm the location of halloysites in halloysite-PCL scaffolds, halloysites were labeled with FITC (Fluorescein isothiocyanate) and observed under the epifluorescence microscope. Then, selected scaffolds were used for cell assays to assess biocompatibility of halloysite-PCL scaffolds.

5.2.1 Preparation of Halloysite-PCL Composites Scaffolds

An electrospinning technique was used for preparing PCL scaffolds, halloysite-PCL scaffolds and drug-loaded halloysite-PCL scaffolds. The electrospinning set-up consist of a syringe pump, syringe, plastic covering to enclose and stabilize the path of the polymer jet, a collector plate, and high voltage electricity source. PCL (poly ε-caprolactone) was used to make scaffolds. PCL beads were dissolved in chloroform over-night. The PCL chloroform mixture was taken in a 1ml syringe and released at 10μl/min. Flat head needles were used to dispense the polymer solution. The voltage supplied was maintained at 17-20KV. The distance between the tip of the needle and the collector

plate was maintained at 15 to 20cm for halloysite-PCL scaffolds and 25-30cm for PCL scaffolds. The scaffolds made were then cut into 1cm^2 squares. In electrospinning, a syringe pump applies constant pressure to the syringe, and a high voltage is used between the tip of the syringe needle and the grounded collector. A polymer jet starts to travel towards the collection plate when the electric field strength is able to overcome the force of surface tension of the solution droplet formed at the needle tip. During the travelling, the solvent evaporates, and the scaffold is formed on the collector. In this project an aluminum plate was used as a collector. Nine weight percent of PCL-chloroform mixture was used for the PCL scaffold. For a halloysite-PCL scaffold, 2wt% halloysites were added to 9wt% PCL-Chloroform mixture to make 2wt% halloysite-PCL scaffold. Similarly, the 5wt% and 7% halloysite PCL scaffold were prepared.

5.2.2 Surface Characterization of PCL/Halloysite-PCL Composites Scaffolds

A scanning electron microscope (SEM) was used to observe the surface topography of the PCL scaffold and the halloysite-PCL scaffold; electrically conductive carbon tapes were used for mounting samples on the SEM pin mount specimen holder.

5.2.3 Halloysite Labeling

Fluorescence was added to halloysites by aminopropyltriethoxysilane functionalization. HNTs were labeled by altering their surface with aminopropyltriethoxysilane (APTES). APTES (500μl) was dissolved in 6.25ml of toluene to this 0.15g of clay powder was added, and then solution was ultrasonically dissolved for 30 minutes. The solution was then refluxed at 120°C for 20 hours with constant stirring. The resultant product was rinsed with toluene six times, followed by drying overnight at 120°C. Then the mixture was rinsed 10 times with DI water followed

by freeze-drying overnight. Three milligrams of these amino functionalized halloysites were then added in 1.5ml of 0.1M carbonate buffer (pH 8.0). To this solution, 100µl of 13mM solution of FITC in DMSO was added. This mixture was kept for 2 days with constant stirring and protected from light. The solution was dialyzed and lyophilized overnight [118]. An epiflurescent microscope was used for finding the location of the labeled halloysite in the halloysite-PCL scaffolds.

5.2.4 Scaffold Sterilization

Scaffolds were cut into 1cm^2 squares, and were then soaked in 95% alcohol for 48 hours. Scaffolds were washed with sterile distilled water two times and kept in HBSS/DPBS -5X pen-strep for 24 hours. Before seeding cells on the scaffolds, they were washed twice with the medium.

5.2.5 DNA (PicoGreen) Assay

The rate of cell proliferation on PCL scaffolds and halloysite-PCL scaffolds was measured by PicoGreen assay. The rate of cell proliferation was determined by quantifying ds DNA content produced by dividing cells growing on PCL scaffolds, halloysite-PCL scaffolds and type 1 collagen coated halloysite-PCL scaffolds. 100µl of the cell lysate sample obtained from the cells grown on PCL scaffolds, halloysite-PCL scaffolds and type 1 collagen coated halloysite-PCL scaffolds were mixed with 100µl of picogreen reagent, followed by incubation in the dark at room temperature for 2-5 minutes. Then from each tube, 100µl was transferred in 96 black well plates to avoid photodegradation. A fluorescence plate reader was used to detect fluorescence emitted by the samples at an excitation wavelength of 485nm and emission wavelength of 528nm.

5.2.6 Coomassie Plus Protein Assay

Fifty microliters (0.05ml) of cell lysate from each sample was pipetted into the appropriate test tube. Thousand five hundred microliters (1.5ml) of the Coomassie® Plus Reagent was added to each test tube and mixed. The test tubes were incubated for 10 minutes at room temperature. The absorbance was measured at or near 595nm with a spectrophotometer [159].

5.2.7 Calcium (Alizarin Red) Assay

The cells gown on PCL scaffolds and halloysite-PCL scaffolds were stained with alizarin red for 10 minutes. All the excess stain was removed, and the scaffolds were destained with 10% cetyl pyridinium chloride in 10mM sodium phosphate solution. This was measured on a spectrophotometer at 410nm.

5.2.8 Statistical Analysis

Analysis of variance (ANOVA) was used for quantitative analysis of Osteoblast cells proliferation, total protein synthesis and calcium deposition. In all these assays, each reading was the mean of three trials to eliminate experimental errors. In this study, ANOVA was used to assess the statistical difference between samples types (PCL scaffold and type I collagen coated halloysite-PCL scaffold) and culture period. Here, α was taken as 0.05. The null hypothesis for this study stated that measured parameters such as osteoblast cells proliferation, total protein synthesis and calcium deposition, are not affected by factor of sample type (PCL scaffold and type I collagen coated halloysite-PCL scaffold) and different culture periods. And alternative hypothesis state that Osteoblast cells proliferation, total protein synthesis and mineralization are affected by sample type and different culture period. Results of different assays will be considered significant when $p<0.05$.

5.3   Results

The electrospinning technique was used for fabricating PCL scaffolds and halloysite-PCL scaffolds. Figure 5.1 shows a digital camera picture of the electrospun PCL scaffold. The PCL fiber organization, the fiber diameter and the position of halloysite in the PCL-halloysite were investigated by a scanning electron microscope (SEM).
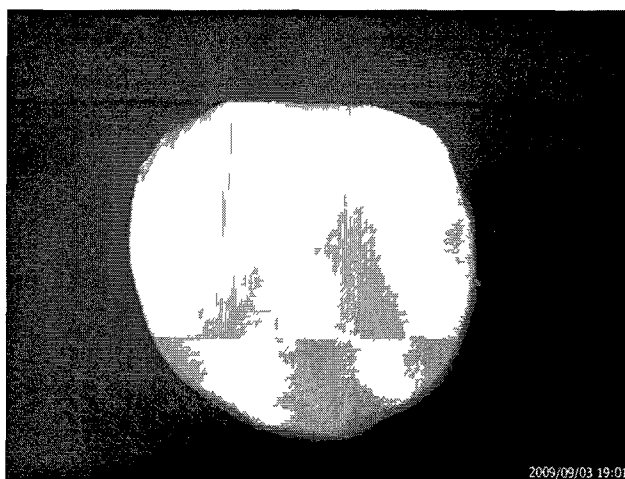
Figure 5.1 PCL Scaffold (4cm × 4cm).

5.3.1   PCL/ Halloysite-PCL Scaffold Characterization

Figure 5.2 shows a SEM image of the PCL scaffold. The average fiber diameter of the PCL scaffold was 7μm according to the SEM microscopic image scale.
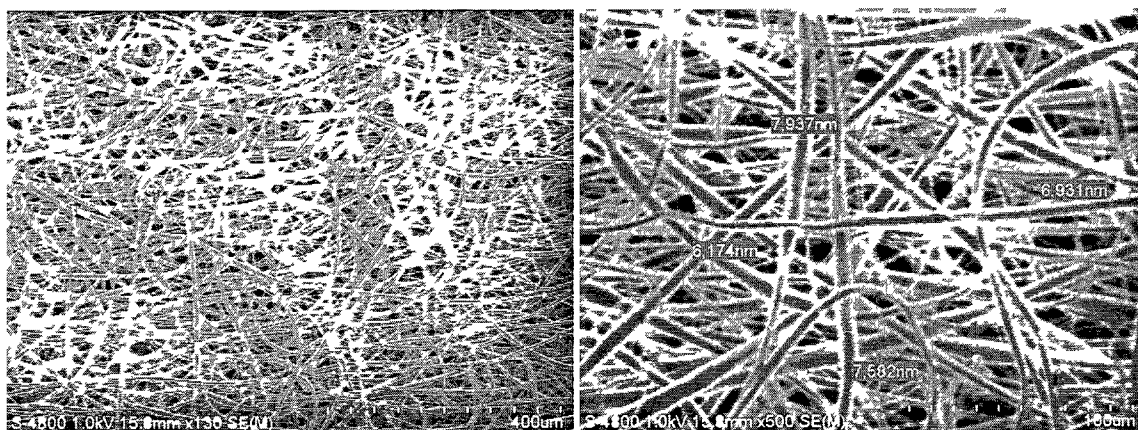
Figure 5.2 SEM Image of PCL Scaffold.

Figure 5.3 shows a SEM image of 2% halloysite-PCL scaffold. Two percent halloysite-PCL scaffolds were fabricated by adding 2wt% of halloysites in 9wt% of PCL chloroform mixture. SEM images show the bead formation, which was absent in the PCL scaffold. Thus, these beads were formed because of the halloysite. This indicates that halloysites get clustered together and form the beads.
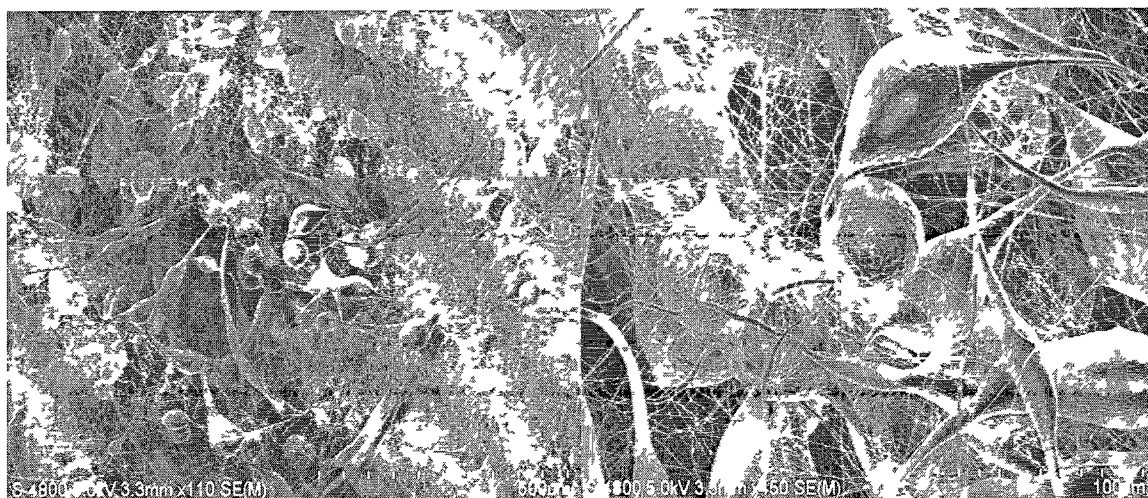
Figure 5.3 2% Halloysite-PCL Scaffold.

Figure 5.4 shows a 5% halloysite-PCL scaffold. Hardly one bead was present in the 5% halloysite-PCL scaffold. Bead formation should have been more than what was observed in the 2% halloysite-PCL scaffold. Here, it looks like most of the halloysite was incorporated into the PCL fiber or halloysites were pelleted at the bottom of the mixture.
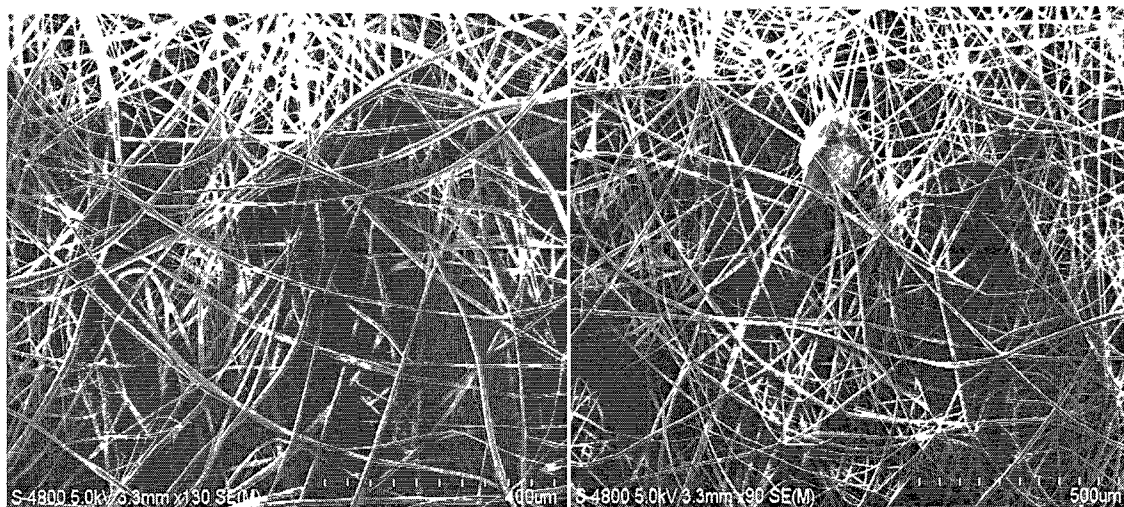
Figure 5.4 5% Halloysite-PCL Scaffold.

Figure 5.5 shows a 7% halloysite-PCL scaffold. Many beads were formed in the 7% halloysite- PCL scaffold. As the results for the 5% halloysite-PCL scaffold were different from the 2% and the 7% halloysite-PCL scaffold, a confirmatory test was done to find out the exact location of the halloysites in the halloysite-PCL scaffold. This confirmatory test involved the fabrication of the FITC labeled halloysite-PCL scaffold.
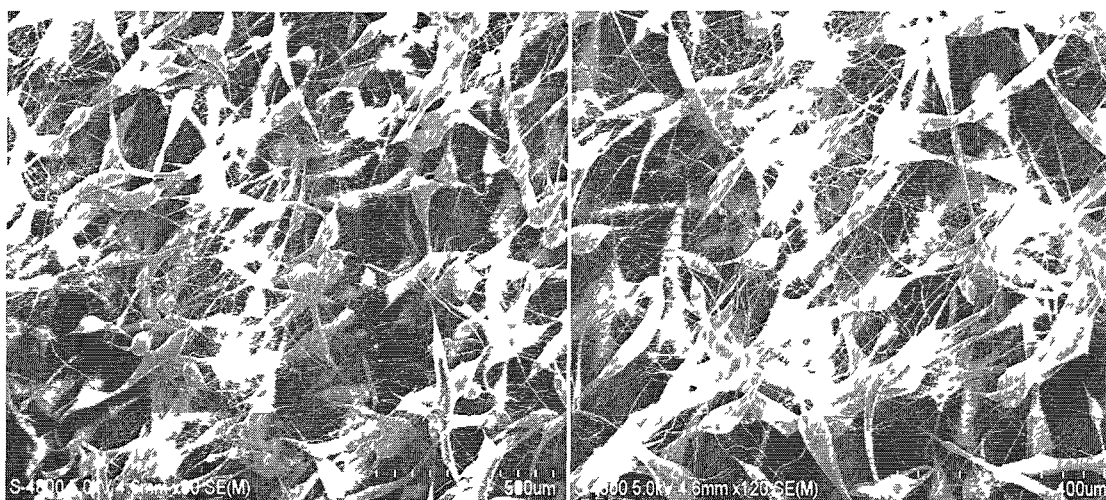
Figure 5.5 7% Halloysite-PCL Scaffold.

5.3.2 FITC Labeled Halloysite-PCL Scaffold Characterization

Here, halloysites were labeled with florescent dye (FITC), and then added into the PCL-chloroform mixture, followed by electrospinning. Therefore, wherever halloysites were present in the scaffold, it would show bright green color under the epifluorescent microscope. Figure 5.6 shows that florescence was present on the beads. This indicates that the halloysites clustered together and formed the beads which were not getting incorporated into the PCL fibers.
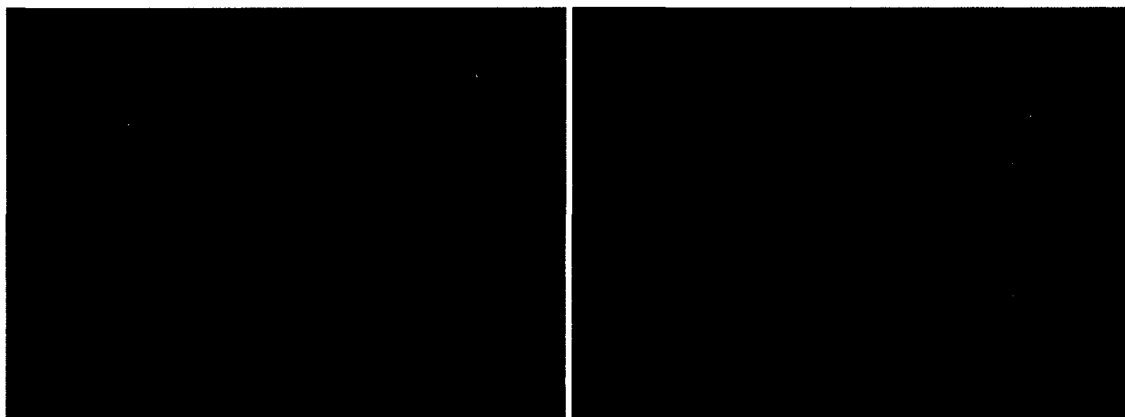
Figure 5.6 FITC Labeled Halloysite-PCL Scaffold.

5.3.3 Analysis of Cellular Response

5.3.3.1 DNA (PicoGreen) Assay for Halloysite-PCL Scaffold

The cell lysate obtained from the osteoblast culture on the type I collagen coated halloysite-PCL scaffold, the halloysite-PCL scaffold, the PCL scaffold, the positive control and the negative control were used for the assay. The assay was performed over a culture period of 21 days, on the days 7, 14 and 21. The lysate were placed in a 96 well plate to evaluate the total DNA content by addition of PicoGreen. The quantity of ds DNA produced was measured from the fluorescing cell lysate sample at 528nm. The standard curves were used to evaluate the quantity of ds DNA produced from the fluorescence of the cell lysate sample. Each fluorescing value was a mean of the triplicate samples employed.

It was observed that the type I collagen coated halloysite-PCL scaffold showed an increased rate of osteoblast proliferation (Figure 5.7) compared to the negative control , the positive control, the PCL scaffold and halloysite-PCL scaffold on day 7.Whereas the uncoated halloysite-PCL scaffold had lower cell proliferation compared to the type I collagen coated halloysite-PCL scaffold, PCL scaffold and positive control. On day 7 the PCL scaffold and halloysite-PCL scaffold both showed lower cell proliferation compared to the positive control. The type I collagen coated halloysite-PCL scaffold showed highest cell proliferation on day 7 compared to days 14 and 21 (Figures 5.7-5.9). For the type I collagen coated halloysite-PCL scaffold, cell proliferation was lowest on Day 21. For uncoated halloysite-PCL scaffold cell proliferation was maximum on day 14 (Figures 5.7- 5.9) compared to day 7 and day 21, but still it was less than cell proliferation

observed on the type I collagen coated halloysite-PCL scaffold. Cell proliferation started

decreasing for both PCL scaffold and positive control after day 7.
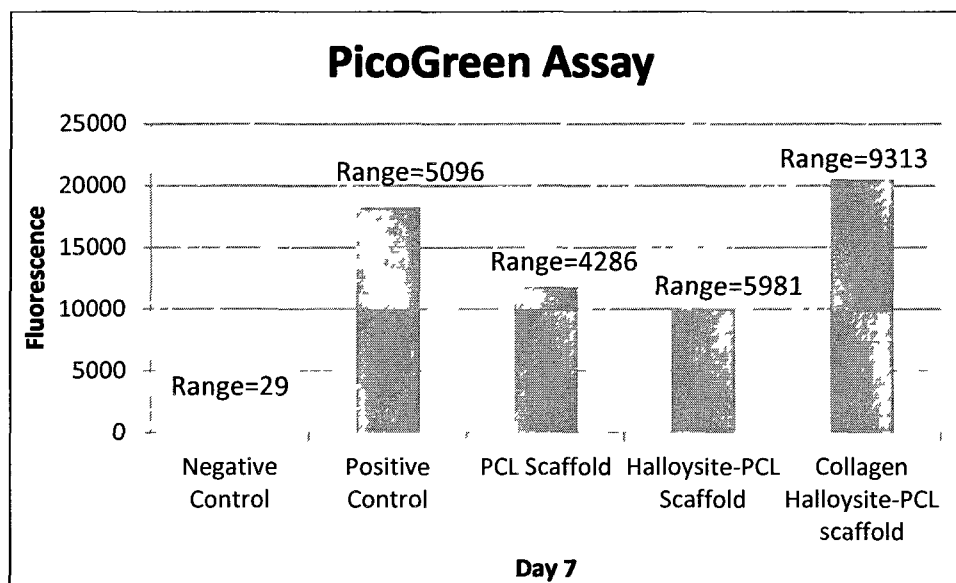
PicoGreen Assay

Figure 5.7 Halloysite-PCL Scaffold Picogreen Assay Day 7($p<0.05$ Statistically Significantly Different).
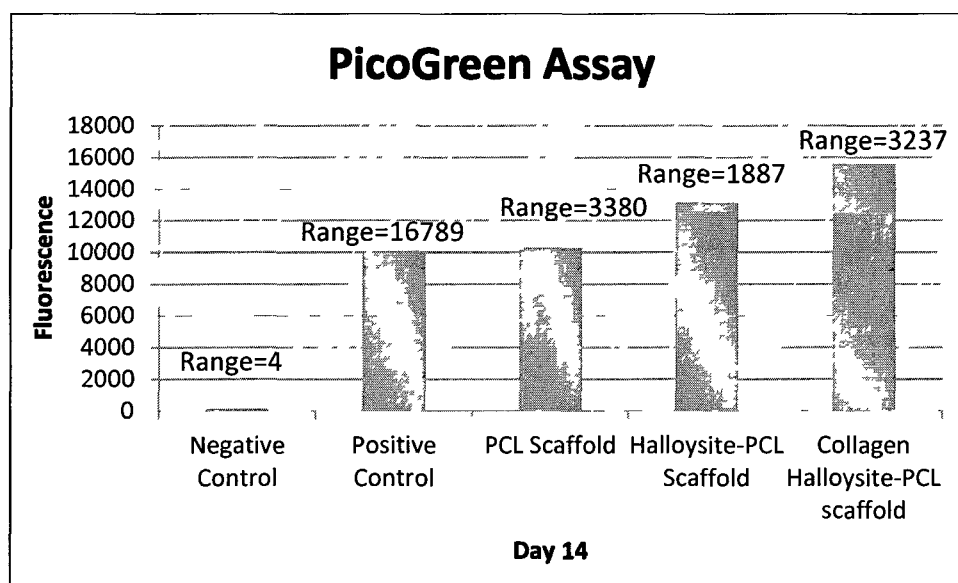
PicoGreen Assay

Figure 5.8 Halloysite-PCL Scaffold Picogren Assay Day 14($p<0.05$ Statistically Significantly Different).
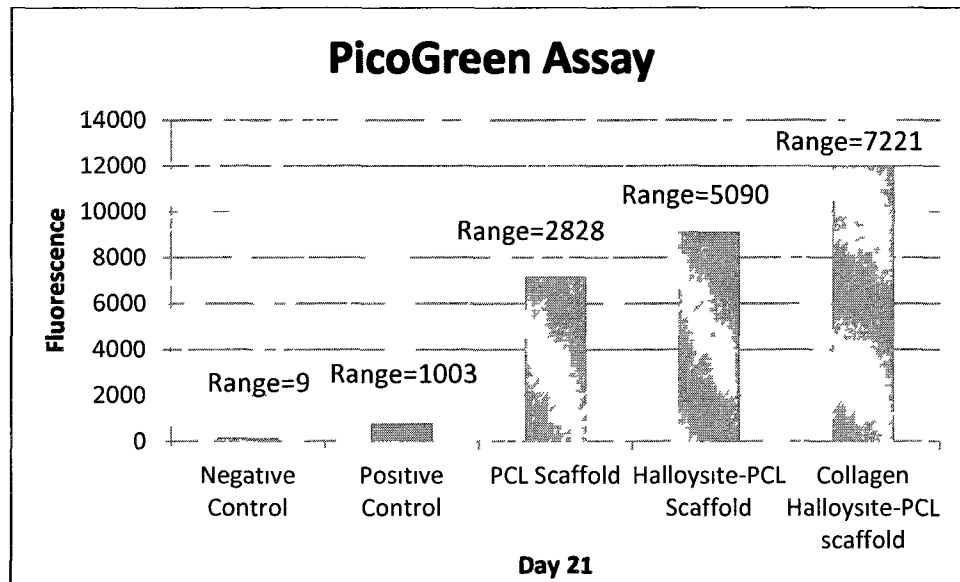
Figure 5.9 Halloysite-PCL Scaffold Picogreen Assay Day 21($p<0.05$ Statistically Significantly Different).

5.3.3.2 Coomassie Plus Protein Assay for Halloysite-PCL Scaffold

The Coomassie Plus protein assay was used to quantify the total protein production. The total protein content was assessed in the cell lysate obtained from the cell culture on the negative control, the positive control, the PCL scaffold, the halloysite-PCL scaffold and the type I collagen coated halloysite-PCL scaffold. Triplicates were used for each sample considered. The lysates of 0.05ml of each sample were mixed with 1.5ml of the Coomassie plus reagent; the resulting colorimetric reaction was measured at 595nm.

Results indicated that the total amount of protein production on the type I collagen coated halloysite-PCL scaffold was more than the negative control, the positive control, the PCL scaffold and the halloysite-PCL scaffold on day 14. Total amount of protein production on the type I collagen coated halloysite-PCL scaffold was highest on day 14 compared to day 7 and day 21 (Figures 5.10-5.12). For the halloysite-PCL scaffold, total protein synthesis was highest on day 21 (Figure 5.12). It was more than the

negative control, the positive control and the type I collagen coated halloysite-PCL

scaffold (Figure 5.12).
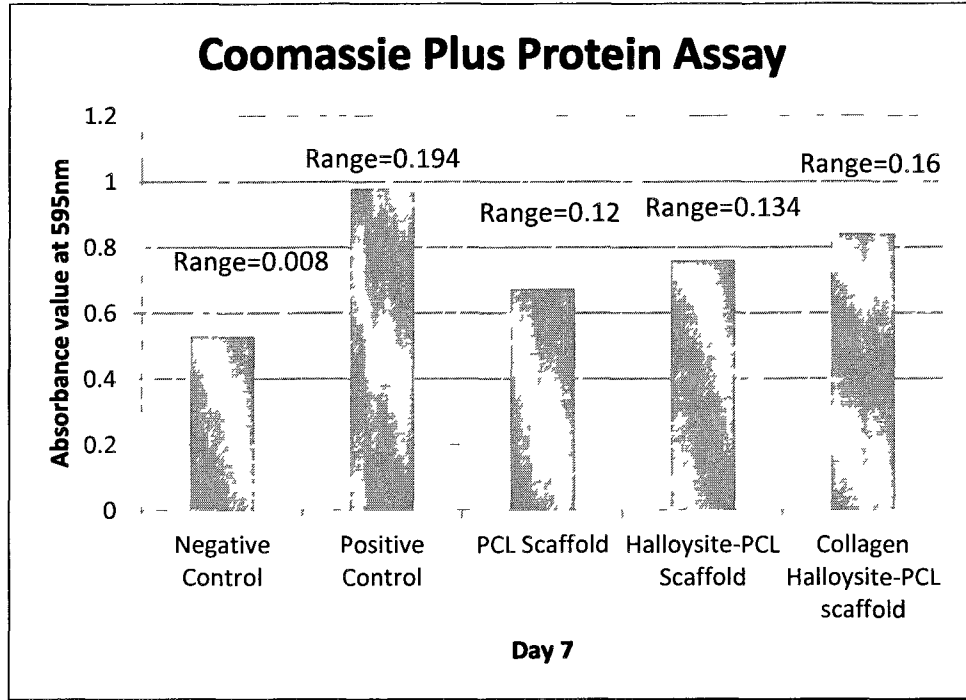
Figure 5.10 Halloysite-PCL Scaffold Coomassie Plus Protein Assay Day 7 ($p<0.05$ Statistically Significantly Different).

Coomassie Plus Protein Assay

Range=0.676 Range=0.448

Range=0.334 Range=0.039

Range=0.216

Negative Control | Positive Control | PCL Scaffold | Halloysite-PCL Scaffold | Collagen Halloysite-PCL scaffold

Day 14

Absorbance value at 595nm
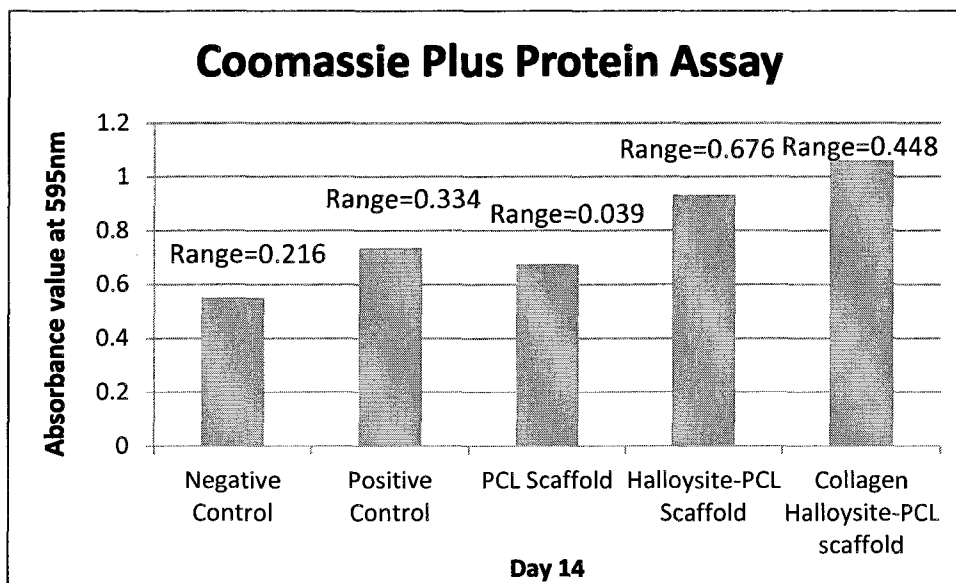
Figure 5.11 Halloysite-PCL Scaffold Coomassie Plus Protein Assay Day 14 ($p<0.05$ Statistically Significantly Different).

Coomassie Plus Protein Assay

Negative Control | Positive Control | PCL Scaffold | Halloysite-PCL Scaffold | Collagen Halloysite-PCL scaffold

Day 21

Absorbance value at 595nm
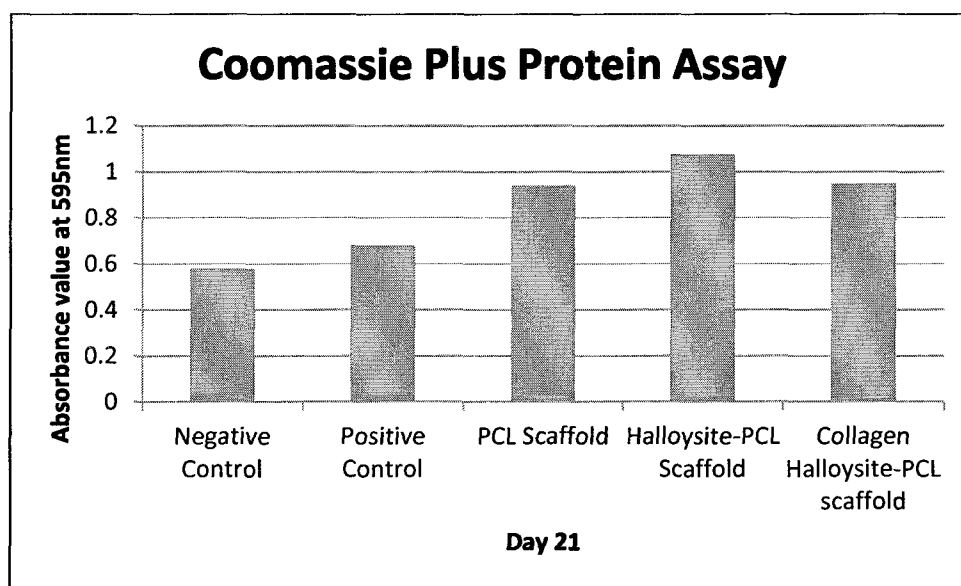
Figure 5.12 Halloysite-PCL Scaffold Coomassie Plus Protein Assay Day 21 ($p>0.05$ Not Statistically Significantly Different).

5.3.3.3 Calcium (Alizarin Red) Assay for
Halloysite-PCL Scaffold

This is a sensitive method for quantification of the ARS in a stained monolayer by distaining with 10% Cetyl Pyridinium Chloride in 10mM Sodium Phosphate solution followed by colorimetric detection at 410nm. Figures 5.13 and 5.14 show the absorbance value of alizarin red stain distained from the monolayer on days 7 and 14, respectively. It was observed that the type I collagen coated halloysite-PCL scaffold showed higher absorbance value than the halloysite-PCL scaffold, the PCL scaffold and the controls on day 7 (Figure 5.13). The absorbance values were almost equal for halloysite-PCL scaffold and the type I collagen coated halloysite-PCL scaffold on day 14 (Figure 5.14). For the PCL scaffold, absorbance value decreased on day 14 compared to day 7 (Figures 5.13 and 5.14).
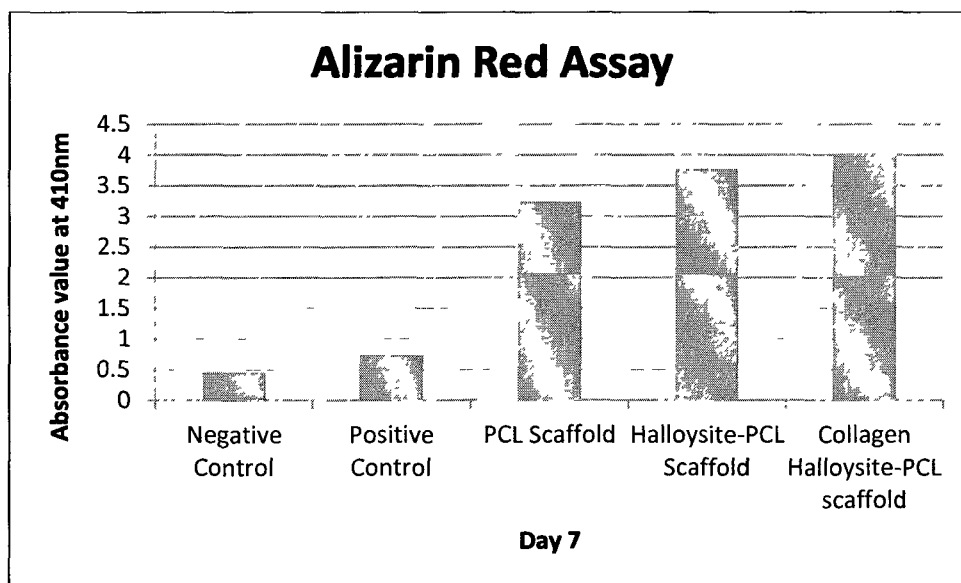
Figure 5.13 Halloysite-PCL Scaffold Alizarin Red Staining Day 7 ($p>0.05$ Not Statistically Significantly Different).
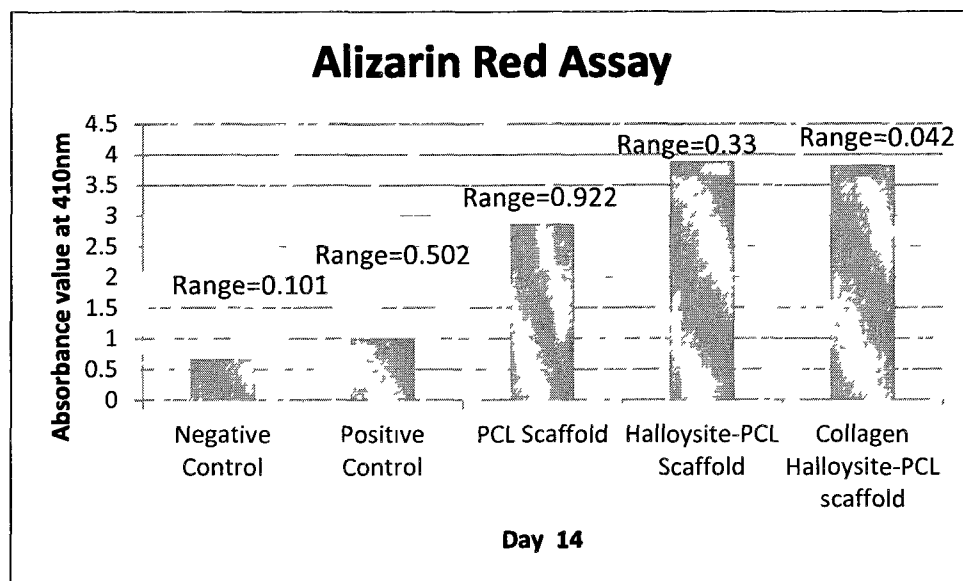
Alizarin Red Assay

Figure 5.14 Halloysite-PCL Scaffold Alizarin Red Staining Day 14($p<0.05$ Statistically Significantly Different).

5.3.3.4 Statistical Analysis of Results

The reading of cell proliferation, total protein synthesis and calcium deposition was the mean of three trials to remove experimental errors. The statistical significance of results with respect to sample type (PCL scaffold and type I collagen coated halloysite-PCL scaffold) and different culture period was analyzed using ANOVA. The calculated p values for cell proliferation assay and total protein synthesis showed statistically significant differences for the different sample types (PCL scaffold and type I collagen coated halloysite-PCL scaffold) on day 7 and 14. Cell proliferation was also statistically significant differences for the different sample types on day 21. The calculated p value for calcium deposition showed significant differences between the sample type (the PCL scaffold and the type I collagen coated halloysite-PCL scaffold) on day 14.

5.4   Discussion

The electrospun PCL and halloysite-PCL fibers were fabricated and characterized using SEM. Porous electrospun fibrous mats can mimic the extracellular matrix for cell attachment, proliferation and differentiation and can be helpful for drug-delivery from the fibers [192, 193, 194, 186]. According to study done by Qi et al., the addition of a small quantity of halloysite does not significantly change the characteristics of the mats [195]. The current study supports the results of previous study showing that the addition of up to 2wt% of the halloysite in the PCL did not change its characteristics much. SEM images of the halloysite-PCL scaffold show the beads formation, which was absent in PCL scaffolds. These beads formed because of the presence of the halloysites. Therefore, here it looks like that halloysites clustered together and formed the beads. A confirmatory test was done to find out the exact location of the halloysite in the halloysite-PCL scaffold. This confirmatory test was a fabrication of FITC labeled halloysite-PCL scaffold. Here, halloysites were labeled with a florescent dye (FITC) which showed a bright green color under the epifluorescence microscope. Since florescence was present only on the beads, it indicates that halloysites clustered together and formed the beads and that they are not getting incorporated into the PCL fibers. In the current study, the type I collagen coated halloysite-PCL scaffold achieved higher cell proliferation, protein synthesis and mineralization faster than halloysite-PCL scaffold and PCL scaffold. Higher cell proliferation results in more cell colonization on the scaffold surface, probably leading to a larger mass of bone tissue around the type I collagen coated halloysite-PCL scaffold. Faster cell differentiation may result in faster maturation of bone around the type I collagen coated halloysite-PCL scaffold.

CHAPTER 6

HALLOYSITE-PCL COMPOSITES SCAFFOLD FOR SUSTAINED DRUG RELEASE

6.1 Introduction

Halloysites are naturally occurring nanotubes. The halloysites can be loaded with different drugs and used for slower drug release [61]. This slower release lengthens the effectiveness of the drug, as the drug comes out of the halloysites slowly. This helps in extending the effectiveness of drugs without increasing dosage strength. Compared with carbon nanotubes (CNTs), halloysite nanotubes are less expensive and have a larger surface area [196, 197]. The advantages of using halloysites in drug-delivery are slower release and reduced toxicity of drug. A drug-loaded halloysite can be added to the PCL to make drug-loaded halloysite-PCL scaffolds that can be used as drug-loaded wound care products. There are a number of potential benefits of these scaffolds, including the elimination of the high initial delivery rate and a better safety profile. By using drug-loaded halloysites, we can deliver drugs more uniformly, which will increase the effectiveness of a clinical dose. Due to this efficiency, lower doses of drugs will be required per patch. There are many different types of wound care products. The drug-loaded halloysite delivery system is designed to offer superior clinical benefits over current wound care systems, especially in the area of burn care. It will reduce the rate at which a bandage needs to be changed. In the current study, we are making halloysite-PCL scaffolds that can be used as a drug-loaded bandage in the future.

6.2   Materials and Methods

6.2.1   Drug-Loading in Halloysites

The method for drug-loading in halloysite follows: Dissolve 20mg drug (Brilliant Green, Chlorhexidine, Iodine, Amoxycilline and Potassium Clavulanate, and Doxycycline) in 1ml of water or alcohol. Sonicate it until the drug dissolves. Once the solution becomes transparent add 50mg of halloysite powder. Sonicate again for 30 minutes. Then keep the solution in a vacuum machine and apply the vacuum for 20 minutes. After 20 minutes, stop the vacuum, remove the tube containing halloysites from the vacuum machine. Keep it in room atmosphere for 20 minutes. Repeat vacuum process three times. Followed by washing with water to remove any extra drug solution left around halloysites. Figure 6.1 shows the drug-loading process in halloysites. When vacuum is applied, air bubbles are removed from the halloysites. When the vacuum is broken drug solution enters in to the halloysites [115]. As Povidone Iodine come in solution form, so 50mg of halloysites were directly added into the 1ml of Povidone Iodine solution. Twenty five milligrams of Curcuma Longa was dissolved in 1ml of water in this solution 50mg of halloysite were dissolved. Followed by vacuum loading. Amoxycillin and Potassium Calvulanate was obtained from Macleods pharmaceuticals, India. Doxycycline was obtained from Shreya life science PVT. LTD, Roorkee, Uttarankhand, India. Brilliant Green was obtained from Sigma.
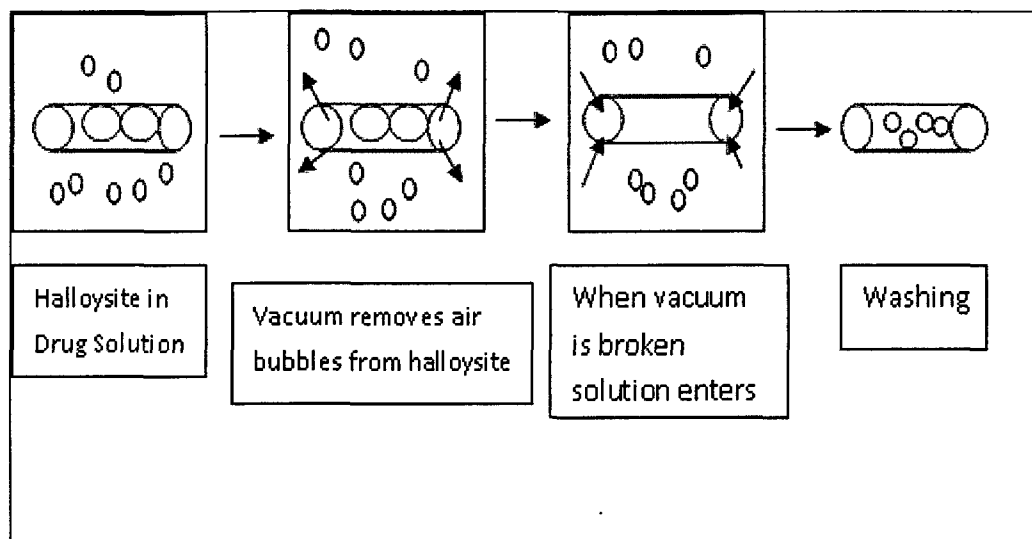
Figure 6.1 Drug-Loading in Halloysite [115].

6.2.2 Fabrication of Drug-Loaded PCL Scaffolds and Halloysites-PCL Scaffolds

First, a PCL chloroform mixture was prepared by adding the appropriate weight percent of PCL in the chloroform. The mixture was kept overnight. To this mixture, the drug-loaded halloysites were added. Then, the solution was sonicated for 10 minutes followed by electrospinning. For more detail see Section 5.2.1.

6.2.3 Fabrication of PCL/Halloysites-PCL Scaffolds Containing Two Different Drugs

Electrospinning of the electrospinning mixture containing one type of drug was performed until the scaffold is sufficiently thick; then electrospinning of the second electrospinning mixture containing the second type of drug was performed over the first layer of the scaffold. In the current study, Brilliant Green and Amoxycillin were used for preparing the scaffold containing two layers of different drugs. Brilliant Green is green and Amoxycillin is white. Then, the fiber organization was observed under the microscope.

6.2.4 Drug Release from Drug-Loaded Halloysites

Drug-loaded halloysites were added into 1ml of water, incubated on magnetic stirrer for 10 minutes, and centrifuged at 7000rpm for 2 minutes. The supernatant was taken into the fresh tube and marked as #1 tube. To the pellet 1 ml of water was added, and it was incubated again on the magnetic stirrer for 10 minutes. Then, centrifuged at 7000rpm for 2 minutes. The supernatant was taken in the fresh tube and marked as #2 tube. To the pellet 1ml of water was added. This process was repeated utill desired. The magnetic stirrer was taken out, and then the concentration of the drug released was measured with the UV Spectrometer and calculated. The difference between absorption maximum and 800nm was taken, than it was multiplied by dilution factor. Concentration at each time was found by adding up concentration. This was divided by total concentration and multiplied by hundred.

6.2.5 Drug Release from PCL scaffolds and Halloysites-PCL scaffolds

Take 0.1gm of the drug-loaded PCL scaffold/drug-loaded halloysite-PCL scaffold, and add 5ml of water. Incubate on magnetic stirrer for 1 month. Take out the supernatant at different time intervals. Measure the concentration of the drug released with the UV Spectrometer.

6.2.6 Bacterial Studies

A bacterial experiment was performed to find out the effect of the drug released from halloysites-PCL scaffold on the bacteria. One liter of LB broth was prepared by mixing 10gm of NaCl, 10gm of tryptone, 5gm of yeast extract, 15gm of agar, and enough distilled water to make a final volume of 1 liter. This LB broth was sterilized by autoclaving at $121^\circ C$ for 15 minutes. After autoclaving, LB broth was poured into

different plates, which were allowed to solidify overnight. The next day, a loop full culture of *Escherichia coli (E. coli)* bacteria was spread on the LB broth plates. Bacteria were allowed to grow overnight. Next day, drops of drug released from halloysite-PCL scaffold were kept on the bacterial culture in the LB broth plate. The effect of the drug was observed the next day.

6.3   Results

Loading of the halloysites with drugs was based on the vacuum cycling of a halloysite suspension in a saturated drug solution, as was described earlier. The air located in the pores of the halloysites was replaced by the drug solution during this process. This cycle was repeated three times in order to get the highest loading. Brilliant Green, Chlorhexidine, Iodine, Curcuma Longa, Povidine Iodine, Amoxycillin and Potassium Calvulanate and Doxycycline drugs were used for loading in the halloysites.

6.3.1   Drug Release from Halloysites

Figures 6.2 - 6.8 show drug release profiles form the halloysites for Brilliant Green, Chlorhexidine, Iodine, Curcuma Longa, Povidone Iodine, Amoxycillin and Potassium Calvulanate, and Doxycyclin respectively. A drug release study was performed in water at room temperature. The suspension of the halloysite nanotubes was constantly stirred with the magnetic stirrer during the entire release process in order to establish an equilibrium condition. Samples for analysis were taken from the suspension by centrifugation. Concentration of the drug was determined by UV spectrophotometer. Here, 96.52% of Brilliant Green was released from halloysites in the first 5 hours (Figure 6.2); 84.95% of Chlorhexidine was released from halloysites in the first 4 hours (Figure 6.3); 92.68% of Iodine was released from halloysites in the first 5 hours (Figure 6.4);

93.4% of Curcuma Longa was released from halloysites in the first 8 hours (Figure 6.5);

76% of Povidone Iodine was released from halloysites in the first 6.5 hours (Figure 6.6);

94.83% of Amoxycillin and Potassium Calvulanate was released from halloysites in the

first 5 hours (Figure 6.7); and 98.73% of Doxycycline was released from halloysites in

the first 4 hours (Figure 6.8).
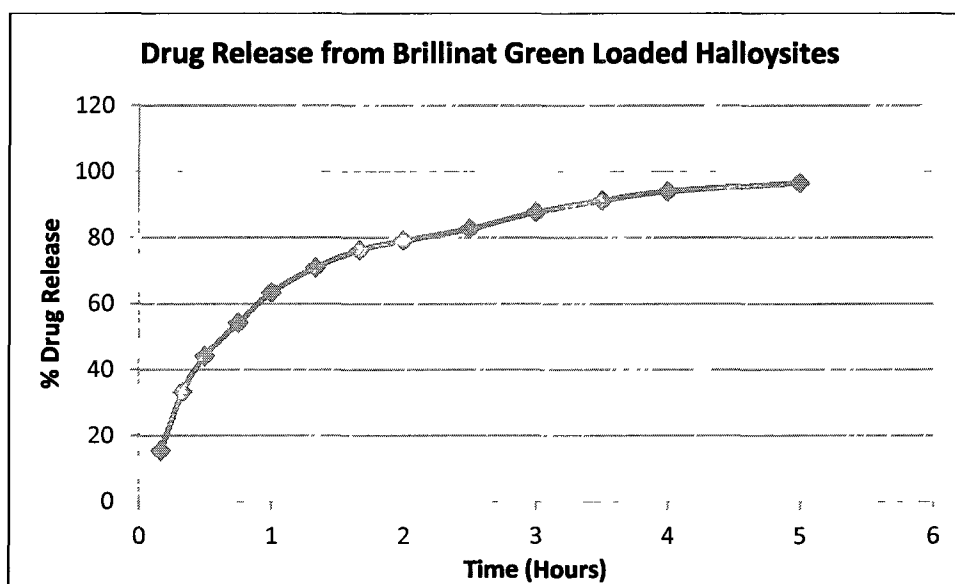
Figure 6.2 Brilliant Green Release Profile from Halloysites.

Drug Release from Chlorhexidine Loaded Halloysites
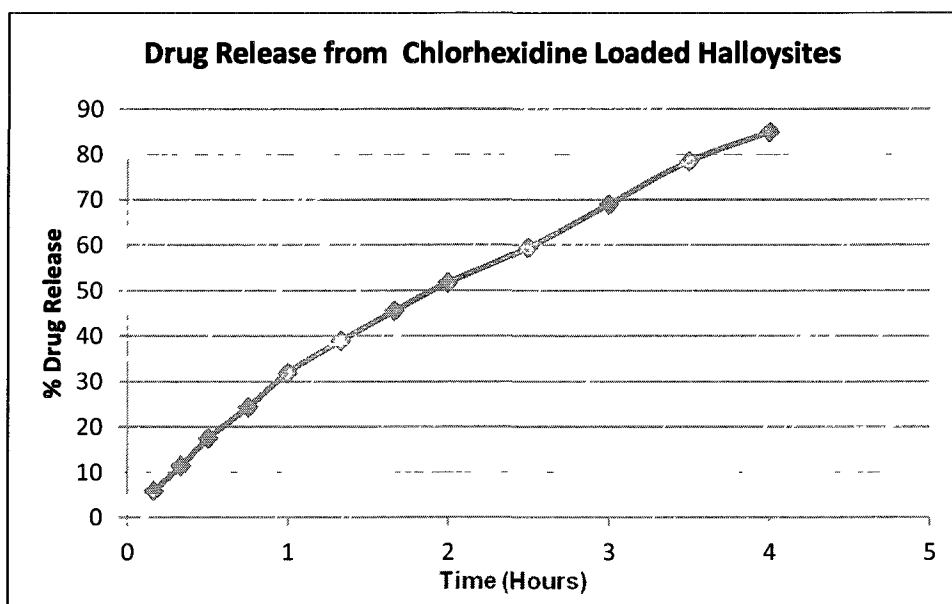
Figure 6.3 Chlorhexidine Release Profile from Halloysites.

Drug Release from Iodine Loaded Halloysites
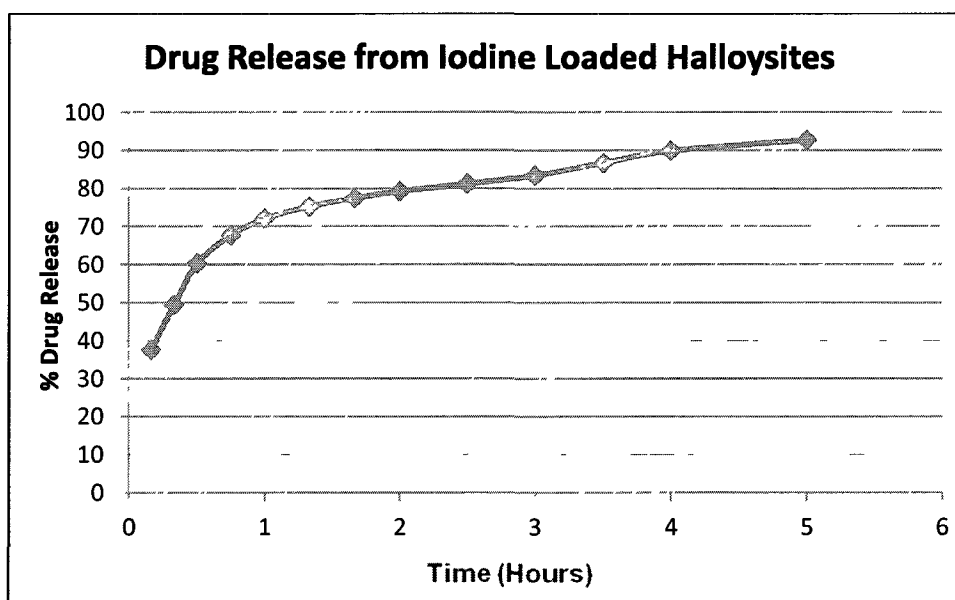
Figure 6.4 Iodine Release Profile from Halloysites.
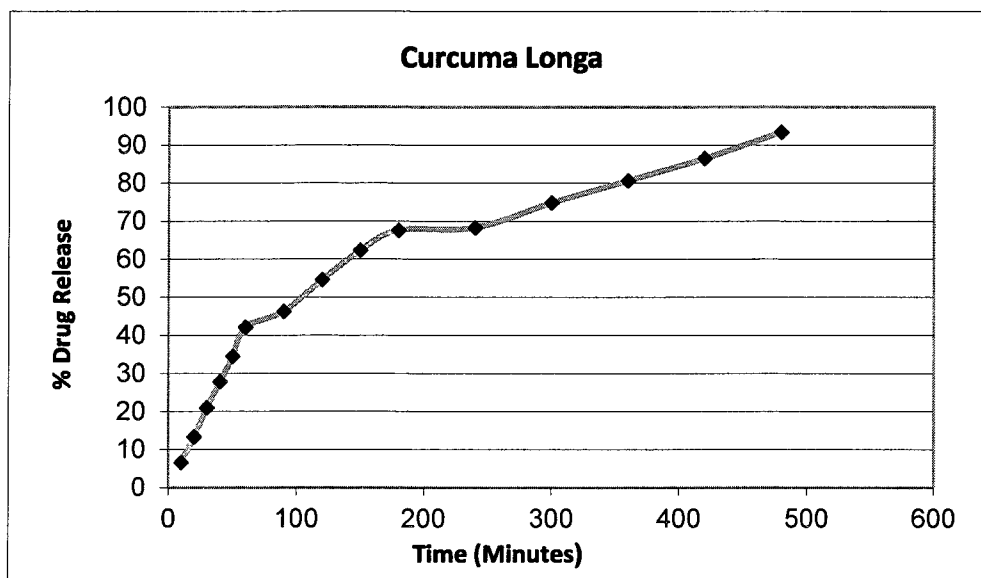
Figure 6.5 Curcuma Longa Release Profile from Halloysites.
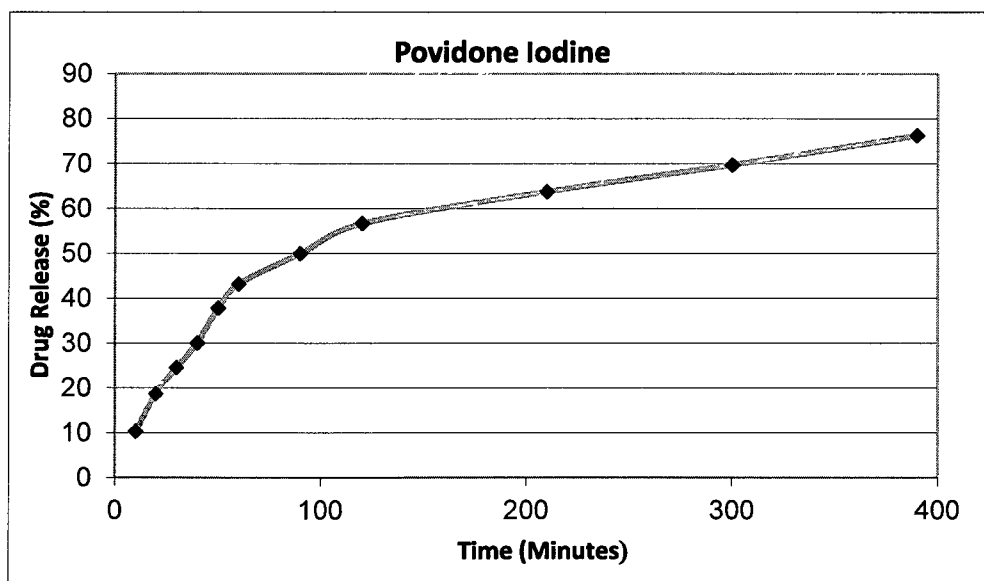
Figure 6.6 Povidone Iodine Release Profile from Halloysites.
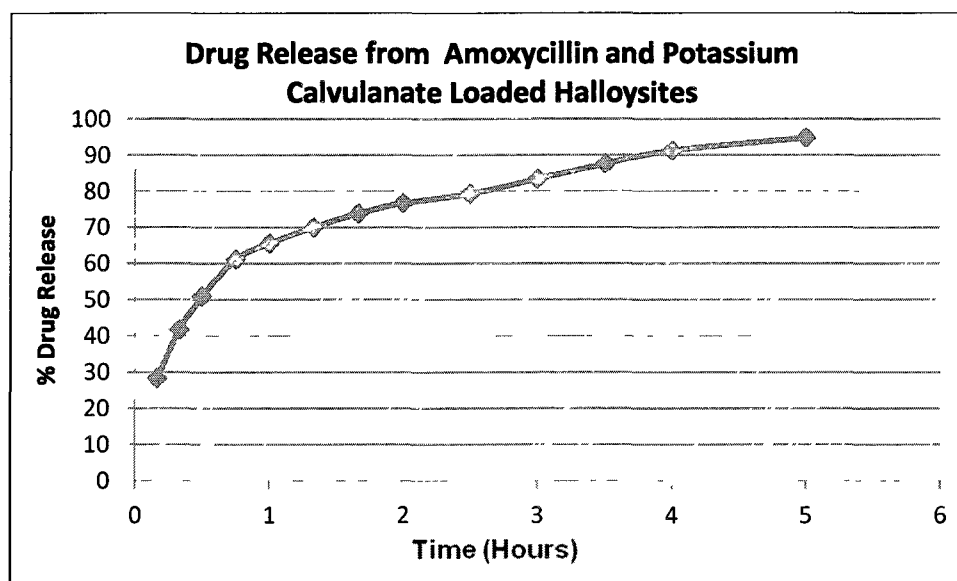
Figure 6.7 Amoxycillin and Potassium Calvulanate Release from Halloysites.
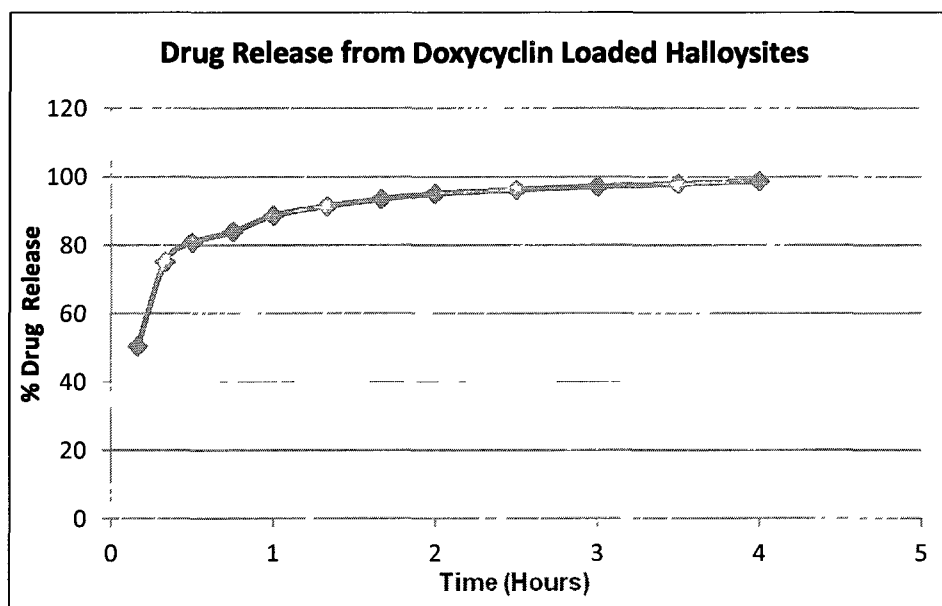
Figure 6.8 Doxycycllin Release from Hallloysites.

6.3.2 Drug Release from PCL/Halloysite-PCL Scaffold

Figures 6.9 and 6.10 show drug release profiles form the Brilliant Green loaded PCL scaffold and the Brilliant Green loaded halloysites-PCL scaffold, respectively. A drug release study was performed in 5ml of water at room temperature. The suspension

containing the drug-loaded scaffold was constantly stirred with the magnetic stirrer during the entire release process in order to establish an equilibrium condition. Samples for analysis were taken at specific time intervals. The concentration of the drug was determined by UV spectrophotometer. It was observed that 98.58% of Brilliant Green was released from the Brilliant Green loaded PCL scaffold in 25 days (Figure 6.9), and 100% of Brilliant Green was released from Brilliant Green loaded halloysite-PCL scaffold in 5 days (Figure 6.10). Figure 6.11 shows the absorption maximum for Brilliant Green. The absorption maximum for Brilliant Green was 623nm. It was seen that 91.67% of Amoxycillin and Potassium Calvulanate was released in 9.6 days from Amoxycillin and Potassium Calvulanate loaded halloysite-PCL scaffold (Figure 6.12) and 97.46% of Amoxycillin and Potassium Calvulanate was released from Amoxycillin and Potassium Calvulanate loaded PCL scaffold in 5.6 days (Figure 6.13). Further, 95.16% of Doxycycline was released from Doxycycline loaded PCL Scaffold (Figure 6.14). Figure 6.15 shows absorption maximum for Amoxycillin and Potassium Calvulanate, which was 274nm.

Drug Release from Brilliant Green Loaded PCL Scaffold
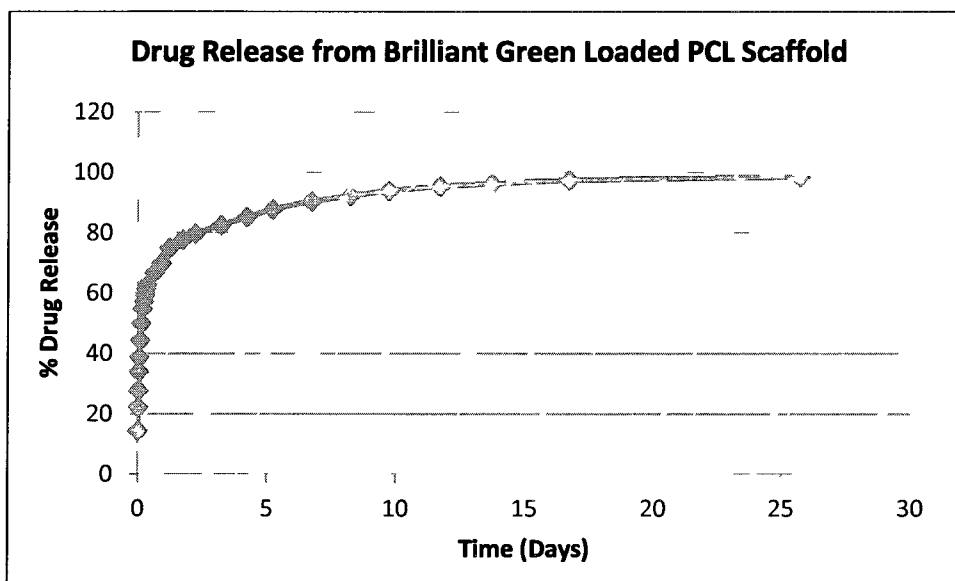
Figure 6.9 Drug Release from Brilliant Green Loaded PCL Scaffold.

Drug Release from Brilliant Green Loaded Halloysite-PCL Scaffold
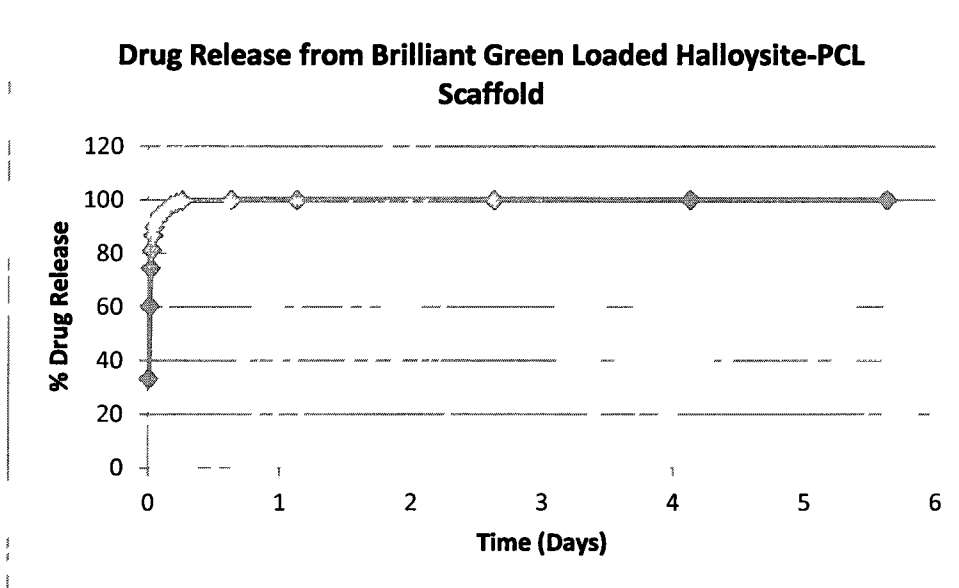
Figure 6.10 Drug Release from Brilliant Green Loaded Halloysite-PCL Scaffold.
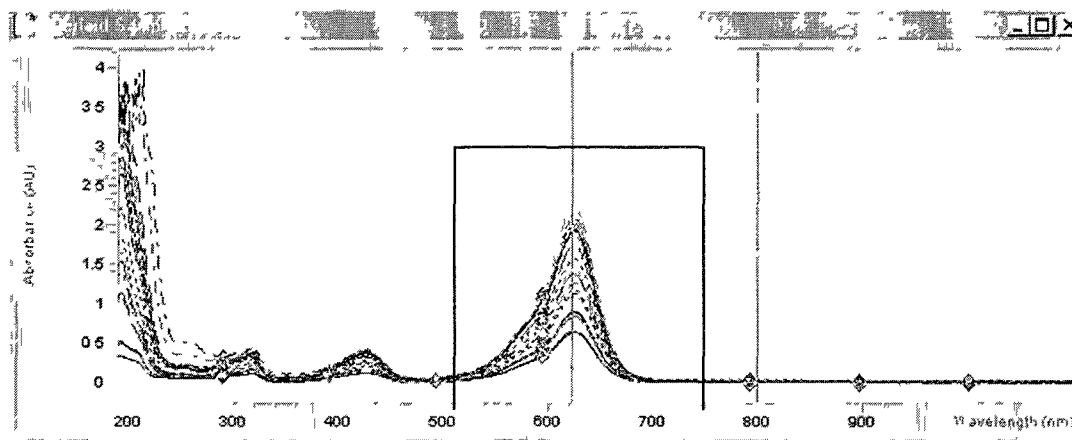
Figure 6.11 Absorption Maximum for Brilliant Green at 623nm.
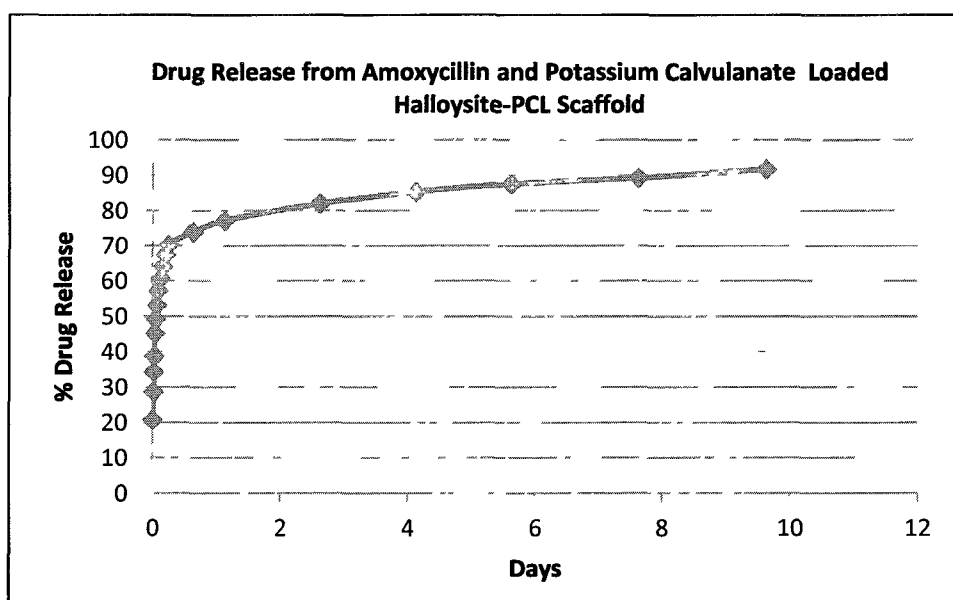
Figure 6.12 Drug Release from Amoxycillin and Potassium Calvulanate Loaded Halloysite-PCL Scaffold.
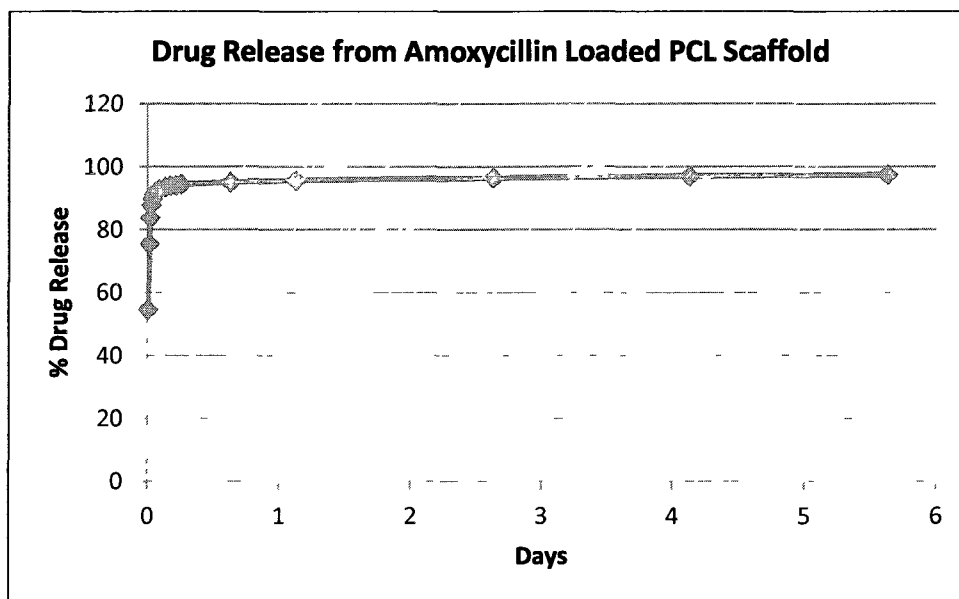
Figure 6.13 Drug Release from Amoxycillin and Potassium Calvulanate Loaded PCL Scaffold.
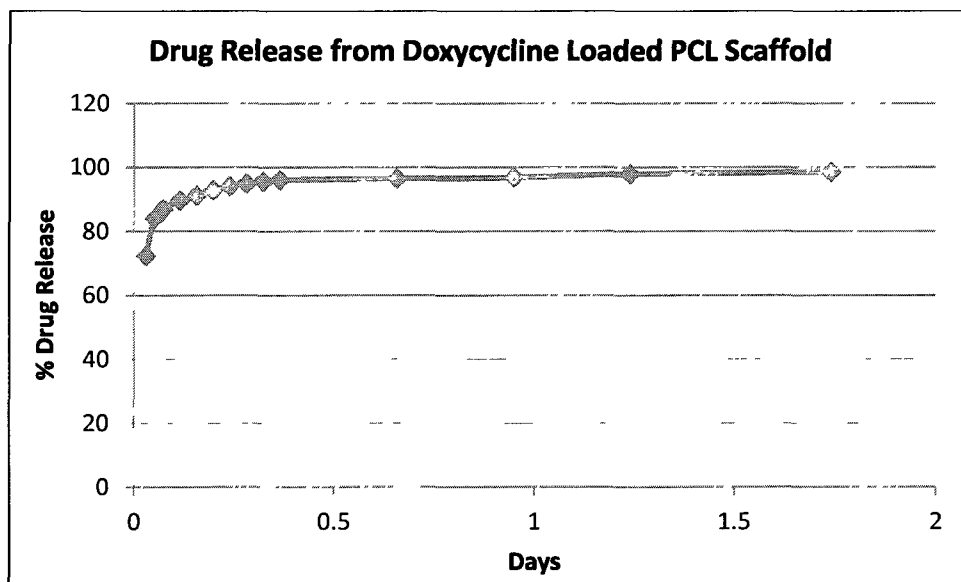
Figure 6.14 Drug Release from Doxycycline Loaded PCL Scaffold.
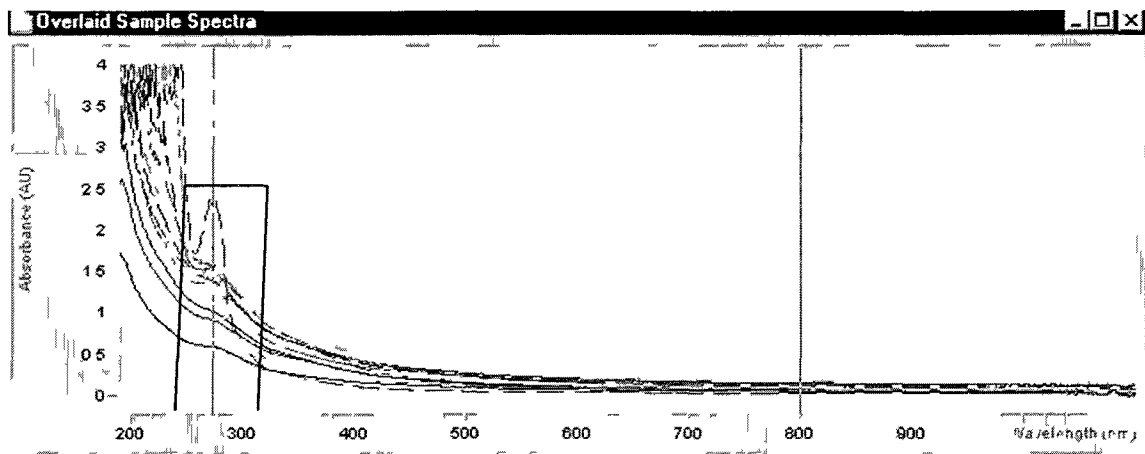
Figure 6.15 Absorption Maximun for Amoxycillin and Potassium Calvulanate at 274nm.

6.3.3 Drug-Loaded PCL Scaffolds and Halloysites-PCL Scaffolds

Scaffolds were examined under the microscope. Figure 6.16 shows fiber arrangement in a band aid obtained from Johnson and Johnson company. These fibers do not contain any drug. Figures 6.17-6.19 show fiber arrangements in an Amoxycillin loaded PCL scaffold, a Brilliant Green loaded PCL scaffold, and a scaffold containing two drug layers (a Brilliant Green loaded PCL layer and an Amoxycillin loaded PCL layer) respectively. The Amoxycillin loaded PCL scaffold showed white color as Amoxycillin is white (Figure 6.17). The Brilliant Green loaded PCL scaffold showed a green color as Brilliant Green is green (figure 6.18); whereas, the scaffold containing two drug layers (a Brilliant Green loaded PCL layer and an Amoxycillin loaded PCL layer) showed both white and bluish green colors (Figure 6.19).
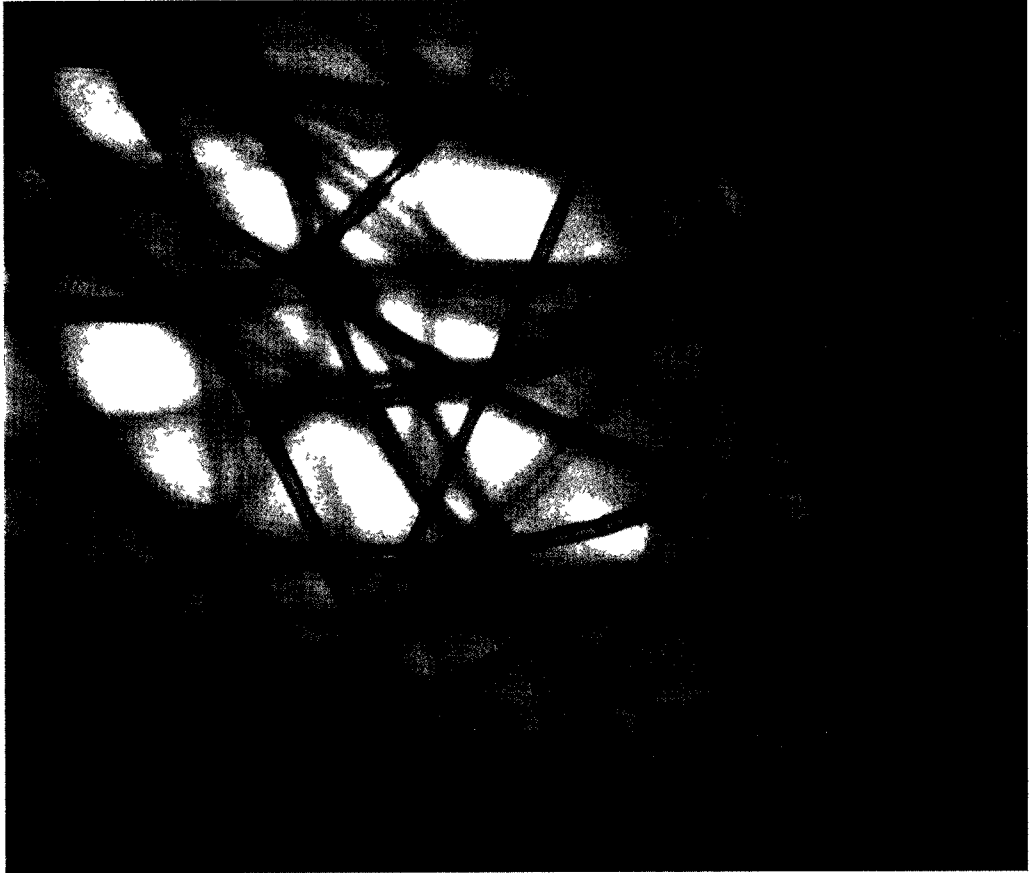
Figure 6.16 Band-Aid (Johnson and Johnson).
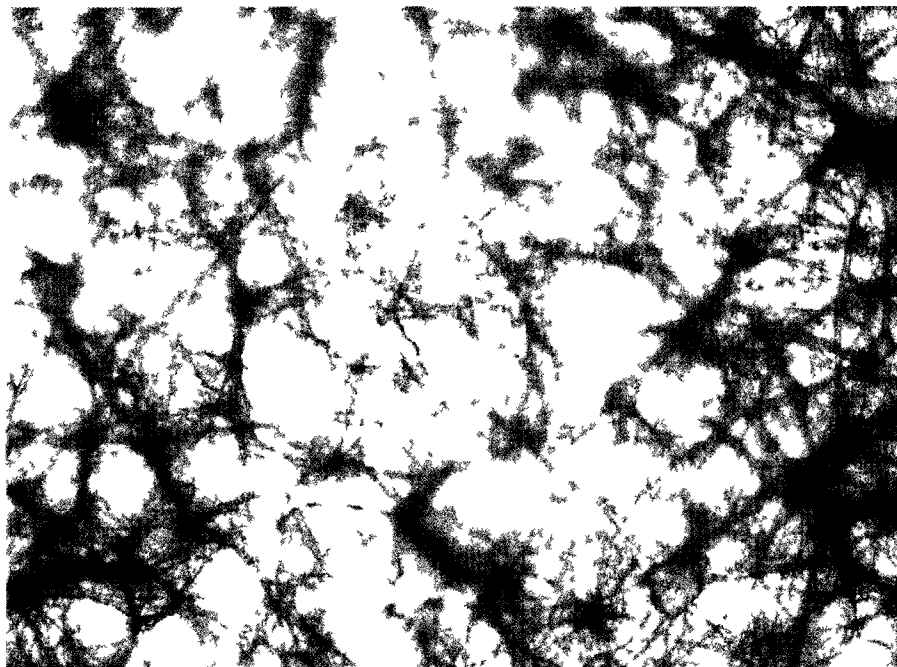
Figure 6.17 Amoxycillin Loaded PCL Scaffold.

Figure 6.18 Brilliant Green Loaded PCL Scaffold.
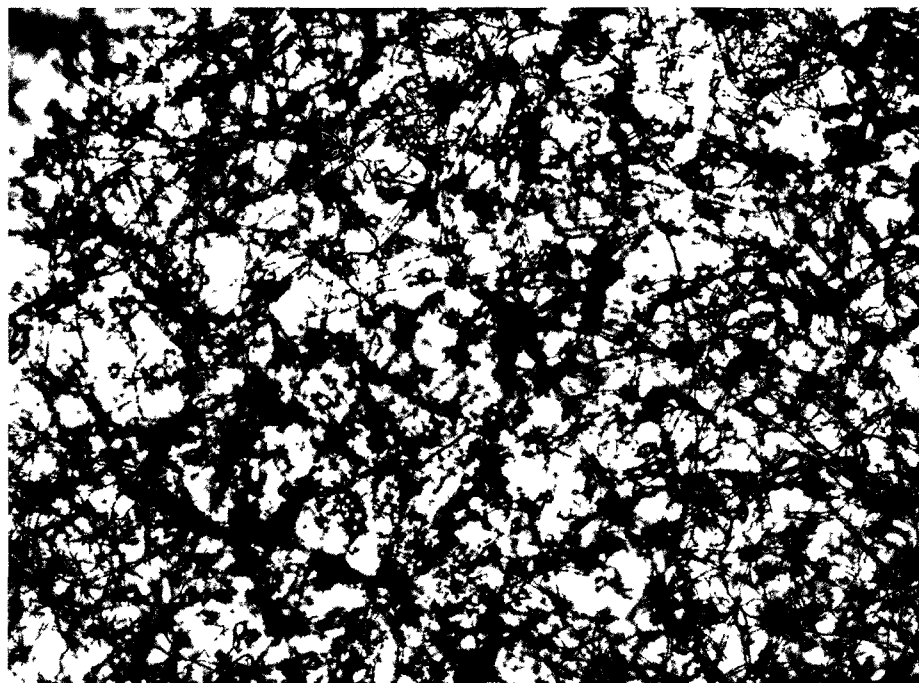
Figure 6.19 Brilliant Green Loaded PCL+ Amoxycillin Loaded PCL Scaffold.

6.3.4 Bacterial Studies

A bacterial study was done to find out the effectiveness of the drug released from the halloysites-PCL scaffold on *E.coli*. A bacterial culture of *E.coli* was spread on an agar plate and lines were drawn on the outside of the plate to create "sectors". These bacterias were allowed to grow overnight. The next day, drops of drug released from halloysites-PCL scaffold was kept in one sector, and the plates were allowed to grow overnight again at 37°C. The next day, bacteria were killed in a region where a drop of the drug released from halloysites-PCL scaffold was kept (Figure 6.20). Here, Amoxycillin and Potassium Calvulanate released from halloysites-PCL scaffold was used. In Figure 6.20 arrow indicates the areas were bacteria were killed.

Figure 6.20 Effect of Amoxycillin and Potassium Calvulanate Released from Halloysite-PCL Scaffold on Bacteria.

6.4   Discussion

Halloysite nanotubes have a high specific surface area [120]. For halloysite nanotubes, the capillary force is very high. This results in a quicker adsorption of materials. Absorption of small molecules mainly takes place by their intercalation into interlayer space [122, 123, 124]; whereas, big molecules and drugs are bound to the outer and inner faces of halloysites [111, 125]. The adsorptive properties of halloysites are significantly affected by their surface charges. These surface charges are pH-dependent [110, 40]. Brilliant Green, Chlorhexidine, Iodine, Curcuma Longa, Povidine Iodine, Amoxycillin and Potassium Calvulanate, and Doxyxycline drugs were successfully loaded into halloysites. A drug release study was performed in water at room temperature. The suspension of the drug-loaded halloysite, the drug-loaded PCL scaffold and the drug-loaded halloysite-PCL scaffold was constantly stirred with a magnetic stirrer during the entire release process in order to establish an equilibrium condition. Samples for analysis were taken from the suspension by centrifugation. The concentration of the drug was determined by UV spectrophotometer. Each drug had a different release profile. This indicated that the halloysite can be used for drug-delivery. Ninety six percent of Brilliant Green was released from the halloysite in the first 5 hours. Ninety eight percent of Brilliant Green was released from the Brilliant Green loaded PCL scaffold in 25 days, whereas, 100% of Brilliant Green was released from the Brilliant Green loaded halloysite-PCL scaffold in 5 days. These results indicate halloysites, PCL scaffold and halloysite-PCL composite scaffolds can be used for sustained drug release. Results of Amoxycillin and Potassium Calvulanate drug release from halloysites, PCL Scaffold and halloysite-PCL scaffold also indicate that drug-loaded halloysites, PCL Scaffold and halloysite-PCL scaffold can be used for sustained drug release. According to this study, we can fabricate

scaffolds containing two or more different drug-loaded layers and we can create a scaffold where drug 1 is loaded into the halloysite, drug 2 is loaded into the PCL fibers and drug 3 is coated on the surface of the scaffold.

CHAPTER 7

CONCLUSION

In this dissertation, two different materials were nanoengineered for application in regenerative medicine. The first material used was titanium and the second was halloysite-PCL scaffold. The present study investigated anodized titanium, as a surface modified nanoporous substrate. Uniform nanopores of 78nm diameter were produced by optimizing the wt% of HF, applying the voltage and using two different molar concentration of H_2SO_4. Nanoporous titanium showed higher cell proliferation, total protein synthesis and mineralization compared to smooth titanium.

The fabrication of the halloysite-PCL scaffold was optimized by using different wt% of the halloysite in the PCL-chloroform mixture. The location of the halloysite in the halloysite-PCL scaffold was finalized by use of SEM and FTIC labeling of the halloysite. 2wt% halloysites in the PCL-chloroform mixture gave the best architecture. Up to 7wt% halloysites produced a fair quality of the halloysite-PCL scaffold. The type I collagen coated halloysite-PCL scaffold achieved higher cell proliferation, protein synthesis and mineralization faster than the halloysite-PCL scaffold and the PCL scaffold.

According to the current study, we can construct a scaffold containing two or more drug-loaded layers. We can also create a scaffold where drug 1 is loaded into the halloysite, drug 2 is loaded into the PCL fibers and drug 3 is coated on the surface. Brilliant Green release from the drug-loaded Halloysites, the drug-loaded PCL scaffold

and the drug-loaded Halloysites-PCL scaffold were observed. Results show that the drug-loaded Halloysites-PCL scaffolds and the drug-loaded PCL scaffold were more effective in delivering drugs over a longer period of time compared to drug-loaded halloysites. Therefore, the PCL/halloysite-PCL scaffold can be used as a drug-loaded band aid for sustained drug release in the future.

CHAPTER 8

FUTURE WORK

Several studies can be done in the future to further build upon the obtained results. Future studies need to be done to advance this development such as:

- Use of local anesthetic drug, anti-inflammatory drugs, growth factors and other drugs for encapsulation and sustained release from halloysite.

- Check the effect of the growth factor loaded halloysite-PCL scaffold on osteoblasts.

- Application of layer-by-layer assembly, using various polymers on the drug-loaded halloysite-PCL scaffold as an additional step for controlled for drug diffusion.

- Elaboration of drug-loading study of halloysite for application in cosmetics.

- Investigate the growth of osteoblasts on nanoporous titanium loaded with growth factors.

- Try a combination of nanoporous titanium and layer-by-layer technique.

- Nanoporous titanium with surface functionalization with bioactive coating such as collagen should be tested.

- Check the hybrid micro/nano-textured titanium surface for osteoblast growth.

- In the SEM image (Figures 8.1 and 8.2) white clay (multani mitti) looks similar to halloysites, so further study should be done to find out its properties.
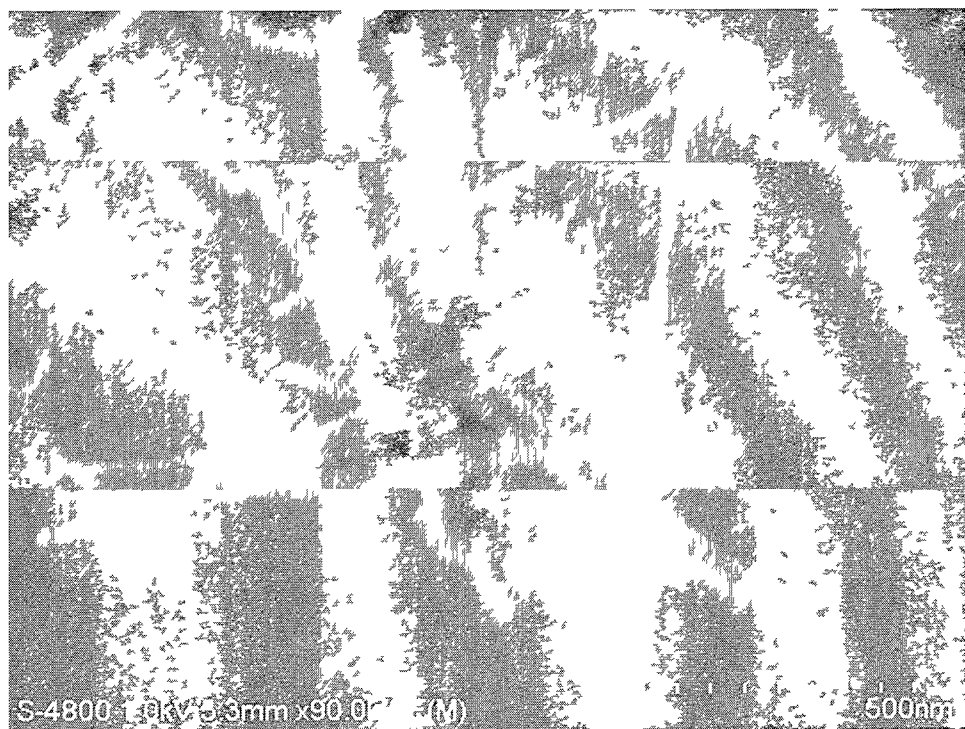
Figure 8.1 SEM Image of White Clay (Multani Mitti).
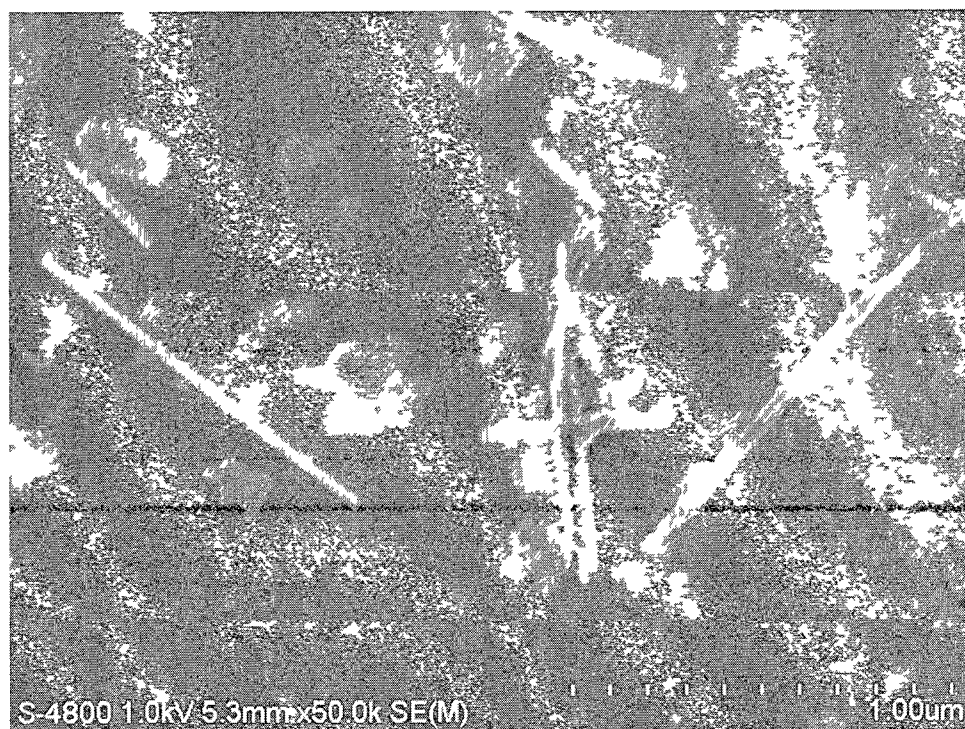
Figure 8 2 SEM Image of White Clay (Multani Mitti).

APPENDIX A

PREPARATION OF COMPLETE α-MEM

Materials and Equipment Needed

αMEM (alpha minimum essential medium), fetal bovine serum and antibiotic (AB) were used.

Method

Complete αMEM (alpha minimum essential medium) is prepared by mixing 90% αMEM with 2mM L-glutamine and 1mM sodium pyruvate without ribonucleosides and deoxyribonucleosides, 10% fetal bovine serum and 1% antibiotics.

APPENDIX B

THAWING CRYOPRESERVED VIALS

Materials and Equipment Needed

Cryovials containing osteoblasts, 75% alcohol, centrifuge tubes, complete αMEM and tissue culture flasks were used.

Method

A liquid nitrogen tank contains different containers labeled with varying colours. Cryovials of different cell lines are placed in different containers. The log book is checked before taking out cryovials from the liquid nitrogen. When removing cryovials from the liquid nitrogen, protective goggles and gloves need to be worn. After removing from the cryovials cap need to be loosened to release liquid nitrogen trapped in the threads of vial. Re-tight the cap and using a float lower half of the vials was placed in water at room temperature to thaw. Sterilize the exposed area of the vial with 75% alcohol before using it. Transfer the suspension to the centrifuge tube from the vial so that nothing will be left in the cryovial. Add complete αMEM to the desired concentration. Centrifuge it. Discard the supernatant, resuspend the pellet in complete αMEM. Plate the desired number of cells on a tissue culture flask. Ensure the uniform distribution of cells in the the flask to avoid clumps of cells. Incubate the cells at 37°C, 5% CO_2 and 95% air in a humidified cell culture incubator.

APPENDIX C

CELL CULTURE

Materials and Equipment Needed

Seventy percent ethanol, cryovial floating membrane or thawing cells, culture dishes, pipetting aids, sterile pipettes, disposable centrifuge tubes, pipette tips, flask and funnel, hemacytometer, light microscope and 37°C incubator were used. Hanks buffer saline solution (HBSS), trypsin and complete media αMEM were also used.

Method

Laminar hood was cleaned with 70% alcohol. The laminar hood was turn on for 30 minutes so that the laminar hood will be sterilized. Then the cell culture works was started. αMEM was taken out from the refrigerator and equilibrate to 37°C. Sterilization of the bottle surface was done with 70% alcohol in sterile hood. Cryopreserved vial of cells was taken out from the liquid nitrogen storage tank. Osteoblasts were obtained from ATCC (7F2 CRL-12557).

Proper protection for the eyes and hands was used. The cryovial of the cells was kept in a 37°C water bath for thawing. Once it was thaw; it was wiped with 70% alcohol. Cells in the cryovial were transferred to the centrifuge tube, containing 5ml of the complete αMEM. It was centrifuged at 1.2rpm for 7 to 10 minutes. The supernatant was discarded because it contains cell freazing media. The pellet was resuspend in 5ml of complete αMEM. It was transfer into culture dishes. Add some more medium if needed. The culture was incubated at 37°C, 5% CO_2 and 95% humidified air.

APPENDIX D

SUBCULTURING OF THE CELLS

Cell Check

Check for the presence of microbial contamination every day. Using a microscope, check for the confluency of the culture every day. Once the cells become confluent, subcultivate them to keep the cells actively growing.

Harvesting of Cells

Pre-warn HBSS, 1X Trypsin and Complete αMEM medium to room temperature. Take out and discard the medium using sterile pipette from the culture dish. Wash the cell monolayer two times with 5ml of HBSS. HBSS washing is followed by, addition 3-5ml of 1X Trypsin and incubate for 5 minutes at room temperature. Check for the detachment of the cells under the microscope. When the cells start detaching, take out all the media with a sterile transfer pipette and transfer it to a centrifuge tube. Centrifuge at 1.2rpm for 10 minutes. Discard the supernatant. Resuspend the pellet in 5ml of Complete αMEM. Transfer it into culture dishes. Add some more medium if needed. Incubate the culture at 37°C, 5% CO_2 and 95% humidified air.

APPENDIX E

CRYOPRESERVATION OF THE CELLS

Materials and Equipment Needed

Extra osteoblast cells, sterile cryovials, liquid nitrogen and cell freezing medium were used.

Method

Extra osteoblast cells were stored in cryovials in liquid nitrogen for long-term use. The temperature of the liquid nitrogen was maintained at -80°C. Extra Osteoblasts were collected in a centrifuge tube. They were counted for cell numbers. They were centrifuge at 1.2rpm for 7 to 10 minutes. The supernatant of complete αMEM was discarded. The cells were resuspended in cell freezing medium (complete αMEM + 10 % DMSO) at a concentration of about $10^6 - 10^7$ cells/ml. The cryovials were filled with 1-1.5ml of cells suspended in a freezing medium. Before the cryovials were stored at -80°C, they were initially stored for about 6 hours at 4°C and then for 24 hours at -20°C.

APPENDIX F

CELL COUNTING

Materials and Equipment Needed

Hemocytometer, osteoblast cells and microscope were used.

Method

A hemocytometer is used for counting the osteoblast cells per unit volume of a suspension. Cover slips used for the counting chambers are thicker than the usual microscopic cover slips. The cover slip is kept over the counting surface then cell suspension is dropped into one of the V-shaped wells. Due to this, the area under the cover slip fills by capillary action. Once the counting chamber is filled, then the counting grid is focused at a low power. The counting chamber has nine large squares. Each square has an area of $1mm^2$ and the depth of 0.1mm. The osteoblast cell suspension was dilute enough so that the cells do not overlap each other and uniformly distribute on the counting chamber. The central large square was selected to perform the count.

REFERENCES

1. **Popat, Ketul.** *Nanotechnology in Tissue Engineering and Regenerative Medicine.* s.l. : CRC Press, 2011.

2. **Andersen, Ronald M, Rice, Thomas H and Kominski, Gerald F.** *Changing the U.S. Health Care System: Key Issues in Health Services Policy and Management .* s.l. : John Wiley and Sons, 2007.

3. **Tomellini, Renzo, Faure, Uta and Panzer, Oliver.** *European Technology Platform on NanoMedicine Nanotechnology for Health.* s.l. : European Commission, 2005.

4. *Nanotechnology in Regenerative Medicine: the Materials Side.* **Engel, Elisabeth, et al.** 2008, Trends in Biotechnology , Vol. 26, pp. 39-47.

5. *Future Impact of Nanotechnology on Medicine and Dentistry.* **Patil, Mallanagouda, Mehta, Dhoom Singh and Guvva, Sowjanya.** 2, 2008, Journal of Indian Society of Periodontology, Vol. 12, pp. 34-40.

6. *Nanotechnology for Regenerative Medicine: Nanomaterials for Stem Cell Imaging.* **Solanki, Aniruddh, Kim, John D. and Lee, Ki-Bum.** 4, 2008, Nanomedicine, Vol. 3, pp. 567-578.

7. *Nanotechnology on Duty in Medical Applications.* **Kubik, T, Bogunia-Kubik, K and Sugisaka, M.** 2005, Current Pharmaceutical Biotechnology, Vol. 6, pp. 17-33.

8. **U, Meyer, et al.** *Fundamentals of Tissue Engineering and Regenerative Medicine.* s.l. : Springer, 2009.

9. **Modo, Miche and Bulte, Jeff W. M.** *Molecular and Cellular MR Imaging.* s.l. : CRC Press, 2007.

10. **Sargent, John F.** *CRS Report for Congress, Nanotechnology and U.S. Competitiveness: Issue and Options.* s.l. : Science, and Industry Division, 2008.

11. *Engineering Structurally Organized Cartilage and Bone Tissues.* **Sharma, B and Elisseeff, J.H.** 2004, Ann Biomed Eng, Vol. 32, pp. 148-159.

12. **Atala, A., et al.** *Principles of Regenerative Medicine.* s.l. : Academic press, 2008.

13. *Stem Cell and Regenerative Medicine.* **Alvarez, Antonia, et al.** 2009, Current Stem Cell Research and Therapy, Vol. 4, pp. 287-297.

14. *Regenerative Pharmacology:The Future is Now.* **Andersson, Karl-Erik and Christ, George J.** 2, 2007, Molecular Interventions, Vol. 7, pp. 79-86.

15. *Engineering Structurally Organized Cartilage and Bone Tissues.* **Sharma, B and Elisseeff, J.H.** 1, 2004, Ann Biomed Eng, Vol. 32, pp. 148-159.

16. *Nanotechnology as Tailored Biological Probes.* **Taton, T.Andrew.** 7, s.l. : Elsevier Science Ltd, 2002, Trends in Biotechnology, Vol. 20, pp. 277-279.

17. **Hosokawa, Masuo, et al.** *Nanoparticle Technoogy Handbook.* s.l. : Elsevier, 2007.

18. **Jain, Kewal K.** *The Handbook of Nanomedicine.* s.l. : Springer, 2008.

19. *Mesoporous Silica Nanoparticles for Drug Delivery and Biosensing Applications.* **Slowing, I.I., et al.** 8, 2007, Vol. 17, pp. 1225-1236.

20. *Nanoparticles as Tools to Study and Control Stem Cells.* **Ferreira, L.** 4, 2009, J. Cell Biochem, Vol. 108, pp. 746-752.

21. *Quantum Dots for Live Cells, in Vivo Imaging, and Diagnostics.* **Michalet, X., et al.** 5709, 2005, Science, Vol. 307, pp. 538-544.

22. **Nalwa, Hari S.** *Nanostructured Materials and Nanotechnology.* s.l. : Gulf Professional Publishing, 2002.

23. *Labelling of Cells with Quantum Dots.* **Parak, Wolfgang J., Pellegrino, Teresa and Christian, Plank.** 2005, Nanotechnolgy, Vol. 16, pp. R9-R25.

24. *New Opportunities: the Use of Nanotechnologies to Manipulate and Track Stem Cells.* **Ferreira, Lino, et al.** s.l. : Elsevier, 2008, Cell Stem Cell, Vol. 3, pp.136-146.

25. **Kumar, Challa S.** *Nanomaterials for Medical Diagnosis and Therapy.* s.l. : Wiley-VCH, 2007.

26. **Prouty, Malcolm D.** Layer-by-layer Self-assembly of Micro-capsules for the Magnetic Activation of Semi-Permeable Nano-shells. s.l. : Louisiana Tech University, 2007.

27. **Pradeep, T.** *Nano the Essentials.* s.l. : McGraw-Hill Professional, 2007.

28. **Kreuter, Jorg.** *Colloidal Drug Delivery Systems.* s.l. : CRC Press, 1994.

29. **Collings, Peter J.** *Liquid Crystals: Nature's Delicate Phase of Matter.* s.l. : Princeton University Press, 2002, 2002.

30. *Nanoparticles in Liquid Crystals: Synthesis, Self-Assembly, Defect Formation and Potential Applications.* **Hegmann, Torsten, Q, Hao and Marx, Vanessa M.** 3, 2007, Journal of Inorganic and Organometallic Polymers and Materials, Vol. 17, pp. 483-508.

31. *Developments in Liposomal Drug Delivery System.* **Maurer, Norbett, Fenske, David B and Cullis, Pieter R.** 6, 2001, Expert Poin.Biol. Ther., Vol. 1, pp. 1-25.

32. **Gregoriadis, Gregory and Florence, Alexander T.** *Liposome in Drug Delivery.* s.l. : CRC Press, 1993.

33. **Webster, Thomas J.** *Safety of Nanoparticles: From Manufacturing to Medical Applications.* s.l. : Springer, 2008.

34. **Yahya, Noorhana.** *Carbon and Oxide Nanostructures.* s.l. : Springer, 2011.

35. **Reich, Stéphanie, Thomsen, Christian and Maultzsch, Janina.** *Carbon Nanotubes: Basic Concepts and Physical Properties.* s.l. : Wiley-VCH, 2004.

36. *Biosensors Based on Carbon Nanotubes.* **Balasubramanian, Kannan and Burghard, Marko.** 2006, Anal Bioanal Chem, Vol. 385, pp. 452-468.

37. *Applications of Carbon Nanotubes in Drug Delivery.* **Bianco, Alberto, Kostarelos, Kostas and Prato, Maurizio.** 6, 2005, Current Opinion in Chemical Biology, Vol. 9, pp. 674-679.

38. **Bhusha, Bharat.** *Handbook of Nanotechnology.* s.l. : Springer, 2007.

39. **Edwards, Steven Alan.** *The Nanotech Pioneers.* s.l. : Wiley-VCH, 2006.

40. *Halloysite Clay Nanotubes for Controlled Release of Protective Agents.* **Lvov, Yuri M, et al.** 5, s.l. : ACS Nano, 2008, Vol. 2, pp. 814-820.

41. *Exploring and Engineering the Cell Surface Interface.* **Stevens, Molly M and George, Julian H.** November 2005, Science, Vol. 310, pp. 1135-1138.

42. *Surface Modification of Polyester Biomaterials for Tissue Engineering.* **Jiao, Yan-Peng and Fu-Zhai, Cui.** 4, 2007, Biomed Mater, Vol. 2, pp. R24-R37.

43. *Nanostructured Biomaterials for Regenerative Medicine.* **Vinoy, Thomas, Derrick, Dean and Yogesh, Vohra.** 3, 2006, Vol. 2, pp. 155-177.

44. **Webster, Thomas.** *Nanotechnolgy for the Regeneration of Hard and Soft Tissue.* s.l. : World Scientific, 2007.

45. *Bone Tissue Engineering Therapeutics: Controlled Drug Delivery in Three-Dimensional Scaffolds.* **Mouriño, Viviana and Boccaccini, Aldo R.** 43, 2009, Journal of the Royal Society, Vol. 7, pp. 209-227.

46. **Ying, Jackie Y and Ying, Jackie Yi-Ru.** *Nanostructured Materials.* s.l. : Academic Press, 2001.

47. *Material Encapsulation and Transport in Core–Shell Micro/Nanofibers.* **Yarin, A.L, et al.** s.l. : Journal Mater.Chem, 2007, Vol. 17, pp. 2585-2599.

48. *A Modified Porous Titanium Sheet Prepared by Plasma-Activated Sintering for Biomedical Applications.* **Tamaki, Yukimichi, et al.** 2010, Journal of Tissue Engineering, Vol. 2010, pp.1-5.

49. *Biomechanical Comparison of Different Surface Modification for Dental Implants.* **Stephen, F. J., et al.** 6, 2008, The International Journal of Oral and Maxillofacial Implants, Vol. 23, pp. 1037-1046.

50. *Nanotechnology for Regenerative Medicine.* **Khang, D, et al.** 4, August 2010, Biomed Microdevides, Vol. 12, pp. 575-87.

51. *The Impact of Tissue Engineering on Dentistry.* **Baum, Bruce and Mooney, David J.** 3, 2000, Journal of the American Dental Association, Vol. 131, pp. 309-318.

52. *Unite State of America Congressional Record Proceedings and Debates of 106th Congress.* s.l. : United State Goverment Printing Office, 2000.

53. *The Kaiser Permanente National Total Joint Replacement Registry.* **Paxton, Elizabeth W.** 3, 2008, The Permanente Journal, Vol. 12, pp. 12-16.

54. **Wise, Donald Lee.** *Encyclopedic Handbook of Biomaterials and Bioengineering: Applications.* s.l. : CRC Press, 1995. Vol. 2.

55. *Adhesion and Proliferation of OCT-1 Osteoblast-Like Cells on Micro- and Nano-Scale Topography Structuredpoly(L-lactide).* **Yuqing, F., et al.** 21, 2005, Biomaterials, Vol. 26, pp. 4453-4459.

56. *Effects of Different Titanium Alloys and Nanosize Surface Patterning on Adhesion, Differentiation, and Orientation of Osteoblast-like Cells.* **Monsees, T.K., et al.** 2005, Vol. 180, pp. 81-95.

57. *Surface Modification and Cell-materials Interactions with Anodized Ti.* **Das, K., Bose, S. and Bandyopadhyay, A.** 2007, Acta Biomaterialia, Vol. 3, pp. 573-585.

58. *Surface Treatments of Titanium Dental Implants for Rapid Osseointegration.* **Guéhennec, L. Le, et al.** 7, 2007, Vol. 23, pp. 844-854.

59. *Role of Nanotechnology in Novel Drug Delivery System.* **Debijit, Bhowmik, Chiranjib, R.Margret, Chandira and B, Jayakar.** 1, 2009, Journal of Pharmaceutical Science and Technolgy, Vol. 1, pp. 20-35.

60. **Muzykantov, Vladimir and Torchili, V.P.** *Biomedical Aspect of Drug Targeting.* s.l. : Springer, 2002.

61. **Jain, Kewal K.** *The Handbook of Nanomedicine.* s.l. : Springer, 2008.

62. *Encapsulation of Anticancer Drug Cisplatin into Nanotubes.* **Hilder, T.A and Hil, J.M.** s.l. : International Conference on Nanoscience and Nanotechnology, ICONN, 2008.

63. **McKay, Robert B.** *Technological Applications of Dispersions.* s.l. : CRC Press, 1994.

64. **Anal, Anil K.** *Recent Patents on Endocrine, Metabolic & Immune Drug Discovery.* s.l. : Bentham Science Publishers, 2007. Vol. 1.

65. **Laurencin, Cato T and Nair, Lakshmi S.** *Nanotechnology and Tissue Engineering: The Scaffold.* s.l. : CRC Press, 2008.

66. *Methods for Fabrication of Nanoscale Topography for Tissue Engineering Scaffolds.* **Norman, James J and Desai, Tejal A.** 1, Annals of Biomedical Engineering, Vol. 34, pp. 89-101.

67. *Precision Extruding Deposition and Characterization of Cellular Poly-ε-caprolactone Tissue Scaffolds.* **Wang, F, et al.** 1, 2004, Precision extruding deposition, Vol. 10, pp. 42-49.

68. *Micromechanical Control of Cell and Tissue Development:Implications for Tissue Engineering.* **Ghosh, Kaustabh and Ingber, Donald E.** s.l. : Advanced Drug Delivery Reviews, 2007, Vol. 59, pp. 1306-1318.

69. *Extracellular Matrix Dynamics in Development and Regenerative Medicine.* **Daley, W. P., Peters, S. B. and Larsen, Melinda.** 07 08, 2008, Journal of Cell Science, Vol. 121, pp. 255-264.

70. *Collective Review: Bioactive Implants Coated with Poly(D,L-lactide) and Growth Factors IGF-I, TGF-beta1, or BMP-2 for Stimulation of Fracture Healing.* **Schmidmaier, G, et al.** 1, 2006, Journal of Long-Term Effect of Medical Implants, Vol. 16, pp. 61-69.

71. *Degradation Rates of Oral Resorbable Implants (Polylactates and Polyglycolates): Rate Modification with Changes in PLA/PGA Copolymer Ratios.* **Robert, A, Miller, John M and Brady, Duane E.** s.l. : 11, 1977, Journal of Biomedical Materials Research, Vol. 5, pp. 711-719.

72. *Third-Generation Biomedical Materials.* **Hench, Larry L and Polak, Julia M.** 2002, Science, Vol. 295.

73. **Brunette, Donald M.** *Titanium in Medicine:Material Science, Surface Science, Engineering, Biological Responses, and Medical Applications.* s.l. : Springer, 2001.

74. **Bailey, Byron J., Johnson, Jonas T and Newlands, Shawn D.** *Head and Neck Surgery-Otolaryngology.* s.l. : Lippincott Williams & Wilkins, 2006.

75. *A Perspective on Nanophase Materials for Orthopedic Implant Applications.* **Balasundaram, Ganesan and Webster, Thomas J.** 2006, Journal of Materials Chemistry, Vol. 16, pp. 3737-3745.

76. *Enhancing Osseointegration Using Surface-Modified Titanium Implants.* **Yang, Y., et al.** 2006, JOM, Vol. 58, pp. 71-76.

77. *Ti Nano-nodular Structuring for Bone Integration and Regeneration.* **Ogawa, T., et al.** 8, 2008, J Dent Res, Vol. 87, pp. 751-756.

78. *Microrough Titanium Surface Affects Biologic Response in MG63 Osteoblast-like Cells.* **Kim, M., et al.** 2006, Journal of Biomedical Materials Research, Vol. 79A, pp. 1023-1032.

79. *Surface Modification of Titanium, Titanium Alloys.* **Liu, Xuanyong, Chu, Paul K and Ding, Chuanxian.** 2004, Materials Science and Engineering, Vol. 47, pp. 49-121.

80. **Donachie, Matthew J.** *Titanium: A Technical Guide.* s.l. : ASM International, 2000.

81. *TiO2 nanotubes functionalized with regions of bone morphogenetic protein-2 increases osteoblast adhesion.* **Ganesan Balasundaram, Chang Yao, Thomas J. Webster.** 2, 2008, Journal of Biomedical Materials Research Part A, Vol. 84A, pp. 447-453.

82. *Fabrication of Titanium Oxide Nanotubes by Rapid and Homogeneous Anodization in Perchloric Acid/Ethanol Mixture.* **Ishibashi, K., et al.** 1, 2008, Journal of the electrochemical society, Vol. 155, pp. K10-K14.

83. **Jackson, Mark J and Ahmed, Waqar.** *Surface engineered surgical tools and medical devices.* s.l. : Springer, 2007.

84. **Sampson, Karen E.** Nanoporous Alumina on Molybdenum and its Substrates for Nano-Heterojunction Solar Cell Applications. s.l. : University of Kentucky, 2006.

85. *Structure of Nanotubular Titanium Oxide Templates Prepared by Electrochemical Anodization in H_2SO_4/HF Solutions.* **Bestetti, M., et al.** 2007, Thin Solid Films, Vol. 515, pp. 5253-5258.

86. *Titanium Oxide Nanotubes Prepared in Phosphate Electrolytes.* **Ghicov, A., et al.** 2005, Electrochemistry Communications, Vol. 7, pp. 505-509.

87. *A Study of Titanium Nanotube Synthesis in Chloride-Ion-Containing Media.* **Panaitescu, E., Richter, C. and Menon, L.** 1, 2008, Journal of The Electrochemical Society, Vol. 155, pp. E7-E13.

88. **Webster, T.J.** *Nanotechnology for Hard and Soft Tissue.* s.l. : world scientific, 2007.

89. **Amir, Mohammad D.** The oxide Barrier Layer is Considered to Contribute to The Improvement of Corrosion Resistance. Ann Arbor, Michigan : The University of Michigan, 2004.

90. *Comparative Study of Titanium Dioxide Thin Films Produced by Electron-beam Evaporation and by Reactive Low-Voltage Ion Plating.* **Balasubramanian, K., Han, X. F and Guenther, K. H.** 28, 1993, Vol. 32, pp. 5594-5600.

91. **Berger, Michael.** *Nano-Society: Pushing the Boundaries of Technology.* s.l. : Royal Society of Chemistry, 2009.

92. *The Basic Science of Peri-implant Bone Healing.* **Kuzyk, Paul RT and Schemitsch, Emil H.** 2, 2011, Indian Journal of Orthopaedics, Vol. 45, pp. 108-115.

93. *Nanobiotechnology: Implications for The Future of Nanotechnology in Orthopedic Applications.* **Sato, Michiko and Webster, Thomas J.** 1, 2004, Orthopedic Nanobiotechnology, Vol. 1.

94. **McDonald, John, Burroughs, Andrew and Feagan, Brian.** *Evidence-Based Gastroenterology and Hepatology.* s.l. : John Wiley and Sons, 2010.

95. **Truskey, G.A., Yuan, F. and D.F. Katz.** *Transport Phenomena in Biological System.* 2. s.l. : Pearson Education, 2009.

96. *Electrospun Nanofiber Scaffolds: Engineering Soft Tissues.* **Kumbar, S. G., et al.** 2008, Biomedical Materials, Vol. 3.

97. *Electrospinning of Nanofibers with Core-sheath, Hollow, or Porous Structures.* **McCann, Jesse T, Li, Dan and Xia, Younan.** 2005, Journal of Materials Chemistry, Vol. 15, pp. 735-738.

98. *Electrospinning: A whipping Fluid Jet Generates Submicron Polymer Fibers.* **Shin, Y. M., et al.** 2001, Applied Physics Letters, Vol. 78, pp. 1149-1151.

99. *Experimental Study on Relationship Between Jet Instability and Formation of Beaded Fibers During Electrospinning.* **Zuo, W. W., et al.** 2005, Polymer Engineering and Science, Vol. 45, pp. 704-709.

100. *Electrospinning of Polyurethane Fibers.* **Demir, M. M., et al.** 2002, Polymer, Vol. 43, pp. 3303-3309.

101. **Badami, Anand Shreyans.** Bioresorbable Electrospun Tissue Scaffolds of Poly(ethylene glycol-b-lactide) Copolymers for Bone Tissue Engineering. Blacksburg, VA : s.n., 2004.

102. *The Effect of Processing Variables on the Morphology of Electrospun Nanofibers and Textiles.* **Deitzel, J. M., et al.** 2001, Polymer, Vol. 42, pp. 261-272.

103. *Continuous Electrospinning of Aligned Polymer Nanofibers onto a Wire Drum Collector.* **Katta, P., et al.** 2004, Nano Lette, Vol. 4, pp. 2215-2218.

104. *Controlling Surface Morphology of Electrospun POIN-StWene Fibers: Effect of Humidity and Molecular Weight in Electrospinng Process.* **Casper, C. L., et al.** 2004, Macromolecules, Vol. 37, pp. 573-578.

105. **Ramakrishna, Seeram.** *An Introduction to Electrospinning and Nanofibers.* s.l. : World Scientific, 2005.

106. *Development and Characterization of PLGA Nanospheres and Nanocapsules Containing Xanthone and 3-methoxyxanthone.* **Teixeiraa, Maribel, et al.** 3, 2005, European Journal of Pharmaceutics and Biopharmaceutics, Vol. 59, pp. 491-500.

107. *Thermal Stability and Flame Retardant Effects of Halloysite Nanotubes on Poly(Propylene).* **Du, Mingliang, Guo, Baochun and Jia, Demin.** 6, 2006, European Polymer Journal, Vol. 42, pp. 1362-1369 .

108. *Nonlinear Optics of Nontoxic Nanomaterials.* **Yelleswarapu, Chandra S., et al.** 2010, Optics Communications , Vol. 283, pp. 438-441.

109. *Halloysite Nanotubes as Biomimetic Nanoreactors.* **Shchukin, Dmitry G., et al.** 5, 2005, Small, Vol. 1, pp. 510-513.

110. *Controlled Drug Delivery with Nanoparticles: Current Possibilities and Future Trends.* **Couvreur, P., Dubernet, C. and Puisieux, F.** 1995, European Journal of Pharmaceutics and Biopharmaceutics , Vol. 41, pp. 2-13.

111. *Modification of Surface Charge Properties during Kaolinite to Halloysite – 7A Transformation.* **Tari, G., et al.** 1999, Journal Colloids and Interface Science, Vol. 210, pp. 360-366.

112. *In-vitro Release Characteristics of Tetracycline HCI, Khellin and Nicotinamide adenine dineculeotide from Halloysite; A Cylindrical Mineral.* **Price, R., Gaber, B. and Lvov, Y.** 2001, Journal of Microencapsulation, Vol. 18, pp. 713-722.

113. *Morphology and Structure of Endellite and Halloysite.* **Bates, T., Hildebrand, F. and Swineford, A.** 1950, American Mineralogist, Vol. 35, pp. 463-484.

114. *Cytocompatibility and Uptake of Halloysite Clay Nanotubes.* **Vergaro, Viviana, et al.** 3, 2010, Biomacromolecules, Vol. 11.

115. *Halloysite Tubes as Nanocontainers for Anticorrosion Coating with Benzotriazole.* **Abdullayev, Elshad, et al.** 7, 2009, Applied Materials and Interfaces, Vol. 1, pp. 437-443.

116. **Bergaya, Faïza, Theng, B. K. G and Lagaly, Gerhard.** *Handbook of Clay Science.* s.l. : Elsevier, 2006.

117. **Essington, Michael E.** *Soil and Water Chemistry: an Integrative.* s.l. : CRC Press, 2004.

118. *Cytocompatibility and Uptake of Halloysite Clay Nanotubes.* **Vergaro, Viviana, et al.** 3, 2010, Biomacromolecules, Vol. 11, pp. 820-826.

119. *The Effect of Halloysite Nanotubes as a Novel Nanofiller on Curing Behaviour, Mechanical and Microstructural Properties of Ethylene Propylene Diene Monomer (EPDM) Nanocomposites.* **Ismaila, H., et al.** 3, 2009, Polymer-Plastics Technology and Engineering, Vol. 48, pp. 313-323.

120. *Characterisation of Halloysite for Use as a Microtubular Drug Delivery System.* **Levis, S. R. and Deasy, P. B.** 2002, International Journal of Pharmaceutics, Vol. 243, pp. 125-134.

121. *Characteristics of Fine Pores in Some Halloysites.* **Churchman, G. J, et al.** 2, 1995, Vol. 30, pp. 89-98.

122. *Behavior of Halloysite Clay Under Formamide Treatment.* **Joussein, E., Petit, S. and Delvaux, B.,.** 2007, Applied Clay Science, Vol. 35, pp. 17-24.

123. *Vibrational Spectra and Structure of Kaolinite: A Computer Simulation Study.* **Bougeard, D., Smirnov, K. S. and Geidel, E.** 2000, Journal of Physical Chemistry, Vol. 104, pp. B9210-9217.

124. *Intercalation of Salts in Halloysite.* **Carr, R. M., Chaikum, N. and Patterson, N.,** 1978, Clay and Clay minerals, Vol. 26, pp. 144-152.

125. *Formulation and Preliminary in vivo Dog Studies of a Novel Drug Delivery System for the Treatment of Periodontitis.* **Kelly, H. M., et al.** 2004, International Journal of Pharmaceutics, Vol. 274, pp. 167-183.

126. **Veerabadran, Nalinkanth G.** Nanoengineered Templates for Controlled Delivery of Bioactive Compounds. Ruston : Louisiana Tech University, 2008.

127. **Walsh, Ronald A.** *Electromechanical Design Handbook.* 3. s.l. : McGraw-Hill, 2000.

128. *Self-organized High Aspect Ratio Porous Hafnium Oxide Prepared by Electrochemical Anodization.* **Tsuchiya, Hiroaki and Schmuki, Patrik.** 1, 2005, Electrochemistry Communications, Vol. 7, pp. 49-52.

129. **McKeen, Laurence W.** *Fluorinated Coatings and Finishes Handbook: The Definitive User's Guide and Databook.* s.l. : William Andrew Publishing, 2006.

130. **Pocius, Alphonsus V.** *Adhesion and Adhesives Technology: An Introduction.* s.l. : Carl Hanser Verlag, 2002.

131. **Granqvist, Claes G.** *Handbook of Inorganic Electrochromic Materials.* s.l. : Elsevier, 1995.

132. **Wheeler, Barbara and Wilson, Lori J.** *Practical Forensic Microscopy: A Laboratory Manual.* s.l. : John Wiley and Sons, 2008.

133. **Reed, S. J. B.** *Electron Microprobe Analysis and Scanning Electron Microscopy in Geology.* 2. s.l. : Cambridge University Press, 2005.

134. **Goldstein, Joseph, et al.** *Scanning Electron Microscopy and X-Ray Microanalysis.* [ed.] 3. s.l. : Springer, 2003. Vol. 3.

135. **Reimer, Ludwig.** *Scanning Electron Microscopy: Physics of Image Formation and Microanalysis.* 2. s.l. : Springer, 1998.

136. **Schatten, Heide and Pawley, James B.** *Biological Low-Voltage Scanning Electron Microscopy.* s.l. : Springer, 2008.

137. *Electrostatic Field-assisted Alignment of Electrospun Nanofibres.* **Zussman, A Theron and Yarin, A L.** 2011, Nanotechnology, Vol. 12, pp. 384-390.

138. **Duquesne, Sophie, Magniez, Carole and Camino, Giovanni.** *Multifunctional Barriers for Flexible Structure.* s.l. : Springer, 2007.

139. *Proceedings of the American Society for Composites: Twentieth Technical Conference.* **Ko, Frank K, et al.** s.l. : DEStech Publications, 2005.

140. **Goddard, William A, et al.** *Handbook of Nanoscience, Engineering, and Technology.* 2. s.l. : CRC press.

141. **Kumar, Challa.** *Tissue, Cell and Organ Engineering.* s.l. : Wiley-VCH Verlag Gmbh and Co, 2006. Vol. 9.

142. **Tateishi, Tetsuya.** *Biomaterials in Asia: in Commemoration of the 1st Asian Biomaterials Congress.* s.l. : World Scientific, 2008.

143. *Electrospinning Process and Applications of Electrospun Fibers.* **Doshi, Jayesh and Reneker, Darrell H.** 1995, Journal of Electrostatics, Vol. 35, pp. 151-160.

144. **Slavík, Jan.** *Fluorescence Microscopy and Fluorescent Probes.* s.l. : Plenum Press, 1998. Vol. 2.

145. **Wilkinson, M and Schut, F.** *Digital Image Analysis of Microbes: Imaging, Morphometry, Fluorometry, and Motility Techniques and Applications.* s.l. : John Wiley and Sons Ltd, 1998.

146. **Hui, Yiu H.** *Handbook of Food Science, Technology, and Engineering.* s.l. : CRC press, 2006. Vol. 4.

147. **Dykstra, Michael J and Reuss, Laura E.** *Biological Electron Microscopy: Theory, Techniques, and Troubleshooting.* 2003.

148. **Nair, Jayakumaran A.** *Principles of Biotechnology.* s.l. : Laxmi Publication.

149. **Mahesh, S.** *Biotechnology-3: Including Molecular Biology Biophysics.* s.l. : New Age International limited, 2003.

150. **Räty, Jukka, Peiponen, Kai-Erik and Asakura, Toshimitsu.** *UV-visible Reflection Spectroscopy of Liquids.* s.l. : Springer, 2004.

151. **Anderson, Rosaleen J, Bendell, David J and Groundwater, Paul W.** *Organic Spectroscopic Analysis.* s.l. : Royal Society of Chemistry, 2004.

152. **Kenkel, John.** *Chemistry: an Industry-based Laboratory Manual .* s.l. : CRC Press, 2000.

153. **Kubic, Thomas and Petraco, Nicholas.** *Forensic Science Laboratory Manual and Workbook.* [ed.] 3. s.l. : CRC Press.

154. **Kotz, John C, Treichel, Paul and Weaver, Gabriela C.** *Chemistry and Chemical Reactivity.* s.l. : Cengage Learning, 2006.

155. FLx800 Fluorescence Microplate Reader. Winooski, Vermont , USA : BioTek Instruments, Inc.

156. Eclipse TS100. Tokyo, Japan : Nikon Corporation.

157. **Freshney, R. Ian.** *Culture of Animal Cells: A Manual of Basic Technique and Specialized Applications.* s.l. : John Wiley and Sons, 2010.

158. Quant-iT™ PicoGreen ® dsDNA Reagent and Kits. Eugene, Oregon, USA : Molecular Probes Invitrogen Detection Technologies, 610, 2008. Vol. MP 07581.

159. Instructions Coomassie Plus-The Better Bradford Assay Kit. Rockford, Illinois, USA : Pierce. Vol. 23236.

160. *An Alizarin Red-based Assay of Mineralization by Adherent Cells in Culture: Comparison with Cetylpyridinium Chloride Extraction.* **Gregory, C.A.** 2004, Analytical Biochemistry, Vol. 329, pp. 77-84.

161. **Bancroft, John D and Gamble, Marilyn.** *Theory and Practice of Histological Techniques.* s.l. : Elsevier Health Sciences, 2008.

162. *Corrosion Characterization of Titanium Alloys by.* **Assis, S'ergio Luiz de, Wolynec, Stephan and Costa, Isolda.** 2006, Electrochimica Acta, pp. 1815-1819.

163. *Processing and Mechanical Properties of Autogenous Titanium Implant Materials.* **Wen, C. E., et al.** 4, Journal of Materials Science: Materials in Medicine, Vol. 13, pp. 397-401.

164. *Corrosion Resistance for Biomaterial Applications of TiO2 Films Deposited on Titanium and Stainless Steel by Ion-beam-assisted Sputtering.* **Pan, J., et al.** 3, s.l. : Journal of Biomedical Materials Research, 1997, Vol. 35, pp. 309-318.

165. *Comparative Investigation of the Surface Properties of Commercial Titanium Dental Implants. Part I: Chemical Compositions.* **Massaro, C., et al.** 6, Journal of Materials Science: Materials in Medicine, Vol. 13, pp. 535-548.

166. *Enhanced Bone Apposition to a Chemically Modified SLA Titanium Surface.* **Buser, D, et al.** 7, 2004, Journal of Dental Research, Vol. 83, pp 529-533.

167. **Young, Barbara, et al.** *Wheater's Functional Histology: A Text and Colour Atlas.* s.l. : Elsevier, 2006.

168. **Currey, J.D.** *Bones Structure and Mechanics.* s.l. : Princeton University Press, 2002.

169. **Shipman, P., Walker, A. and Bichell, D.** *The Human Skeleton.* 1985.

170. **Luiz, C. L., Jose, C. and McGraw-Hill.** *Basic Histology Text and atlas.* 11. 2005.

171. **Guyton, C. A. and Hall, J.** *Textbook of Medical Physiology.* 11. s.l. : Elsevier Saunders, 2006.

172. **Lieberman, Jay R and Friedlaender, Gary E.** *Bone Regeneration and Repair: Biology and Clinical Applications.* s.l. : Humana Press, 2005.

173. **Johnson, Ann L, Houlton, John E. F and Vannini, Rico.** *AO Principles of Fracture Management in the Dog and Cat.* s.l. : Thieme, 2005.

174. *Principles of Bone Healing.* **Kalfas, I. H.** 2001, Neurosurg Focus, Vol. 10, pp. 7-10.

175. **Barnes, Steven J and Harris, Lawrence P.** *Tissue Engineering: Roles, Materials and Applications.* s.l. : Nova Publishers, 2008.

176. **Cappabianca, Paolo.** *Cranial, Craniofacial and Skull Base Surgery.* s.l. : Springer, 2009.

177. **White, Timothy D and Folkens, Pieter A.** *The Human Bone Manual .* s.l. : Academic Press, 2005.

178. **Wheeler, Russell C.** *A Textbook of Dental Anatomy and Physiology.* s.l. : Saunders, 1958.

179. **Sarandha.** *Textbook of Complete Denture Prosthodontics.* 2007.

180. **Hobkirk, John A, Watson, Roger M and Searson, Lloyd J.** *Introducing Dental Implants.* s.l. : Elsevier Health Sciences, 2003.

181. **Drago, Carl J.** *Implant Restorations: A Step-by-step Guide.* s.l. : Wiley-Blackwell, 2007.

182. *Self-Organized Porous Titanium Oxide Prepared in H2SO4/HF Electrolytes.* **Beranek, R, Hildebrand, H and Schmuki, P.** 3, 2003, Electrochem. Solid-State Letters, Vol. 6, pp. B12-B14.

183. *Titanium Oxide Nanotube Array Prepared by Anodic Oxidation.* **Gong, Dawei, Grimes, Craig A and Varghese, Oomman, K.** 12, 2001, Journal of Material Science Research, Vol. 16, pp. 3331-3334.

184. *Bioreactor Development for Cartilage Tissue Engineering.* **Wick, Timothy and Farooque, T.** Melbourne, Australia : s.n., 2009. CSIRO. pp. 1-7.

185. *Tissue Engineering:Despite Technical and Regulatory Challenges, the Prospects for Tissue Engineering are Good.* 2000, Nature Biotechnology, Vol. 18, pp. IT56-IT58.

186. *In vivo Bone Tissue Engineering using Mesenchymal Stem Cells on a Novel Electrospun Nanofibrous Scaffold.* **Shin, M., Yoshimoto, H. and Vacanti, J. P.** 2004, Tissue Engineering, Vol. 10, pp. 33-41.

187. *Review: Polymeric Biomaterial for Tissue and Organ Regeneration.* **Seal, B.L., Otero, T.C. and Panitch.** 2001, Material Science and Engineering, Vol. 34, pp. 147-230.

188. *Electrospinning of Polymeric Nanofibers for Tissue Engineering Applications:A Review.* **Pham, Q. P., Sharma, U. and Mikos, A.** 2006, Tissue engineering, Vol. 12, pp. 1197-1121.

189. *Biomanufacturing for Tissue Engineering: Present and Future Trends.* **Bartolo, J., et al.** 4, s.l. : Taylor and Francis, 2009, Virtual and Physical Prototyping, Vol. 4, pp. 203-216.

190. *Micro- and Nanoscale Structures for Tissue Engineering Constructs.* **Desai, Tejal A.** 2000, Medical Engineering and Physics, Vol. 22, pp. 595-606.

191. *Review: Biomaterials and Scaffolds for Ligament Tissue Engineering.* **Ge, Zigang, et al.** 2005, Journal of Biomedical Materials Research, pp. 639-652.

192. *Polymeric Biomaterials for Tissue and Organ Regeneration.* **Seal, B.L., Otero, T.C. and Panitch, A.** 4, 2001, Materials Science and Engineering, Vol. 3, pp. 147-230.

193. *Nano-fibrous Scaffolding Architecture Selectively Enhances Protein Adsorption Contributing to Cell Attachment.* **Woo, K.M., Chen, V.J. and Ma, P.X.** 2, 2003, Journal of Biomedical Materials Research, Vol. 67A, pp. 531-537.

194. *Biodegradable Nanofiber Scaffold by Electrospinning and Its Potential for Bone Tissue Engineering.* **Yoshimoto, H, et al.** 12, 2003, Biomaterials, Vol. 24, pp. 2077-2082.

195. *Electrospun Poly(lactic-co-glycolic acid)/Halloysite Nanotube Composite Nanofibers for Drug Encapsulation and Sustained Release.* **Qi, Ruiling, et al.** 2010, Journal of Material Chemistry, Vol. 20, pp. 10622-10629.

196. *Study on the Adsorption of Neutral Red from Aqueous Solution onto Halloysite Nanotubes.* **Luo, Peng, et al.** 5, 2010, Water Research, Vol. 44, pp. 1489-1497.

197. *Interactions Between Halloysite Nanotubes and 2,5-Bis(2-Benzoxazolyl) Thiophene and Their Effects on Reinforcement of Polypropylene/Halloysite Nanocomposites.* **Liu, Mingxian, et al.** 20, 2008, Nanotechnology, Vol. 19.